NANOWIRE-EPOXY INTERACTION AND ITS EFFECTS ON MECHANICAL

PROPERTIES OF NANOWIRE-BASED EPOXY COMPOSITES

A Dissertation

by

YIXI CHEN

Submitted to the Office of Graduate and Professional Studies of
Texas A&M University
in partial fulfillment of the requirements for the degree of

DOCTOR OF PHILOSOPHY

Chair of Committee,	Sreeram Vaddiraju
Committee Members,	Mustafa Akbulut
	Micah Green
	Arun Srinivasa
Head of Department,	Arul Jayaraman

December 2020

Major Subject: Chemical Engineering

ABSTRACT

One-dimensional nanomaterials, such as carbon nanotubes (CNTs) and nanowires, are promising for various applications. Although CNTs have been used as reinforcements in composites owing to their high mechanical strength and high surface-area-to-volume ratio, the use of nanowires as reinforcements has not been examined extensively. This is especially surprising, given that nanowires have not only been successfully synthesized, but also demonstrated to exhibit novel mechanical properties. One of the challenges for the applications of nanowires is that translating the successes achieved in the laboratory to commercial products requires mass production of nanowires, if possible, in a byproduct-free manner. In view of this, the first objective of this dissertation is to produce byproduct-free nanowires. This was accomplished using Zn_3P_2 nanowires as an illustration. Herein, Zn foams were obtained and used as substrates to grow Zn_3P_2 nanowires. These foams were obtained *in situ* by heating consolidated mixtures of Zn flakes and a sacrificial salt, NH_4Cl. This approach aided in the uniform heating of the foams and the complete conversion of Zn into Zn_3P_2 nanowires.

The second objective is aimed at the fabrication of nanowire-based composites and examination of the effects of nanowires on the mechanical properties of nanocomposites. Herein, Zn_3P_2 and TiO_2 nanowires were selected as reinforcements. To understand nanowire-epoxy interaction, various coupling agents were applied to nanowires to modify their surface characteristics. Overall, functionalization affected both interfacial adhesion

and the degree of dispersion of nanowires. Ultimately, this was observed to alter the mechanical properties of these nanocomposites.

Lastly, to fabricate nanocomposites in a manner similar to that employed for fiber-reinforced composites, foams of interconnected nanowires were prepared by heating the functionalized nanowire mixtures with sacrificial salt microcrystals. The idea here is that optimal mechanical performance of nanocomposites is achieved when a continuous filler network is established, while preventing nanowire agglomeration. These nanowire foams were infused with a shape memory polymer (SMP) and the mechanical properties of the resulting composites were studied. These composites exhibited mechanical properties superior to those obtained by merely mixing fillers and a matrix material.

ACKNOWLEDGEMENTS

CONTRIBUTORS AND FUNDING SOURCES

NOMENCLATURE

4ATP	4-aminothiophenol
4tBTP	4-tert-butylthiophenol
AAO	Anodic aluminum oxide
APTMS	3-(aminopropyl)trimethoxysilane
ASTM	American Society for Testing and Materials
BET	Brunauer-Emmett-Teller
CNT	Carbon nanotube
CTAB	Cetyltrimethylammonium bromide
CVD	Chemical Vapor Deposition
DMA	Dynamic Mechanical Analysis
DSC	Differential Scanning Calorimetry
EDS	Energy Dispersive X-ray Spectroscopy
FTIR	Fourier-transform Infrared Spectroscopy
GPTMS	3-(glycidoxypropl)trimeothoxysilane
HOPG	Highly oriented pyrolytic graphite
MWCNT	Multiwalled carbon nanotube
NGDE	Neopentyl diglycidyl ether
PCM	Polycarbonate membrane
PS	Polystyrene
PVD	Physical Vapor Deposition

PVP	Polyvinylpyrrolidone
SAM	Self-assembled monolayer
SCCM	Standard cubic centimeter per minute
SDS	Sodium dodecylsulphate
SEM	Scanning Electron Microscopy
SMA	Shape memory alloy
SMP	Shape memory polymer
SMPC	Shape memory polymer composite
STM	Scanning Tunneling Microscopy
TEM	Transmission Electron Microscopy
TGA	Thermogravimetric Analysis
VLS	Vapor-liqud-solid
VS	Vapor-liquid
XPS	X-ray Photoelectron Spectroscopy
XRD	X-ray Diffraction

TABLE OF CONTENTS

Page

LIST OF FIGURES

LIST OF TABLES

xvi

CHAPTER I

INTRODUCTION

Background

In this section, a brief introduction to some of the key concepts in this dissertation is given. More in-depth discussion relevant to the experimental work performed in this dissertation can be referred to the following section, Literature Review.

Nanowires

Nanomaterials have a dimension on the order of 1–100 nm and typically exhibit distinct properties from their bulk counterparts. For example, it has been reported that metal nanoparticles exhibit reduced melting points (melting point depression) [1, 2] and have enhanced catalytic activities [3, 4] compared to their bulk form, because of the presence of a significant amount of surface atoms or functional groups with respect to their volume. Nanoparticles have been used in many applications, such as lubricant additives [5, 6], catalysts [7, 8], light emitting diodes [9, 10], drug delivery [11, 12], and fluorescent labels of protein or DNA [13, 14].

In some applications, one-dimensional nanomaterials, *e.g.*, nanowires, nanorods, nanobelts, and nanotubes, may be superior to their zero-dimensional counterparts, i.e., nanoparticles. Among the common one-dimensional nanomaterials, nanowires are one of the most widely studied materials due to their excellent properties. For example, as our group has reviewed previously, nanowires have reduced thermal conductivity due to

phonon scattering while maintaining a good electrical conductivity, leading to potential applications in high-performance thermoelectric devices [15]. It has also been reported that nanowires exhibit higher mechanical strength and higher flexibility (higher strain at failure) compared to their bulk counterparts, which was also observed in our lab with Zn_3P_2 nanowires[16-19]. Besides, some nanowires, such as ZnO nanowires, are also found that they can be used to produce good UV-light laser and highly sensitive UV-light switches [20]. Up to now, nanowires with different chemical compositions, dimensions, and crystal phases have been successfully synthesized in the laboratory using various techniques [21, 22].

Polymer Composites

Composite materials are a class of materials that are composed of two or more distinct materials, while each component remains separate within the final structure [23]. For each of these constituents, the discrete phase is termed the fillers and the continuous one is called the matrix. Typically, the properties of a composite are combinations of those of the constituent phases, and consequently a material with properties different from conventional metals, ceramics, and polymers can be produced [23]. For example, the composite materials developed for aerospace applications, composed of a thermosetting (e.g., epoxy) or thermoplastic (e.g. Nylon 6.6) matrix reinforced by carbon fibers [24], possess extraordinary properties, such as high stiffness, high strength, high corrosion resistance, and low densities [23].

Polymer composites can be classified into two major categories depending on the geometry of the fillers, namely, fiber-reinforced and particulate-reinforced composites. Fiber-reinforced composites are widely used in aerospace and structural applications, in which fibers or filaments with high strength and stiffness are aligned along a plane within a matrix. Due to this anisotropic arrangement of fibers, the as-produced planes, also known as laminas, exhibit anisotropic mechanical properties; namely, the plane is significantly stronger in the normal direction than the orthogonal one, with respect to the fiber alignment [23]. Typically, the fiber component takes up more than 50 vol.% in the composite, and the polymer component serves as the binding agent [23].

On the other hand, for particulate-reinforced composites, particles are dispersed in a matrix and serve as reinforcements, in which the matrix is the major constituent. The common fillers include carbon black and silica [23]. Although reinforcement by particles is not as significant compared to fibers mentioned above, the addition of particles to a polymeric matrix can append new properties not native to the matrix [24]. For example, the use of conducting particles, e.g., graphite, makes an insulating polymer conductive. Most of nanocomposites also fall under this category.

Nanowire-based Polymer Composites

The significant reinforcement effect of carbon nanotubes (CNTs) as fillers for polymeric materials is well-known for decades, due to the fact that CNTs possess one of the highest mechanical strength and stiffness among all the materials ever known to humankind [25, 26]. However, compared to CNT-based composites, which were first

studied by Ajayan *et al.* in 1994 [27] (CNTs were first discovered by Iijima in 1991 [28]), nanowire-based composites are less investigated or understood in terms of their mechanical properties. Probably the first systematic study in this area was performed by Vivekchand *et al.* in 2006, who examined the enhancement in elastic modulus of polyvinyl alcohol composites reinforced by SiC or Al_2O_3 nanowires [29].

In effect, nanowires are promising materials as reinforcements because of their high aspect ratios, which enable an effective load transfer from a host matrix to fillers [30, 31]. What is more, similar to electrical percolation, which can be achieved at a much lower concentration for fillers with a higher aspect ratio [30, 32], mechanical properties can be enhanced owing to mechanical percolation [33, 34]. Namely, when a continuous network of fillers is formed within a matrix, elastic modulus of a nanocomposite can be improved dramatically. Some computational studies also showed that nanowires are more effective than nanoparticles for enhancement in mechanical properties of polymeric materials [35, 36]. Some of the most widely used models that predict the mechanical properties of a composite include the Guth [37] and Halpin-Tsai [38, 39] equations.

It is worth noting that the capability of mass production of nanowires is a prerequisite to fabricate a polymer composite, considering that multiple bulk dumbbell-shape specimens need to be prepared for tensile testing. The synthesis method for mass production depends on the specific type of nanowires, and some of the common approaches include hydrothermal [40-43], PVD [44-47], and CVD [16, 48-51].

Shape Memory Polymer Composites

Shape memory polymers (SMPs), a class of materials that are capable of memorizing the original shape even after deformed to a different shape, are also known as smart materials. These materials can be activated and transformed from a temporary shape to a permanent shape under certain conditions, and one of the most common stimuli to induce shape recovery is temperature. These materials have been shown to be promising for biomedical and aerospace applications [52, 53]. SMPs possess several advantages relative to their metal counterparts, shape memory alloys (SMAs), including lower densities, higher recovery strains, and ease of processabilities [54]. However, SMPs suffer from a few disadvantages, including lower recovery speeds, lower recovery stresses, and lower cyclability [55, 56]. The intent of improving these mechanical properties led researchers to fabricate shape memory polymer composites (SMPCs) reinforced by a filler component [57, 58]. To date, a variety of materials have been examined as fillers for SMPCs, including carbon black [59-62], SiC [60, 61, 63-65], clay [66-69], carbon fibers [60, 61, 70, 71], and carbon nanotubes (CNTs) [72-76].

Literature Review

Herein, the literature relevant to the experimental studies performed in this dissertation is reviewed. First, the common synthesis approaches of nanowires are delineated, and the nanowire growth mechanism of each approach is discussed. Subsequently, the challenges in fabrication of nanocomposites are introduced. Finally, aiming to produce an effectively reinforced nanocomposite, a technique to improve the

5

interfacial adhesion between nanowires and a polymeric matrix, known as functionalization, is presented.

Synthesis of Nanowires

Many synthesis approaches have been developed to produce metal and semiconducting nanowires, e.g. vapor-phase synthesis, solution-phase synthesis, and template-assisted synthesis. These approaches, also known as bottom-up synthesis, are very successful to produce high-quality nanowires in the laboratory. In contrast, a few studies also investigated top-down synthesis of nanowires, e.g. nanolithography and focused ion beam, because of its high cost and low productivity.

The following sections will discuss the various synthesis techniques and their mechanisms for growing nanowires. The mass production approach of a specific type of nanowires used in this dissertation will be discussed in Chapter II, Chapter III, and Chapter IV.

Physical Vapor Deposition

Physical Vapor Deposition (PVD) is a common technique to produce thin films or protective coatings in the industry, and it is also widely applied to produce semiconducting nanowires in the laboratory [21, 77]. PVD is also called thermal evaporation method or evaporation-physical transport-condensation method [78].

Figure 1 shows the major steps in which nanowires are grown by PVD in a reactor. In a PVD chamber, a precursor, usually a powder, is placed in the upper stream, whereas

6

a substrate to collect the product is located in the lower stream. At elevated temperatures, the solid precursor sublimes and transports through the chamber, along with the carrier gas, to the lower stream. The substrate is usually maintained at lower temperatures than the upper stream, where the hot vapors of the precursor condense and crystallize as a form of nanowires. Some of the common nanowires synthesized by this technique include ZnO [78], TiO_2 [79], and SnO_2 [80] nanowires. Normally, nanowires grown by PVD are controlled by the Vapor-solid (VS) growth mechanism.
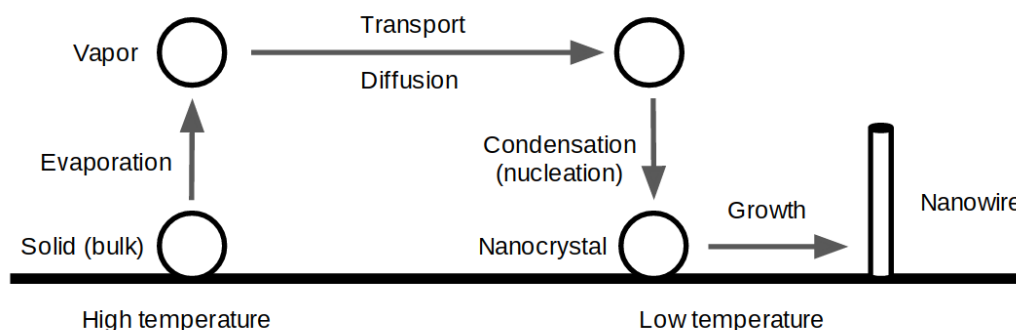
Figure 1 A scheme of synthesis of nanowires by PVD, in which a solid material (usually a powder) is heated to a high temperature and evaporated, transported along a reactor by a carrier gas, and then condensed on a cold substrate in to form nanowires

Vapor-solid Growth Mechanism

VS is one of the most common growth mechanisms in vapor-phase synthesis for nanowires, and a variety of semiconducting nanowires synthesized in the laboratory can be attributed to it [81]. As shown in **Figure 2**, VS growth of nanowires involves multiple steps in the interface between a vapor and a surface: (i) diffusion from a vapor to a surface, (ii) adsorption/desorption on a surface, (iii) diffusion across a surface to a desired

7

nucleation site, (iv) nucleation on a surface, and (v) anisotropic growth of a nanowire [82].

It is worth noting that the surface is not just the bulk surface of a substrate, but it can also

be the surface of individual nanowires. The main driving force of this process is the

minimization of chemical potential (Gibbs free energy), the rate determining steps being

the second and last steps, namely, adsorption and anisotropic growth [82].
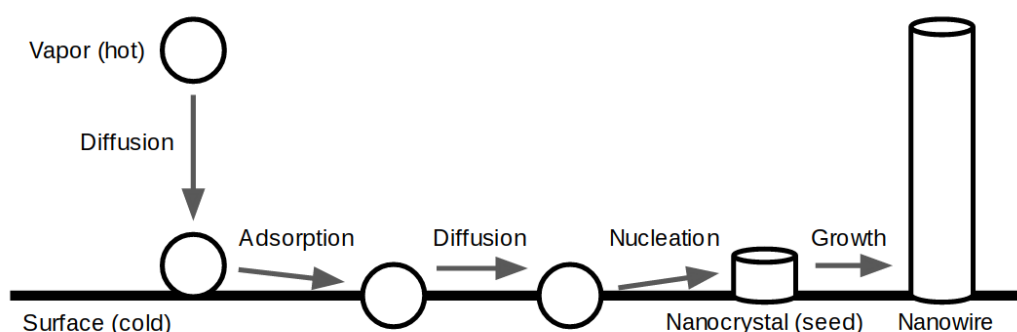
Figure 2 A scheme of growth of a nanowire by the VS mechanism, in which the growth of nanowires is achieved by the anisotropic crystal growth due to their anisotropic crystal structure

An anisotropic growth of nanowires is generally originated from different growth

rates (which can vary even by the orders of magnitude) of different planes due to a specific

crystal structure [83]. For example, <0001> and <1000> planes in a hexagonal crystal

structure typically have different growth rates. Accordingly, the aspect ratio and the

diameter of nanowires are likely to be controlled by temperature, as the growth rate of

each type of planes is a different function of temperature. In some cases, crystal structure

defects, such as screw dislocations, or the formation of oxide sheathe, can also lead to the

formation of nanowires [81, 84].

One of the well-studied nanowires grown by VS is ZnO nanowires. Ye *et al.* reported the formation of different morphologies of ZnO nanostructures by VS [78]. In this study, a mixture of ZnO and graphite powders (precursor) was loaded in the upper stream of a horizontal tube furnace, and multiple Si wafers were place downstream to collect the product in different locations. The precursor was quickly heated to 1050 °C, and the products with various nanostructures were obtained in the lower stream due to the difference in temperature at different locations. It was concluded that the morphology of ZnO depends on the degree of supersatuation in the vapor (depending on the solubility of the precursor and the change in temperature) and surface energy of the crystal. Other minor factors include temperature, heating rate, and gas flow rate. In general, a low supersaturation, namely a small temperature difference between the upper and lower streams, is better for nanowire growth, whereas high supersaturation produces bulk crystals, due to the fact that all the crystal planes will grow significantly [78].

Chemical Vapor Deposition

Chemical Vapor Deposition (CVD) is another common method to synthesize semiconducting nanowires in the laboratory. Its overall process is similar to that of PVD, and the main difference is that this process involves chemical reactions during crystal growth [85]. In order to promote the growth of nanowires, a catalytic material, either a foreign material or a self-catalyst, is required [85]. Since the catalytic material melts and becomes liquid droplets during the synthesis, this process is also called a Vapor-liquid-solid (VLS) growth of nanowires.

Vapor-liquid-solid Growth Mechanism

Research in a VLS growth of semiconducting nanowires dates back to the early 1960s, when Wagner and Ellis first proposed this mechanism for a growth of microscale silicon whiskers with the presence of Au particles [86, 87]. Later, in 1998, the size of whiskers was successfully decreased to a nanoscale by Lieber's group, in which a laser ablation technique was applied to produce nanoscale Au seeds for growing Si nanowires [88]. Subsequently, the direct observation of a VLS growth of Si nanowires was successfully performed using *in-situ* Transmission Electron Microscopy (TEM) by Wu *et al.* in 2001, which concluded that three distinct stages exist in a VLS mechanism, namely metal alloying, crystal nucleation, and axial growth of nanowires [89]. As illustrated in **Figure 3**, during a VLS growth of Si nanowires, vapor-phase silane first decomposes and the resulting Si adatoms dissolve into a molten Au nanodroplets. When the Si-Au alloy droplet becomes supersaturated with respect to Si, a solid-phase Si will continuously precipitate out as a nanowire. Eventually, the growth of Si nanowires is terminated by poisoning of Au droplets or insufficiency in thermal energy or reactants, and these liquid droplets solidifies and forms a round tip of each individual nanowire [89]. It was also found that the termination of Si nanowire growth is caused by diffusion of Au droplets [90].
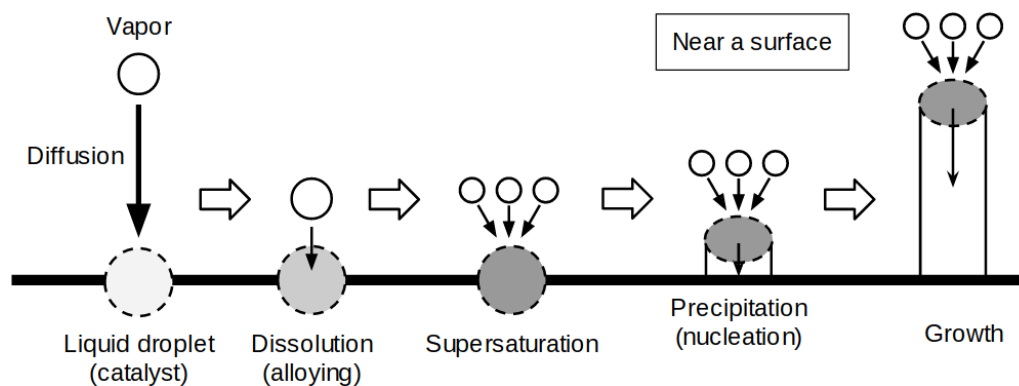
Figure 3 A scheme of a VLS growth of nanowires, in which a liquid nanodroplet serves as a catalyst and creates a vapor-liquid-solid asymmetrical interface to facilitate the anisotropic crystal growth

In general, the diameter of nanowires grown by VLS is strongly affected by the size of these droplets and always larger than that of droplets [82, 91]. For the choice of a catalyst material, equilibrium phase diagrams should be referred to extract key information, e.g., temperature, chemical composition and crystal structures of the product. In addition to foreign metals, e.g., Au, pools of low melting metals, e.g., Ga, can catalyze/self-catalyze the nucleation and basal growth of nanowires [92]. Here, multiple nanowires can be grown by basal attachment from a large, molten droplet, e.g., Ga, based on the VLS mechanism [93].

Hydrothermal Synthesis

Hydrothermal synthesis is a long-known method for creating a bulk crystal based on the solubility change of a salt at different temperatures at a high pressure. It is also commonly applied in the synthesis of one-dimensional nanomaterials in the laboratory,

11

[94]. This method, sometimes also called Solution-solid method, is usually carried out in an autoclave enclosed in a furnace, in order to apply a high pressure and temperature simultaneously.

For a hydrothermal method, the use of appropriate surfactants or capping agents, such as poly(vinylpyrrolidone) and cetyltrimethylammonium bromide, is important to stabilize the solution system and produce high-quality nanowires, because these materials will passivate on the surface of growing crystals and thus reduce their surface energy [95-97]. Additionally, the pH value of a solution and the concentration of reactants are also known to play important roles in the size and the shape of nanowires obtained, due to the fact that the concentration of OH^- (or H^+) significantly affects the crystal growth and the reactions employed for nanowire production [98, 99].

Electrochemical Deposition

Nanowires are also commonly synthesized by electrochemical deposition, or simply electrodeposition, which is widely used to produce thin films in the industry. In general, templates with desired pores can facilitate nanowires to grow in a controlled manner, and the most common templates used are anodic aluminum oxide (AAO) [100], polycarbonate membrane (PCM) [101], and highly oriented pyrolytic graphite (HOPG) [102].

One of the critical factors that control the morphology of one-dimensional nanostructures by electrodeposition is the relative strength of the adhesion between depositing materials and different surfaces [82, 103]. As shown in **Figure 4**, hollow

nanotubes can be produced if the adhesion between the depositing materials and the substrate is stronger, in which the deposition starts with the inner walls of pores and continues inwardly. On the other hand, if nanowires are preferred, an appropriate substrate needs to be selected in order for deposition to start with the bottom and continue along a pore.
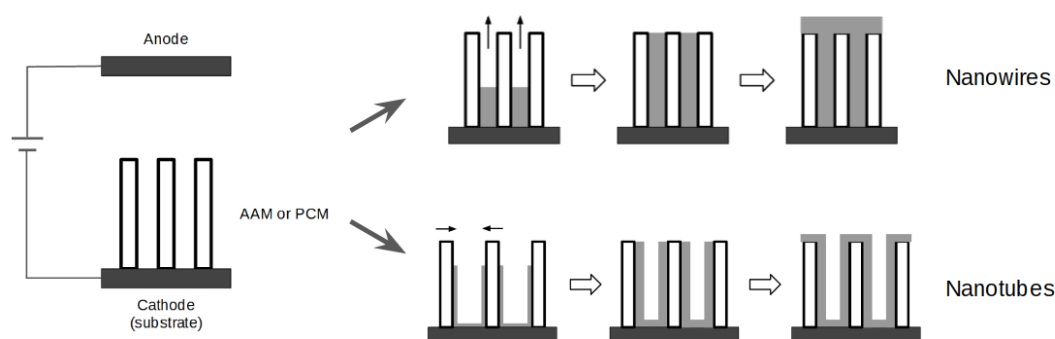
Figure 4 A scheme of producing nanowires by electrochemical deposition, in which the morphology of nanomaterials is dependent on the degree of adhesion between the depositing materials and the substrate

Many studies have successfully produced metal and semiconducting nanowires with various chemical compositions by electrodeposition, such as Ag, Cu, Ni, ZnO, and Bi_2Te_3 nanowires [104-107]. The main advantage of electrodeposition in nanowire synthesis is that this technique is able to produce a well-aligned array of nanowires with well-controlled diameter and length on a desired substrate [106, 108]. However, single-crystalline nanowires are usually difficult to be produced by template-assisted electrodeposition, and the length of nanowires is intrinsically limited by the depth of template pores [103]. It is also worth noting that the synthesis process involves multiple

13

steps, the output is limited, and as-synthesized nanowires can be damaged or deteriorated when the template is removed [103].

Processing of Nanowire-based Polymer Composites

Nanowires are typically dispersed in a polymer matrix by one of three approaches: solution mixing, melt blending, and *in-situ* polymerization [109, 110]. In the first approach, nanowires are dispersed in a solvent (by mechanical mixing, magnetic stirring, and/or sonication), then well mixed into a polymer solution at room temperature or slightly elevated temperatures, and finally casted in a mold to form desired shapes. In the second method, on the other hand, nanowires and polymer melt are directly mixed and processed at high temperatures with high shear forces by extrusion or injection machines, which eliminates the need for solvents. *In-situ* polymerization is another common technique to fabricate a composite, in which nanowires or a nanowire dispersion are mixed with monomers and polymerized by the addition of an initiator or a curing agent. Epoxy-based composites are usually synthesized in this manner.

One of the major issues of processing a nanocomposite is the degree of dispersion of nanofillers. In order to take full advantages of these nanofillers, they must be homogeneously dispersed in a polymer matrix without any agglomeration. The reason is that a poor dispersion of nanofillers leads to a non-uniform distribution of applied forces within the host matrix, while the agglomerates of nanofillers will cause inter-filler slippage and thus an inefficient load transfer to nanofillers [109]. A common but effective practice is to mix nanowires using a high-speed mechanical stirrer for a long period of time, so that

14

nanowire bundles will be dissociated into individual nanowires under high shear forces. Another approach is sonication, either by a tip sonicator or a sonication bath, but this technique may damage and shorten the nanowires if used too aggressively [111, 112]. Accordingly, sonication should be used for a long duration. Additionally, surface functionalization of nanofillers is an effective approach to preventing aggregates and improve dispersity [113-115]. For example, Yang *et al.* reported that functionalization of multi-walled carbon nanotubes (MWCNTs) with triethylenetetramine contributes to the uniform dispersion of MWCNTs in an epoxy matrix, leading to the enhancement in mechanical and thermal properties of the nanocomposite [116].

Another important factor to create an effective nanocomposite is nanofiller-polymer interaction. The surface area of fillers increases tremendously as their size changes from micro- to nano-scales [117], and therefore the interactions between the fillers and a host matrix become more significant. Namely, good interfacial adhesion between nanofillers and a matrix ensures an efficient load transfer and thereby enhances the mechanical properties of a nanocomposite [118, 119]. If fillers and the matrix are poorly adhered, dewetting or debonding will occur, causing a mechanical failure at the interfaces [120, 121]. To achieve high interfacial adhesion between nanofillers and a matrix, functionalization of nanofiller surface, chemically or non-chemically, is an effective approach [122-124]. For chemical functionalization, the most common coupling agents are amines [125, 126], thiols [127, 128], and organosilanes [129-131]. On the other hand, in a non-chemical approach, a low molecular weight polymer or a surfactant is used to wrap up filler materials to be compatible (i.e., better wetting) with the matrix [132].

Typical surfactants employed for this purpose are poly(vinylpyrrolidone) (PVP), polystyrene (PS), cetyltrimethylammonium bromide (CTAB), and sodium dodecylsulfate (SDS) [133, 134]. These methods demonstrated in the past that surface-modified nanofillers showed stronger interactions with the polymer matrix and enhanced mechanical performance of a composite [135-137].

Functionalization of Filler Materials

Coupling agents, also known as molecular linkers, possess two or more functional groups that are capable of linking inorganic and organic compounds to improve filler-matrix interaction. It is of importance to understand the effect of the chemistries of various coupling agents and their deposition mechanisms on the interfaces between the fillers and the matrix. This is discussed in detail below.

Thiolation

One of the most extensively studied coupling agents is thiols. They are typically applied to coinage metals such as Au [138-140] and Cu [140-142]. Because of their strong affinity for the surface metal atoms through thiolate bond formation, thiols readily attach to the metal surface and form a self-assembled monolayer (SAM).

Typically, the thiol functional groups, also called ligand or head groups, anchor spontaneously onto the metal surface, whereas the terminal functional groups at the other end tailor the surface properties of the substrate [143]. During the thiolation process, initially, when the surface coverage is low, thiol molecules are absorbed to the surface in

16

a "lying-down" manner, namely the alkyl chains being parallel to the substrate [144]. Subsequently, when the exposed surface is fully covered by thiol molecules, "standing-up" configuration will be established, in which thiol molecules nucleate in an ordered manner to form a crystalline, closed-packed structure [144].

In addition to coinage metals such as Au and Cu, the functionalization of III-V semiconductor compounds with thiols, including InP [145-147], GaP [147], and GaAs [148], has also been studied by some groups. For these compounds, it has been reported that the sulfur atoms typically bind to the atoms of the Group III element through thiolate bonds.

Silanization

Another common type of coupling agent is organosilanes. They have been extensively used to tailor the surface characteristics of glasses and metal oxides in the industry [149]. The alkoxy groups of the silanes are hydrolysable and readily react with the surface hydroxyl group on the substrate, whereas the organic functional group will interact with polymeric materials [149]. If the functional group is reactive, the organosilane serves as a molecular linker and establish strong covalent bonding with an organic material such as polymers. On the other hand, if an unreactive and nonpolar functional group, i.e., hydrocarbon or fluorocarbon, is present, the surface will become hydrophobic.

Multiple steps are involved in grafting an organosilane to a surface [150]. Firstly, the silane monomers are hydrolyzed and forms silanol groups (Si-OH), either through

reaction with water in the aqueous solution or residual water from the surface of a substrate. Next, some of the silane monomers may also self-condense before being grafted to the substrate and form oligomers during the hydrolysis step [150]. Subsequently, silane monomers or oligomers diffuse to the surface and bind with surface hydroxyl groups via hydrogen bonding. Finally, the silanol groups coordinated with surface hydroxyl groups will form covalent bond by releasing water [150]. In fact, these steps occur simultaneously, although described sequentially. After silanization is completed, each silane molecule is typically linked to the substrate by one bond, whereas other two silanol groups are either linked to other silane molecules or present in a free form [149].

Up to date, organosilane functionalization is usually performed by a solution-phase process for various substrates, and almost exclusively for the materials in a powder form. However, quality control of a SAM produced via a solution-phase route is demanding, which depends on many factors such as temperature, the presence of water, the type of solvent, and the concentration of organosilane coupling agents [151]. Among these factors, the amount of water present in the system is the most difficult factor to control, since water may come from atmosphere, solvent, or fillers themselves. Due to the fact that silane hydrolysis is highly sensitive to the concentration of water in the system, the quality of a SAM may differ from batch to batch. Namely, if the amount of water is not strictly controlled, agglomerates of organosilane will form on the substrate. Besides, especially for powders, any solution-phase process will lead powders to agglomerate by capillary force, and therefore it typically requires post-treatment to break up the agglomerates. A solution-phase silanization process also generates significant amounts of waste, which is

a serious economic or environmental issue [152]. On the other hand, the quality of a SAM produced via a vapor-phase route is superior and more consistent [151, 152]. The deposition takes place in a self-limiting manner, which reduces self-polymerization, and the effect of water can be minimized since the deposition is carried out under a vacuum. Additionally, the vapor-phase approach also eliminates the necessities of filtering/washing or other equivalent cleaning processes. Accordingly, vapor-phase silanization could be an effective approach to introducing high-quality SAM to nanomaterials and preventing powder agglomerates owing to their interactions with a solvent.

Gap in Literature

Following literature review, the purpose of this section is to identify some gaps existing in the current research. Filling these gaps in literature, as discussed in detail in the next section, is the main goal of this dissertation.

Byproduct-free Production of Nanowires

Nanowires have been demonstrated to be useful in the fabrication of many types of devices, including solar cells, thermoelectrics, lithium-ion batteries, and sensors [93]. Translating the successes achieved in the laboratory into commercial production and deployment of nanowire-based devices requires mass production of nanowires. This nanowire mass production is also important in the laboratory for ensuring that bulk nanowire devices exhibit devices performances similar to those accomplished in individual nanowires or small-scale nanowire arrays and mats.

Most of the current reports on nanowire synthesis only demonstrate production of nanowires in the scale of micrograms to a few milligrams, although they do discuss the possibility of scaling up the reported processes [93]. Only a handful of reports show the production of gram and kilogram quantities of nanowires [16, 51, 153-164]. Additionally, in most of the reports discussing the mass production of nanowires, the quality of nanowires is generally missing [165]. It is entirely possible that some unreacted reactants remain with the nanowires (e.g., Au catalyst remaining either at the tips or within silicon nanowires [166]) or some byproducts are generated along with the nanowires (e.g., nanoparticles and bulk crystals [167]). As separation of nanoparticles and other byproducts from nanowires is not a trivial task, it is ideal to obtain nanowires in a byproduct-free manner. Besides, it is ideal to directly obtain the nanowire product in the desired form, e.g., *in-situ* surface functionalized nanowires, to prevent any unwanted surface oxidation of the nanowires [16]. Some of the preliminary work regarding the byproduct-free nanowire mass production was done in collaboration with Mr. Rakesh Polinnaya [168].

Mechanical Properties of Nanowire-based Polymer Composites

Research investigating the mechanical properties of nanowire-based polymer composites is a relatively new field, and the number of publications is still very limited, as summarized in **Table 1** and **Table 2**. Here the key results are tabulated from the articles which investigated the mechanical performance of nanowire-based polymer composites in bulk and thin-film forms, respectively, including elastic modulus (ε), tensile strength

(σ), and flexural strength (σ$_F$). For the simplicity, other properties, such as electrical properties, are omitted in these tables. Readers who are interested in understanding the effect of nanowire addition on the electrical properties of the resulting nanocomposites are referred to these review articles [169, 170]. As shown in **Table 1** and **Table 2**, only a small number of studies have been performed to investigate the effects of nanowires on the mechanical properties of polymeric materials.

Table 1 A summary of studies in mechanical properties of bulk nanowire-based polymer composites

	Filler						
Type	Maximum Loading	Diameter [nm]	Length [μm]	Matrix	Studied Properties	Maximum Change	Ref
SiC	0.125 wt.%	50	<400	Epoxy	σ_F	13%	[171]
SiC	0.5 wt.%	40–200	<100	Epoxy	σ, σ_F	22%, 18%	[172]
SiC	0.5 phr	50	A few	Epoxy	σ_F	34%	[173]
SiC	15 vol.%	50–70	A few	Epoxy	σ	341%	[174]
R. Ni[*]	0.42 wt.%	250	40	PDMS	E	36%	[175]
A. Ni[†]	0.24 wt.%					28%	
Ni	5 vol.%	150	>10	PDMS	E	80%	[30]
Ni	15 vol.%	100	-			30%	
Cu	1 wt.%	-	-	PA6	E	77%	[176]
Cu	4 vol.%	25	1.29	PS	E, σ	28%, 0	[177]
Au	1 wt.%	1.8	<4	PU	σ	50%	[127]
Ag/C	3 wt.%	100–300	<10	Epoxy	σ	34%	[178]
WS$_2$	0.5 wt.%	40–120	2-20	PTT	E, σ	11%, 10%	[179]
WS$_2$	0.5 wt.%	30–150	1-20	PLLA/HA	E, σ	25%, 54%	[180]
MoS$_2$	1 wt.%	<100	<1000	iPP	E, σ, σ_F	40%, 41%, 23%	[181]
Mo$_6$S$_3$I$_6$	2 wt.%	50–600	<100	PA12	E, σ	14%, -3%	[182]
Mo$_6$S$_3$I$_6$	5 wt.%	57	-	PCL	E, σ	0, -20%	[183]
Titanate	2 wt.%	10	-	PA11	E, σ	17%, 0	[184]
Titanate	2 wt.%	10	-	PA11	E, σ	26%, 0	[185]

[*] Randomly distributed Ni nanowires
[†] Aligned Ni nanowires

Table 2 A summary of studies in mechanical properties of nanowire-based polymer composite films

Filler				Matrix	Studied Properties	Maximum Change	Ref
Type	Maximum Loading	Diameter [nm]	Length [μm]				
SiC	0.8 vol.%	~100	<10	PVA	E, σ	90%, 69%	[29]
Al_2O_3	0.4 vol.%	~100	<10			58%, 70%	
Ni	5 vol.%	200	50	P(VDF-TrFE)	σ	75%	[32]
Ag	0.24 vol.%	60	8	PLA	E, σ	34%, 41%	[186]
Ag	1.5 vol.%	-	-	PU	E, σ	57%, -23%	[187]
TiO_2	1 wt.%	9.6	0.118	PS	E, σ	18%, 26%	[129]
Titanate	5 wt.%	9.2	-	PU	E, σ	64%, 50%	[188]
SiO_2	10 wt.%	<50	~1	P(VDF-HFP)	σ	30%	[189]

Among these studies, nanowires were usually incorporated into an epoxy resin or a polymer dispersion by simple mixing. It has been reported that excellent mechanical performance of a nanocomposite can be achieved when a continuous network of filler materials is established within a polymeric matrix, also known as percolation [33, 34, 190, 191]. Nevertheless, only a very few of studies actually synthesized a nanowire-based polymer composite at a loading where percolation of nanowires was achieved, and their mechanical properties were typically not reported [192].

Besides, the major approach to fabricating a nanocomposite is to blend nanofillers into an epoxy resin or a polymer melt, in which no direct interactions among nanofillers can be established. Additionally, some common issues, such as agglomeration and nonuniform dispersion of fillers within a polymeric matrix at high nanowire loadings,

prevent the formation of a filler network within the composites. The occurrence of these issues at high loadings is typically attributed to the increased viscosity of the epoxy resin or the polymer melt, resulting in the increased difficulties in processing, e.g., a powerful tool being required for mixing or nanowires being pre-dispersed in a low-viscosity solvent [117, 134]. An alternative approach, therefore, is to pre-fabricate an interconnected structure of nanofillers and infiltrate a polymer dispersion or an epoxy resin into the structure [192-195]. Several strategies have been attempted to fabricate an intercalated structure of nanowires, so-called nanowire foams. Some of the common approaches include freeze-casting [196-198] and gelation [199-201]. Nevertheless, these techniques are typically time-consuming and very difficult to be scaled up. Therefore, an alternative approach to prefabricate an interconnected nanowire network is of necessity.

Objective of Work

Overall, the main objective of this dissertation was to understand the effects of nanowires on the mechanical properties of nanocomposites, especially the effects of nanowire-epoxy and nanowire-nanowire interactions. Furthermore, the shape memory properties of the nanocomposite were examined, given that the epoxy used herein shows the shape memory effects. In order to achieve this, several sequential goals were proposed. Herein, a technique based on powder metallurgy with a space holder was helpful and useful in achieving these goals.

The first goal was to produce byproduct-free nanowires. It is worth noting that the capability of mass production of nanowires with no byproducts or impurities is a

prerequisite to fabricate a nanocomposite, considering that multiple sets of bulk dumbbell-shape specimens need to be prepared for tensile test. Therefore, an approach to production of byproduct-free nanowires is discussed in the first part of this dissertation. It was based on a previous work from our group in which nanowires were synthesized from metal foils [16]. In the study performed in this dissertation, porous metal foams, which were produced by consolidating mixtures of metal flakes and sacrificial salts, were used as substrates for mass producing nanowires in a byproduct-free manner. Unlike individual metal flakes, these porous metal foams allowed for uniformly heated the metal sources and thereby aided in the uniform production of nanowires of metal compounds.

The second goal was to examine nanowire-epoxy interface and study its effect on the mechanical properties of nanocomposites. Many studies have reported that surface functionalization via various coupling agents is an effective strategy to modify the filler-matrix interface, and the mechanical properties of a nanocomposite can be enhanced by the use of appropriate coupling agents. Nevertheless, most of these studies only claimed that coupling agents can improve interfacial adhesion while no quantitative examination was performed on the interface itself. In this dissertation, different nanowire-epoxy interfaces were created by applying various coupling agents to nanowires. The interactions between nanowires and epoxy monomers were examined to understand the effect of coupling agents on interface as well as the mechanical properties of a nanocomposite.

The third goal was to construct an interconnected structure of nanowires within an epoxy matrix and examine the effect of nanowire-nanowire interaction on the mechanical properties of the resulting nanocomposite. In the majority of studies, nanomaterials are

simply blended with a polymer to fabricate a nanocomposite, in which no direct connection among nanofillers can be established. Considering that the mechanical properties of a nanocomposite can be significantly improved when the filler loading exceeds the percolation threshold, a truly intercalated structure of fillers will enable further improvement. Accordingly, a continuous network of nanowires was synthesized and served as reinforcements for an epoxy. It needs to be emphasized here, similar to the approach adopted to synthesize nanowires in a byproduct-free manner in the first goal, this nanowire network was constructed by assembling nanowires into nanowire foams by powder metallurgy with a space holder. This technique is a powerful method to fabricate porous structures, both at micro- and nano-scales.

CHAPTER II

BYPRODUCT-FREE PRODUCTION OF NANOWIRES[*]

Introduction

Zn_3P_2 is a p-type semiconductor with a direct band gap of 1.5 eV at room temperature, which makes it ideal for applications in thin-film photovoltaic cells [202, 203]. It is composed of elements that are environmentally benign, inexpensive, and abundant in the earth's crust, unlike some of the common commercial photovoltaic materials, e.g., CdTe.

Nanowires are one-dimensional nanomaterials that have been demonstrated to be useful in the fabrication of many types of devices, including solar cells, thermoelectrics, lithium-ion batteries, and sensors [93]. A few groups have reported various approaches to synthesizing Zn_3P_2 nanowires in the laboratory. Shen *et al.* synthesized zigzag-shaped single-crystalline Zn_3P_2 nanowires via a thermochemical method, in which a mixture of ZnS and GaP powders was heated to 1400 °C for 1 hour under a vacuum in a vertical tube furnace [204]. Wu *et al.* produced single crystalline Zn_3P_2 nanowires via a catalyst-free physical evaporation process using zinc grains and InP powders [205]. Besides, our group proposed a facile approach to gram-scale production of Zn_3P_2 nanowires via a direct reaction of Zn foils and phosphorus powders by Chemical Vapor Deposition (CVD) [16].

The work presented here was built upon the previous study by our group, where Zn_3P_2 nanowires were synthesized in large quantities via a self-catalysis scheme on large-area Zn foils [16]. Here, Zn droplets at the tips of the nanowires self-catalyzed the growth of the Zn_3P_2 nanowires. Zn being a component of the materials of the nanowires, it did not lead to contamination of the nanowires. However, as the nanowires were obtained on the top of Zn foils in this process, a tedious scraping procedure needed to be employed to collect nanowires. A logical extension would be the production of nanowires using Zn powders to ensure that all the starting Zn powders could be completely converted into nanowires. However, heating individual Zn microparticles spread in a thin layer format over a substrate in a vacuum chamber is untrivial. This issue leads to the formation of nanowires in a very inefficient manner, and the obtained nanowires always contained associated byproducts and unreacted reactants, namely polycrystalline Zn_3P_2 and unreacted Zn.

With the intent of solving this issue, in this study, the pellets composed of a mixture of Zn and a sacrificial salt, NH_4Cl, were employed as the starting material. The sublimation of NH_4Cl by decomposition in the early stages of the reaction produced highly porous pellets composed of only Zn microparticles. This highly porous structure allowed for inward diffusion of phosphorus as well as outward diffusion of Zn, resulting in the complete conversion of Zn into Zn_3P_2 nanowires. This method produced nanowires without the associated production of any other byproducts such as bulk crystals. Furthermore, no unreacted reactants remained mixed with the nanowire product. This byproduct-free nanowire production thus circumvented the need for collecting nanowires

28

from a mixture of products and reactants after their synthesis. Additionally, NH$_4$Cl also aided in removal of any native oxide layer present on the Zn microparticles that might prevent their reaction with phosphorus vapors. It is essential to note here that although demonstrations were made using Zn$_3$P$_2$ as an example, this procedure can be extended to obtain nanowires of many other binary compound semiconductors.

Experimental Details

Materials

Zn flakes and NH$_4$Cl powders were obtained from Alfa Aesar and Amresco, respectively. Red phosphorus powders were obtained from Alfa Aesar. All the chemicals were used without purification.

Procedure

The procedure for the byproduct-free synthesis of Zn$_3$P$_2$ nanowires from Zn particles comprises of two main steps: (i) the preparation of highly porous Zn pellets, and (ii) CVD-based reaction of the Zn pellets with phosphorus vapors for the formation of Zn$_3$P$_2$ nanowires.

The procedure employed for fabrication of Zn/NH$_4$Cl pellets is described below. Zn flakes and NH$_4$Cl powders were mixed in a weight ratio of 1:4 and grinded using a mortar and pestle. The finely ground powder mixture was consolidated using uniaxial pressing at room temperature and at a pressure of 200 MPa. A custom-built stainless-steel

die with 2 cm in diameter was employed for this purpose, the schematic of which is shown in **Figure 5**. The mass of each pellet obtained, post consolidation, is 1200 mg.
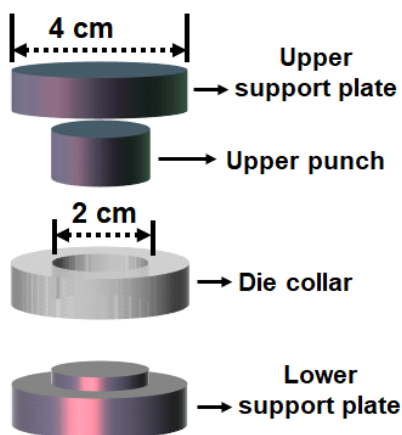
Figure 5 A scheme of the custom-built die set employed for making the pellets composed of Zn and NH₄Cl powders

Figure 6 shows the experimental setup for synthesizing Zn_3P_2 nanowires from the Zn/NH₄Cl pellets. Six consolidated pellets were placed on a glass substrate and placed in Zone 1. An alumina crucible filled with 800 mg red phosphorus powders was placed Zone 3. The CVD chamber was evacuated to a base pressure of 200 mTorr. H_2 carrier gas was then continuously supplied into the chamber at a rate of 100 SCCM, while maintaining the chamber pressure at 600 mTorr. **Table 3** shows the temperature profiles of the three heating zones. Zone 1 and zone 2 were heated from room temperature to 410 °C in 5 minutes and held at 410 °C for a duration of 40 minutes. Zone 3 was heated to 485 °C in 25 minutes and kept at 485 °C for 20 minutes. The heating ramp rate of zone 3 was intentionally maintained at a lower rate than those of zones 1 and 2. This ensured that Zn pellets were ready for reaction with the incoming phosphorus vapors at 410 °C by the time

the phosphorus supply was stabilized. Following the reaction, the system was naturally cooled down to room temperature.
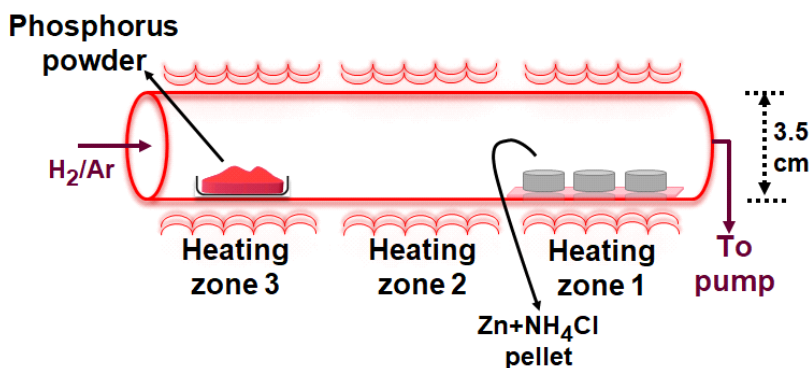
Figure 6 A scheme of the CVD setup for the production of Zn₃P₂ nanowires from Zn/NH₄Cl pellets

Table 3 Experimental conditions for synthesis of Zn₃P₂ nanowires from Zn/NH₄Cl pellets

	Zone 1	Zone 2	Zone 3
Temperature [°C]	410	410	485
Preheating time [min]	10	10	25
Reaction time [min]	35	35	20

<u>Characterization</u>

The morphology of Zn₃P₂ nanowires was characterized by scanning electron microscopy (SEM). The crystallinity and the growth direction of the nanowires were characterized by transmission electron microscopy (TEM). X-ray diffraction (XRD) was performed to confirm the lattice parameters and chemical composition of the nanowires.

Results

<u>Characterization of Porous Zn Pellets</u>

Figure 7 shows the representative scanning electron micrograph of the highly porous structure of the as-synthesized Zn pellet after NH_4Cl was removed by thermal evaporation under vacuum (namely, without a reaction with phosphorus vapors). These pores and channels within the Zn pellets facilitated diffusion of phosphorus vapors into the Zn pellet and allowed phosphorus vapors to react with the whole substrate.
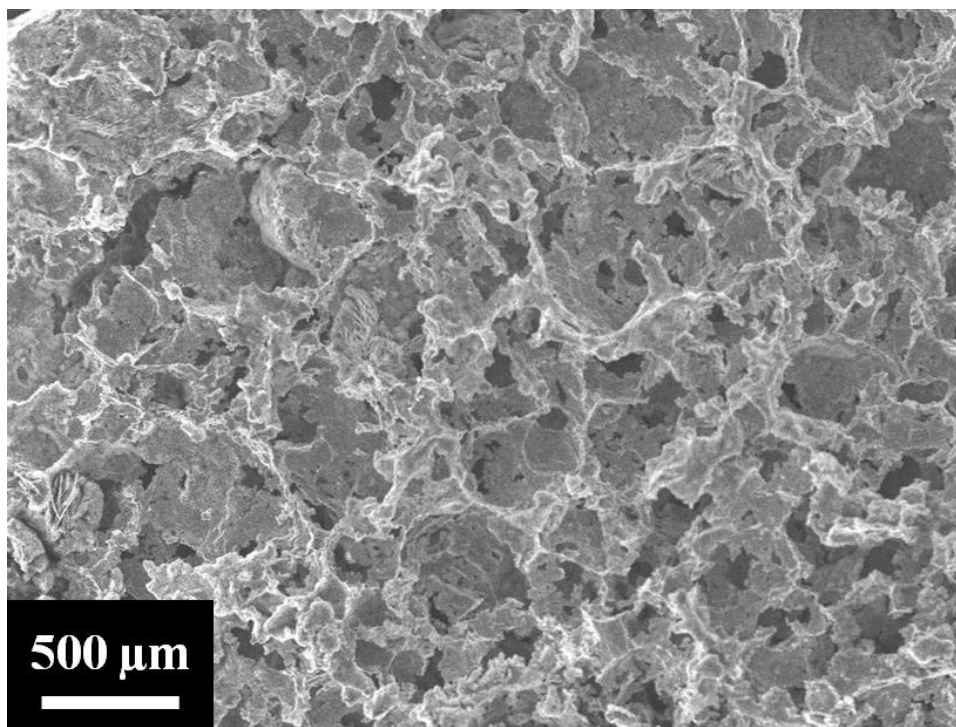
Figure 7 A scanning electron micrograph of a highly porous Zn skeleton obtained after NH4Cl was removed by sublimation at 350 °C

Characterization of Zn_3P_2 Nanowires

A photograph of 2 cm-diameter, 2 mm-thick pellets obtained by consolidating a mixture of Zn flakes and NH_4Cl powders are presented in **Figure 8(a)**. These shiny silver pellets turned orange upon their reaction with phosphorus vapors via CVD, as shown in **Figure 8(b)**. After crushing the orange pellets using a mortar and pestle, brown powders were obtained (**Figure 8(c)**).
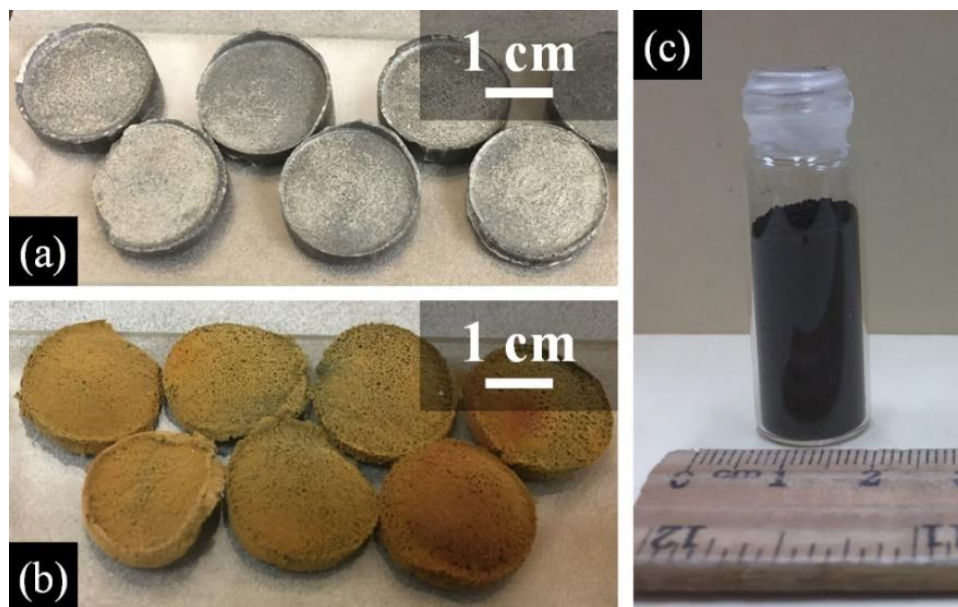
Figure 8 Representative photographs of (a) Zn/NH_4Cl pellets prepared by uniaxial pressing, (b) the pellets composed of Zn_3P_2 nanowires obtained by a reaction with phosphorus vapors, and (c) Zn_3P_2 nanowire powders obtained by gently crushing the pellets with a mortar and pestle

The SEM analysis of the surfaces of the pellets indicated that they were composed of only nanowires, 90–120 nm in diameter and few tens of microns long, as shown in **Figure 9(a)-(c)**. **Figure 9(d)-(f)** show the scanning electron micrographs of the inside

regions of the pellets (obtained by carefully stripping the top layers) and also indicated that they were composed of nanowires. It is worthwhile to note here that although there appear to be three-dimensional bulk crystals underneath the nanowires in the low magnification images, a closer examination at higher magnification showed that these were nanowire agglomerates and composed exclusively of nanowires. An XRD analysis of the nanowires confirmed that they were composed of tetragonal Zn_3P_2 with lattice parameters of a = 8.095 Å and c = 11.47 Å. No other impurities such as Zn, ZnO, or NH_4Cl were detected (**Figure 9(g)**). As postulated above, the reaction between red phosphorus and the pellets composed of consolidated mixtures of Zn and NH_4Cl led to the formation of Zn_3P_2 nanowires. The reaction was complete, and in most of the cases no unreacted Zn or polycrystalline Zn_3P_2 byproduct was observed. nanowires were observed throughout the pellet. TEM analysis of a nanowire (**Figure 9(h) and (i)**) indicated that it is single-crystalline with a growth direction of [110]. Growth along the [110] direction is typical in self-catalytic schemes for nanowire synthesis [16, 206].
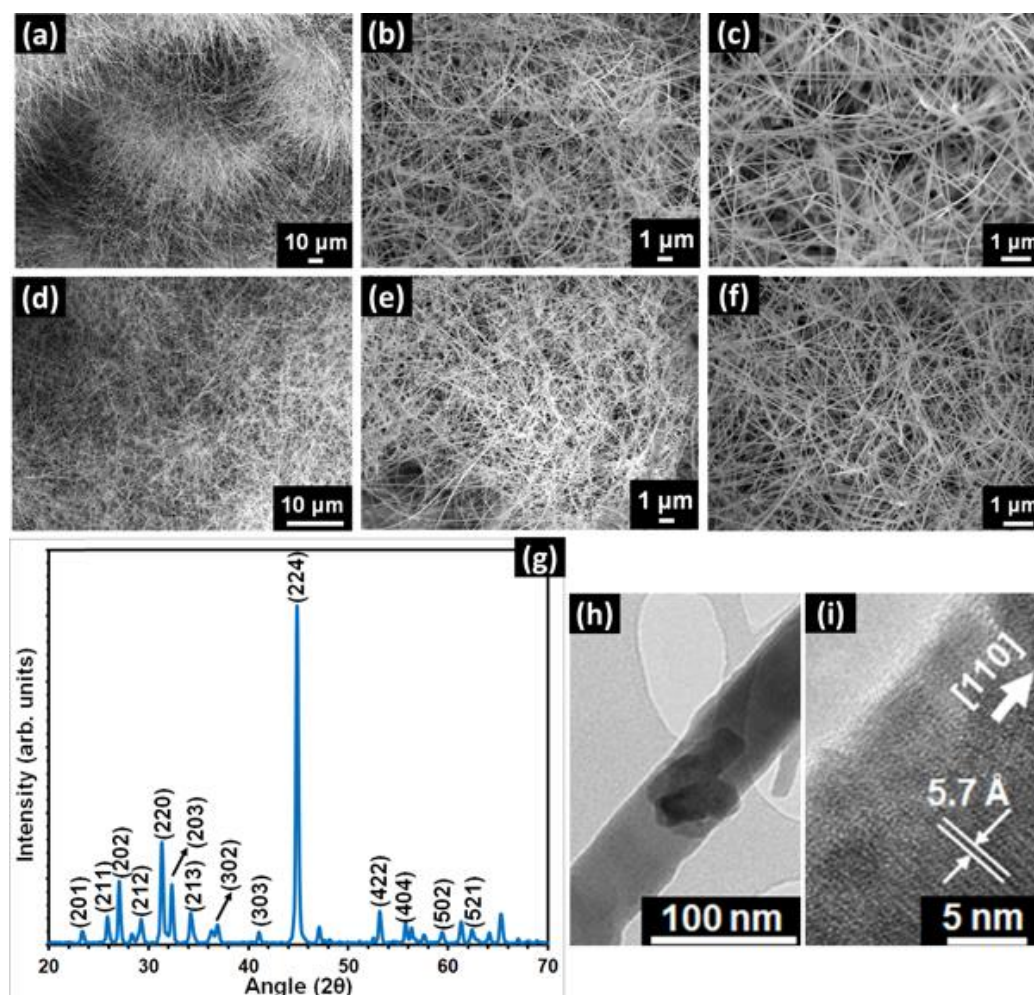
Figure 9 (a)-(f) Scanning electron micrographs of the as-obtained Zn₃P₂ nanowires. Images (a)-(c) are those of nanowires observed on the surfaces of the pellet, while (d)-(f) represent those observed on the inside of the pellet. (g) An XRD spectrum of the nanowires produced using CVD. (h) Low- and (i) high-resolution transmission electron micrographs of a Zn₃P₂ nanowire

Discussion

Selection of Sacrificial Salt

The criteria for selecting an appropriate sacrificial salt are, ideally, (1) removal of the sacrificial salt does not involve other chemicals and (2) no contaminations are

introduced into the system after they are removed. Based on the criteria, NH_4Cl was chosen for the sacrificial salt in this study, given that it decomposes completely into HCl and NH_3 gases at 338 °C. Given that the reaction between Zn and phosphorus vapors takes place at 410 °C, a skeleton of Zn can be easily produced by heating a pellet for a period of time at a preheating stage.

The ratio of Zn to NH_4Cl is an important factor in this study, considering that the porosity of a pellet is dependent on the amount of NH_4Cl subliming from it. With a low fraction of NH_4Cl, the pellet does not have enough pores for phosphorus vapors to diffuse through, which results in the inner region of the pellet to be not fully reacted. On the other hand, if the fraction of NH_4Cl is too high, the pellet does not have enough strength to maintain its shape. In this study, a weight ratio of 1 to 4 was chosen, since the pellets with lower ratios started to shrink or even collapse after the reaction.

Growth Mechanism of Nanowire Pellets

Major steps involved in the conversion of Zn pellets into Zn_3P_2 nanowires are depicted in **Figure 10**. In the pre-heating stage of the reaction, NH_4Cl powders dissociate into NH_3 and HCl vapors and sublime [207], leaving behind highly porous Zn pellets for reaction with phosphorus vapors. Unlike Zn particles supported on the quartz substrate, these highly porous pellets are thermally conducting in nature and ensure that they are sufficiently thermally activated for a reaction with phosphorus vapors. The HCl formed upon decomposition of NH_4Cl also aids in removing native oxide formed on Zn and makes it highly reactive [16, 206]. Furthermore, the high porosity of the pellets allows for the

36

inward diffusion of phosphorus vapors and outward diffusion of Zn, leading to the formation of nanowires throughout the pellets.
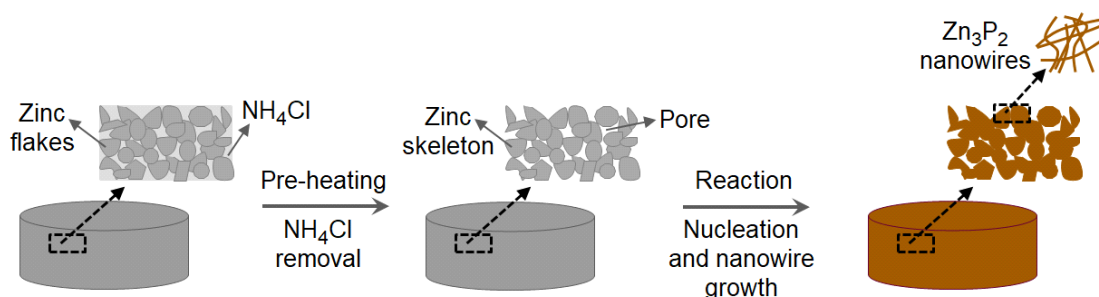
Figure 10 A scheme of the major steps involved in the formation of Zn₃P₂ nanowires in this study. Porous Zn pellets, formed upon decomposition and sublimation of NH₄Cl powders, allow for the outward diffusion of Zn and inward diffusion of phosphorus, leading to the formation of nanowires all throughout

The formation of Zn_3P_2 nanowires is believed to occur by a self-catalysis scheme, as illustrated in detail in our previous publications [16, 206, 208]. The formation of Zn_3P_2 nuclei, followed by selective wetting of the nuclei with Zn and the formation of Zn droplets, and finally liquid phase epitaxy through the Zn droplets leads to the formation of Zn_3P_2 nanowires.

Thermal Conductivity of Porous Pellets

Data discussing the thermal conductivity of cellular foams (porous foams) could be used to confirm that the pellets have higher thermal conductivities than those of the Zn powders supported on glass substrates. Thermal conductivities of cellular foams, κ, can be approximated using the following relationship:

$$\kappa = \kappa_S \left(\frac{\rho}{\rho_S}\right)^n \quad [209]$$

Here, κ_S is the thermal conductivity of solid Zn, ρ and ρ_S are respectively the densities of the cellular Zn and the solid Zn, and n is an exponent. n is normally expected to be in the 1.65–1.8 range [209], and it was reported to be about 1.54 for Zn [210]. As the densities of the porous pellets are higher than those of Zn micropowders, it can be deduced that Zn pellets have higher thermal conductivities. Moreover, the interconnections between Zn in the pellets aid in enhancing thermal conductivities of the porous Zn pellets, unlike Zn micropowders supported on glass substrates.

It is entirely possible to obtain the same result if another method of making highly porous Zn pellets whose surface is devoid of native oxide is employed. For example, Zn foams (made without any additives) are useful for the production of the nanowires. However, they have to be cleaned off surface oxides before they could be reacted with phosphorus for the formation of Zn_3P_2 nanowires.

Conclusions

In conclusions, a novel approach to synthesizing byproduct-free semiconducting nanowires was developed in this study. NH_4Cl was chosen for the sacrificial salt because of the ease of its removal through a sublimation process. The as-grown Zn_3P_2 nanowires were observed through the entire pellets, with diameters of 90–120 nm and lengths of a few tens of µm. As one of the advantages, this method introduces no foreign catalysts, e.g., Au or In, nor bulk substrate through post-synthesis processing. The scale of production can easily be increased by using large sheets of such a porous structure instead

38

of small pellets. This technique can be extended and allowed for synthesis of other type of semiconducting nanowires in a byproduct-free manner. For instance, TiO_2 nanowires, which were studied in the next chapters in this dissertation, were produced by exposing titanium salts to oxygen plasma [51]; Similar TiO_2 nanowires can be synthesized in a byproduct-free manner through the approach developed in this chapter.

CHAPTER III

FABRICATION OF ZN_3P_2 NANOWIRE-EPOXY COMPOSITES

<u>Introduction</u>

Epoxy is a common thermosetting polymer that is extensively used in many applications, including coatings, adhesives, and structural materials [23]. However, because of its relatively low mechanical strength and stiffness, the use of epoxy for high-strength structural components, such as in aerospace or automobile industry, is limited. In order to enhance its mechanical properties, its composites are typically fabricated, one of the most common types being microfiber-reinforced epoxy composites. Recently, a variety of nanoscale materials have been studied as filler materials, such as nanoclays [211], carbon nanotubes (CNTs) [212], and silica nanoparticles [213], given that a small fraction of nanofillers are able to improve the performance of epoxy without having a significant negative impact on its processability and density [214]. Nanowires have also attracted great attention in the field of nanocomposites because of nanowires' high aspect ratio and surface-area-to-volume ratio [134].

In this study, firstly, an epoxy composite embedded with Zn_3P_2 nanowires was fabricated and its mechanical properties were examined. Epoxy is a common thermosetting polymer widely used in many applications, including coatings, adhesives, insulators for electronic devices, and fiber-reinforced composites. It is usually fabricated by crosslinking of two types of monomers with epoxide and amine functional groups, respectively. In order to enhance its mechanical strength, a variety of materials have been

added to an epoxy resin as filler materials, such as carbon black [215, 216], nanoclays [211, 217], silica nanoparticles [213, 218], and CNTs [212, 219]. In a previous study, we successfully mass produced Zn_3P_2 nanowires [16]. It was found that Zn_3P_2 nanowires with diameters less than 50 nm were mechanically flexible and able to elastically recover to the original shape after multiple bending at large angles [220]. Therefore, Zn_3P_2 nanowires have great potential in reinforcing an epoxy as filler materials.

Secondly, to understand the effect of interface between nanowires and an epoxy matrix on the mechanical properties of the composites, 4-aminothiophenol (4ATP) and 4-tert-butylthiophenol (4tBTP) were used to functionalize the nanowires. Here the thiol and amine groups from 4ATP are expected to bind to Zn_3P_2 nanowires and epoxy, respectively, to generate a strong interface. On the other hand, tert-butyl groups from 4tBTP are expected to hinder any bonding between nanowires and epoxy, resulting in a poor interface. Therefore, a systematic approach involving functionalization of Zn_3P_2 nanowires with various coupling agents and their ultimate effect on the mechanical properties of Zn_3P_2 nanowire-based composites has also been explored in this work.

Experimental Details

Materials

EPON 826, neopentyl glycol diglycidyl ether (NGDE), and poly(propylene glycol) bis(2-aminopropyl ether) (known as Jeffamine D230) were purchased from Hexion, TCI America, and Sigma-Aldrich, respectively. These three monomers were thermally

crosslinked to form epoxy. A sheet of Zn metal ($\geq$99.98% metals basis and 0.25 mm thickness) and red phosphorus powders were obtained from Alfa Aesar. The Zn sheet and red phosphorus power were used to synthesize the Zn_3P_2 nanowires. Commercially-available Zn_3P_2 powder, used as a reference in Fourier-transform Infrared (FTIR) analysis, was obtained from Sigma Aldrich. In order to modify the surface characteristics of Zn_3P_2 nanowires, 4ATP and 4tBTP were obtained from TCI America and Alfa Aesar, respectively. All chemicals were used as received.

Procedure

Zn_3P_2 nanowires were synthesized by chemical vapor deposition (CVD), as previously reported by our laboratory [16]. Briefly, a roll of Zn sheet (6×30 cm) was washed twice with deionized water, acetone, and ethanol, respectively, followed by etching by HCl to remove the native oxide layer. The Zn roll was then placed at the downstream in a CVD reactor, while an alumina crucible containing 600 mg red phosphorus powders was placed at the upstream. The pressure in the CVD chamber was reduced to 200 mTorr by a rotary pump, and 20 SCCM hydrogen carrier gas was introduced into the system. The temperatures of the Zn roll and red phosphorus powders were ramped up to 410 and 485 °C in 10 minutes, respectively. After 30 minutes, the reactor was shut off, allowing the CVD reactor to cool down to room temperature naturally. Subsequently, the nanowire powders were scraped off from the Zn substrate by razor blade and gently grinded by a mortar and pestle to break up large agglomerates.

The functionalization of Zn_3P_2 nanowires with 4ATP or 4tBTP was performed *in situ* via a vapor-phase route. After synthesis of Zn_3P_2 nanowires was completed, a vapor of 4ATP or 4tBTP was supplied into the CVD reactor through a bubbler when the substrate was cooled down to 80 °C. The bubbler was maintained at a temperature of 120 °C throughout the process. This *in-situ* functionalization not only modified the surface characteristics of nanowires, but also prevented oxide formation on the nanowires.

The epoxy was fabricated by an *in-situ* polymerization approach reported by Xie and Rousseau [221, 222]. Firstly, EPON 826, NGDE, and Jeffamine D230 were fully mixed at a mole ratio of 3:1:2. Then the resin was casted into a mold and degassed in a vacuum chamber at 100 mTorr for 120 minutes. Finally, the resin was polymerized and cured at 100 °C for 90 minutes and 130 °C for 60 minutes in an oven, respectively. For the composite specimens, before mixed with EPON 826 and NGDE, nanowires were dispersed in Jeffamine D230 by magnetic stirring and sonication, followed by the rest of the procedure. In this study, 0.1, 0.5, and 1 wt.% unfunctionalized Zn_3P_2 nanowires (u-NWs), 0.1, 0.5, 1, and 2 wt.% 4ATP-functionalized Zn_3P_2 nanowires, and 1 wt.% 4tBTP-functionalized Zn_3P_2 nanowires were added to the epoxy resin. The samples examined in this study have been listed in **Table 4**.

Table 4 A list of all the epoxy and composite samples prepared and characterized in this study

Sample Name	Nanowire Type	Nanowire Loading
Epoxy	-	-
U0.1	Unfunctionalized	0.1 wt.%
U0.5	Unfunctionalized	0.5 wt.%
U1	Unfunctionalized	1 wt.%
A0.1	4ATP-functionalized	0.1 wt.%
A0.5	4ATP-functionalized	0.5 wt.%
A1	4ATP-functionalized	1 wt.%
A2	4ATP-functionalized	2 wt.%
B1	4tBTP-functionalized	1 wt.%

Characterization

The morphology of Zn_3P_2 nanowires was observed by Scanning Electron Microscopy (SEM). Fourier-transform Infrared Spectroscopy (FTIR) was performed under dry nitrogen purging using Nicolet IR100 (Thermo Fisher Scientific) to confirm that the nanowires were successfully functionalized with 4ATP or 4tBTP.

Thermal stability of the samples was studied by Thermogravimetric Analysis (TGA) using TGA Q50 (TA instruments). All the measurements were carried out at a heating rate of 5 °C/min from room temperature to 600 °C under nitrogen gas flow. Differential Scanning Calorimetry (DSC) was carried out to examine the crystallinity and glass transition temperature (T_g) of the samples. All the experiments were performed

44

under nitrogen gas flow using DSC Q200 (TA instruments). The specimens were heated/cooled/heated at a heating/cooling rate of 10 °C/min, and the DSC results from the 2nd (cooling) and 3rd (heating) cycles are reported. T_g was obtained from the saddle point of a DSC curve. The Dynamic Mechanical Analysis (DMA) experiments were performed using a DMA 1 (Mettler Toledo) in a tension mode. The thickness of the specimens was 1.2-1.4 mm. All the measurements were made at a heating rate of 3 °C/min, a frequency of 1 Hz, and a strain of 8 μm. The glass transition was determined from the maxima of a tanδ curve with respect to temperature, where tanδ is the ratio of loss and storage moduli. These two moduli represent the elastic and viscous portions of the material, respectively.

Finally, the mechanical properties of the samples were studied by tensile test using Instron 5567, in which dumbbell-shape specimens (ASTM D638-V) were pulled at a strain rate of 1 mm/min with a span of 25.4 mm at room temperature.

Results

Characterization of Zn_3P_2 Nanowires

A scanning electron micrograph that represents the morphology of Zn_3P_2 nanowires used in this study is displayed in **Figure 11**. Typically, most of these nanowires had diameters of 30–50 nm and lengths of tens of micrometers. Our previous study confirmed that the chemical composition of the nanowires is Zn_3P_2 (through X-ray Diffraction (XRD analysis), and that the nanowires are single-crystalline in nature (through Transmission Electron Microscopy (TEM) characterization) [16, 165].
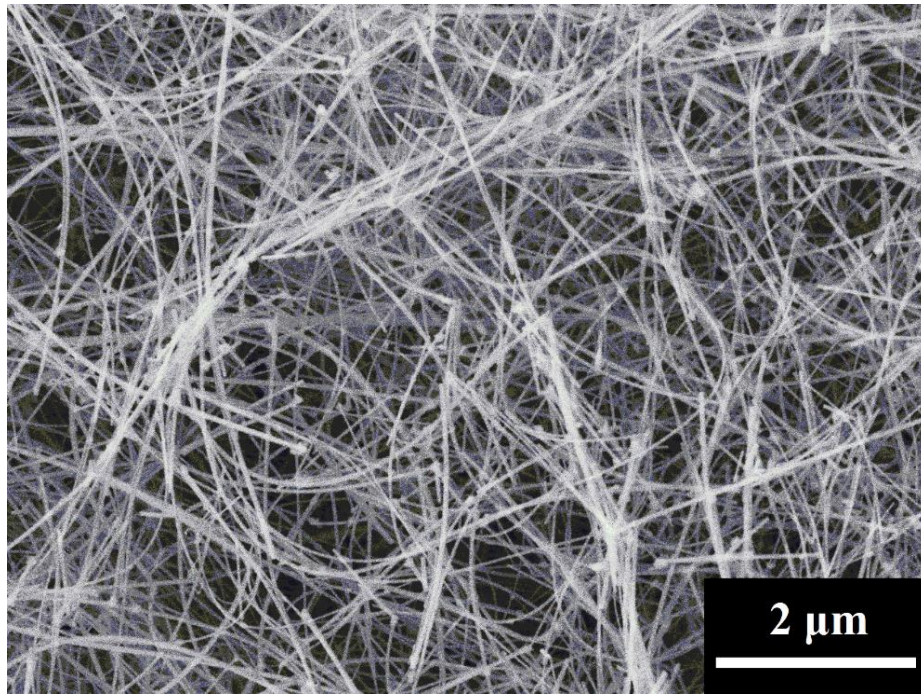
Figure 11 A scanning electron micrograph of Zn$_3$P$_2$ nanowires used in this study

Figure 12(a)-(c) show the chemical structures of three monomer components of epoxy used in this study. The polymerization of this epoxy involves a reaction between two parts of epoxides (from EPON 826 and NGDE) and one part of amine (from Jeffamine D230) to form a continuous three-dimensional network. As shown in **Figure 12(d)**, 4ATP allows nanowires and the epoxy network to be covalently bonded and thus improves nanowire-matrix interfacial adhesion, while 4tBTP hinders bond formation by terminating the nanowires with inactive tert-butyl groups, resulting in poor interfacial adhesion.
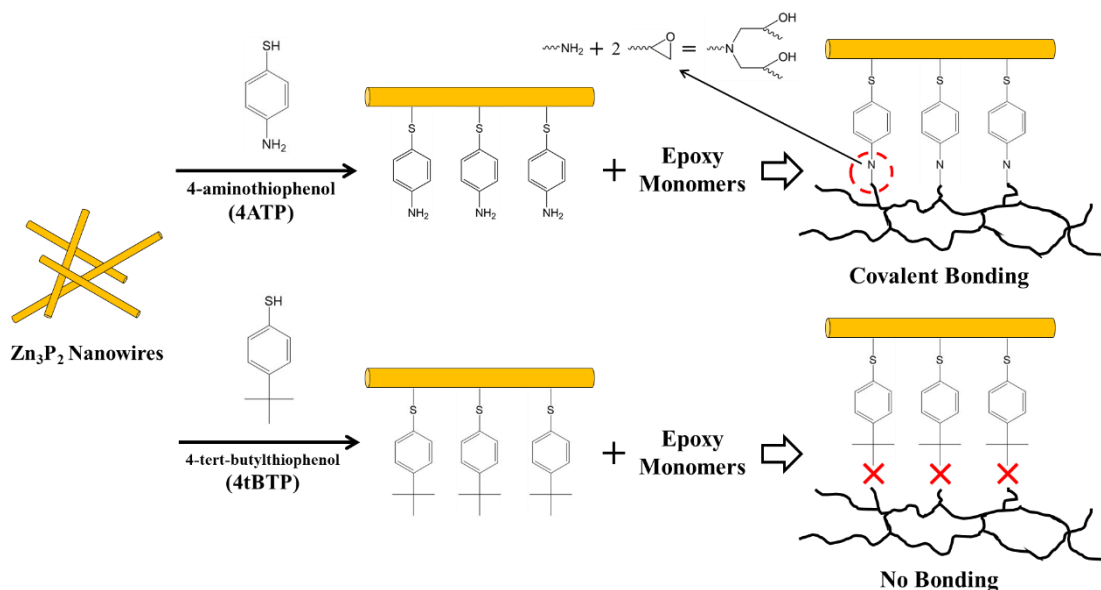
Figure 12 Chemical structures of the epoxy monomers used in this study: (a) EPON 826 (n = 0.085), (b) NGDE, and (c) Jeffamine D230 (n = 2.5). (d) A scheme of the effect of coupling agents on nanowire-matrix interface. 4ATP forms covalent bonds and improves interfacial adhesion with the epoxy network, whereas 4tBTP prevents any bond formation

Figure 13(a) shows the FTIR spectrum of bulk Zn_3P_2 powders. Several peaks at 1100–900 and 700–500 cm^{-1} were observed because of the presence of PO_4^{3-} groups from $Zn_3(PO_4)_2$ [223, 224] (the oxide layer of Zn_3P_2 [16]). A broad peak at 3500–3000 cm^{-1} corresponds to O-H stretching from hydroxyl groups and absorbed water, and a peak at 1625 cm^{-1} is attributed to the bending mode of absorbed water. Given that $Zn_3(PO_4)_2$ typically occurs as a hydrate ($Zn_3(PO_4)_2 \cdot 4H_2O$), the hydroxyl and water peaks were probably originated from this oxide layer of Zn_3P_2 nanowires. No change in FTIR spectrum was observed for Zn_3P_2 nanowires compared to bulk Zn_3P_2 (**Figure 13(b)**).

Figure 13(d) shows the FTIR spectrum of 4ATP-functionalized nanowires, in which the features at 1600 and 1250 cm^{-1} correspond to N-H bending and C-N stretching,

47

respectively, proving the presence of amine groups on 4ATP-functionalized nanowires [225]. Peaks for aryl C-C stretching and C-H bending out of plane of the para-disubstituted benzene rings were observed at around 1500 and 810 cm⁻¹, respectively. For 4tBTP-functionalized nanowires, as shown in **Figure 13(c)**, strong peaks appeared at 3000–2800 cm⁻¹ corresponding to C-H stretching from tert-butyl functional groups. It is worth noting that, because of the large number of C-H bonds from tert-butyl groups, the intensities of C-H peaks were much stronger than those from 4ATP-functionalized nanowires.
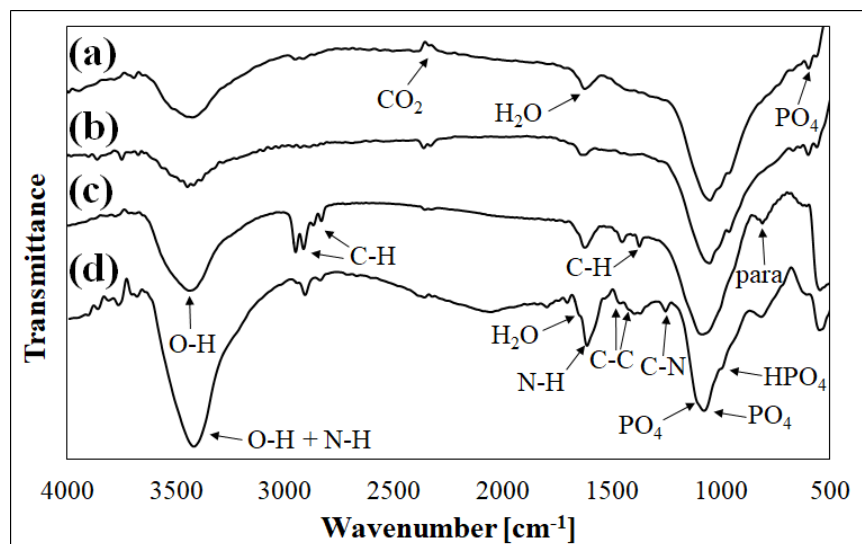
Figure 13 FTIR spectra of (a) bulk Zn_3P_2, (b) unfunctionalized nanowires, (c) 4tBTP-functionalized nanowires, and (d) 4ATP-functionalized nanowires

Based on an X-ray photoelectron spectroscopy (XPS) analysis from our previous study, it was concluded that thiol molecules directly attached to Zn atoms of Zn_3P_2 nanowires by thiolate bonds [16]. It was also reported from other groups that thiolation on

InP and GaP takes place in a similar manner, where sulfur atoms bind to indium or gallium atoms through the formation of thiolate bonds [226].

Physical and Thermal Properties of Nanocomposites

Figure 14(a) and (b) illustrate the typical DSC curves of the epoxy and composite samples at cooling and subsequent heating cycles, respectively. No crystallization or melting processes were observed for all the specimens. This is because epoxy is an amorphous material by nature, and incorporation of fillers makes this material system remains amorphous. No filler-induced crystallization was observed. It was also found that addition of 4ATP-functionalized nanowires into this epoxy had no impact on T_g, as tabulated in **Table 5**.

Typical storage modulus (E') and tanδ curves obtained from the DMA measurements are plotted in **Figure 14(c)**, and the E' and T_g values of each sample are summarized in **Table 5**. No significant change in T_g was observed by the addition of 4ATP-functionalized nanowires into the epoxy, which was in agreement with the DSC characterization. It was also observed that the storage modulus at lower temperatures (glassy region) increased by embedding 4ATP-functionalized nanowires into the epoxy. This increase in storage modulus can be attributed to the strong chemical boding between the epoxy matrix and nanowire fillers established by a coupling agent, 4ATP, which results in an effective load transfer from a weaker matrix to a stronger fillers [147, 227]. This result is also confirmed by tensile test performed in this study.

Figure 14(d) shows a typical TGA thermograph of the epoxy and composites. The curves of the composites with 0.1 wt.% and 0.5 wt.% 4ATP-functionalized nanowires are omitted from this figure for clarity. The onset temperature at which 10% degradation occurs ($T_{10\%}$), onset temperature at which 80% degradation occurs ($T_{80\%}$), and the residual material remaining at 600 °C are given in **Table 5**. Based on the TGA data, it was found that, although 4ATP-functionalized nanowires didn't change the thermal stability of the epoxy at lower temperatures (~300 °C), they were able to prevent severe decomposition at higher temperatures, as higher residual weights were obtained for the composites reinforced by 4ATP-functionalized nanowires compared to that of epoxy. It was also observed that the thermal stability is enhanced with increasing nanowire loadings. This result might be attributed to a strong nanowire-epoxy interfacial adhesion, where 4ATP-functionalized nanowires helped maintain the structural integrity of the composites at higher temperatures [180]. Furthermore, it suggests that 4ATP-functionalized nanowires might also help dissipate heat more evenly within the matrix and prevent severe local heating, leading to improvement in thermal stability [179, 228].
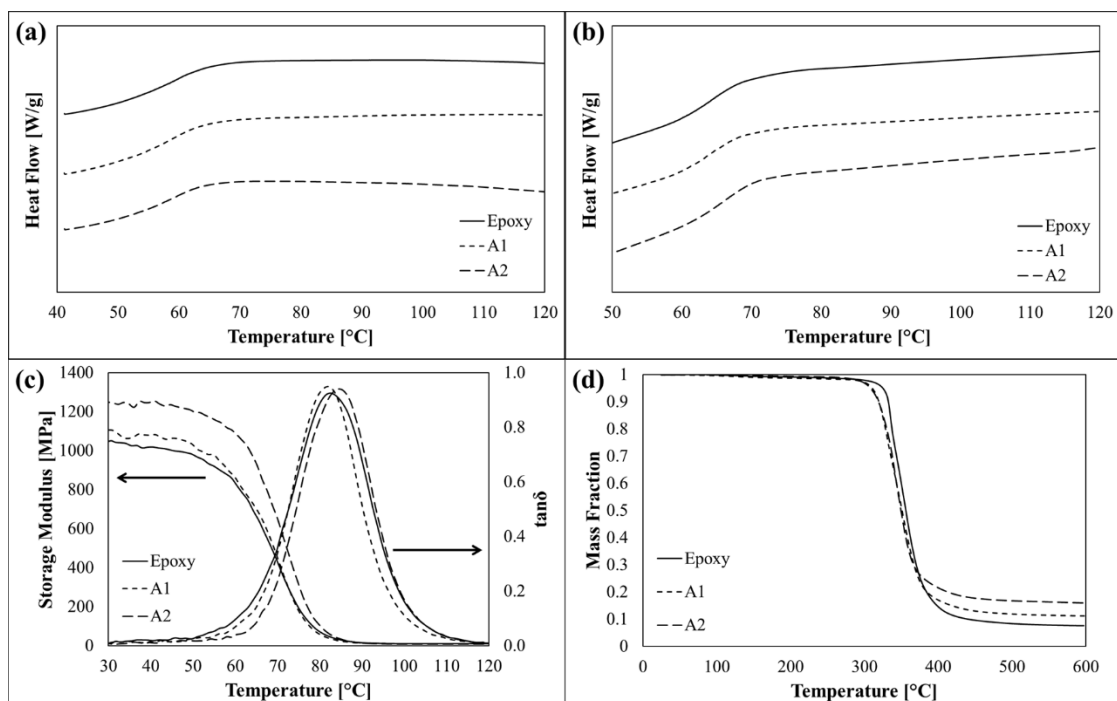
Figure 14 DSC thermograms of the epoxy and the composites during a (a) cooling cycle and (b) a subsequent heating cycle. Water absorbed by the epoxy was removed during the first heating cycle. (c) The storage modulus and tanδ curves with respect to the temperature of the epoxy and the composites measured by DMA. (d) A TGA thermogram of the epoxy and the composites

Table 5 A summary of TGA, DSC, and DMA data for the epoxy and the composites reinforced by 4ATP-functionalized nanowires

Sample	TGA			DSC	DMA	
	$T_{10\%}$ [°C]	$T_{80\%}$ [°C]	Residual Weight	T_g [°C]	E' at 35°C [MPa]	T_g [°C]
Epoxy	332	384	7.7%	64.6	1029	82.7
A1	319	386	11.3%	63.5	1089	82.2
A2	319	414	16.1%	65.6	1247	84.7

Shape Memory Properties of Nanocomposites

        The epoxy used in this study exhibits shape memory effects [221, 222]. In order to confirm that addition of nanowires does not deteriorate shape memory properties of the epoxy, a simple shape recovery experiment was performed in hot water. Two stripes of the epoxy and A2, with a dimension of 1.27×5.08 mm (**Figure 15(a)**), were first bent at a large angle once they became rubbery upon immersion in hot water at ~85 °C (**Figure 15(b))**. Then the shape of these two stripes was fixed by immersing them in cold water maintained at room temperature. They were then dropped in hot water again to initiate shape recovery. **Figure 15(c)-(h)** show a series of snapshots of shape recovery process, in which both bent stripes recovered back to the original form quickly. Therefore, both epoxy and composite samples were capable of recovering back to their original shape when they were thermally activated. This suggests that the addition of Zn_3P_2 nanowires didn't deteriorate the shape memory properties of the epoxy. Based on DMA and DSC, it was confirmed that T_g of epoxy didn't change at low nanowire loadings, and therefore the switching temperature to induce shape recovery was the same. Furthermore, given that storage modulus was improved by the addition of 4ATP-functionalized nanowires, the recovery stress (the stress generated during shape recovery process) may have improved.
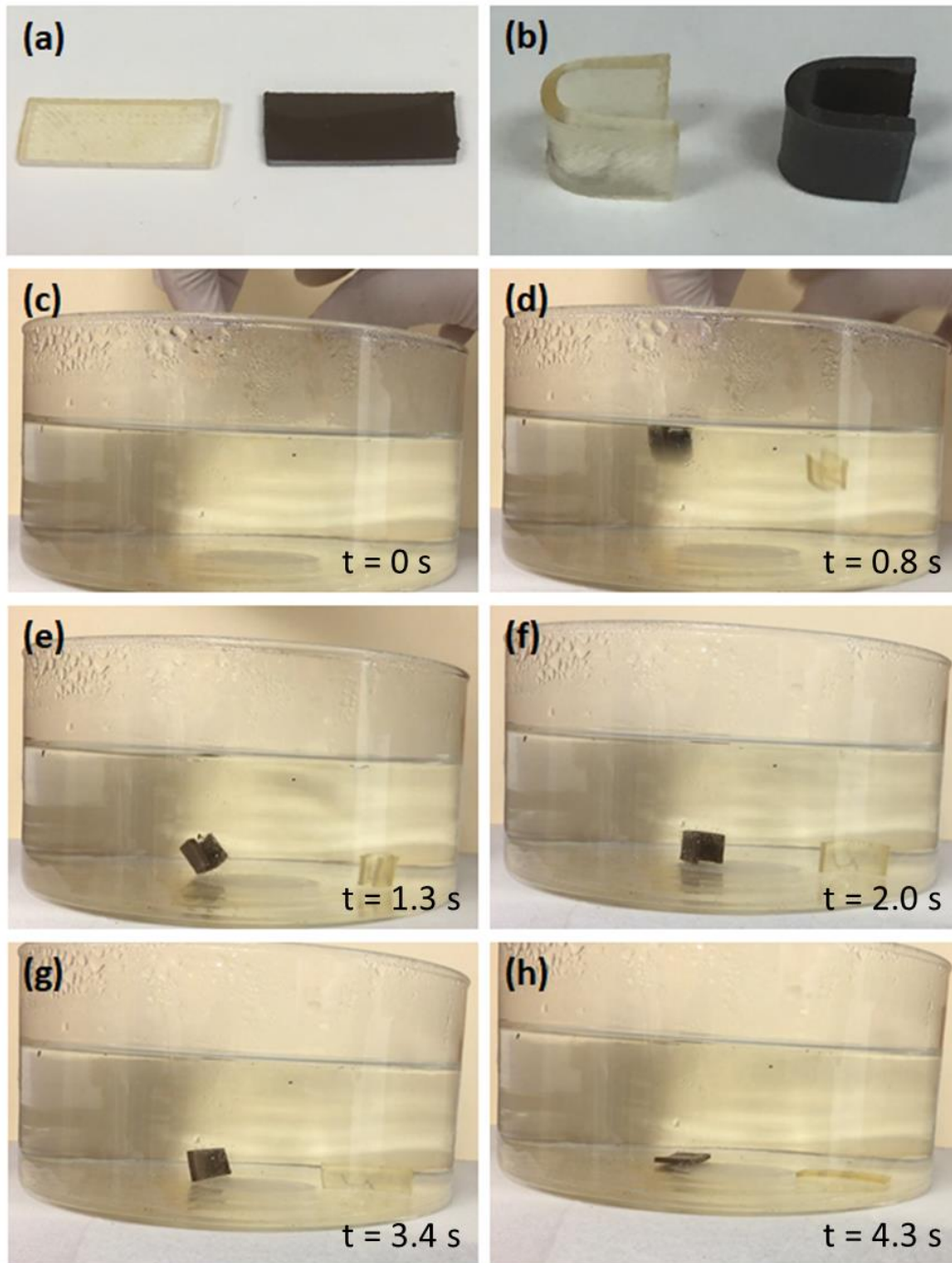
Figure 15 Photographs of (a) the permanent shape and (b) the temporary shape of the epoxy and the composite. Both stripes were bent at a very large angle. (c)-(h) A series of snapshots of shape recovery process. Both samples recovered back to the original shape quickly, no significant differences being observed in the recovery time

Mechanical Properties of Nanocomposites

The typical stress-strain curves for epoxy and composite samples are shown in **Figure 16**. **Table 6** also summarizes the experimental results obtained from the tensile test. It was found that unfunctionalized nanowires were unable to improve either tensile strength or elastic modulus at any nanowire loading; in fact, although the differences among these values were not statistically significant enough because of their large standard deviations, the elastic modulus seem to be reduced with respect to nanowire loading. These measurements were performed only at room temperature.
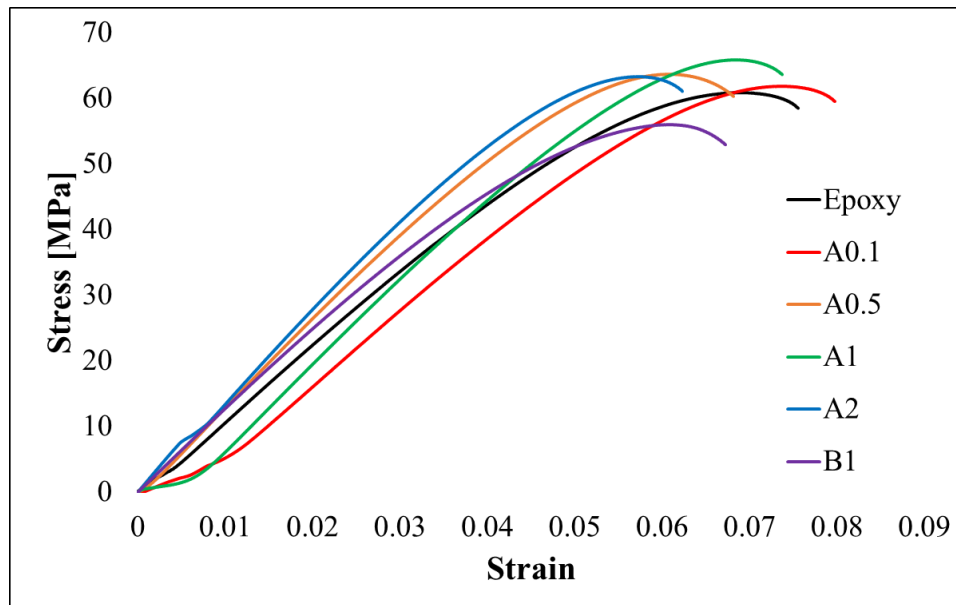
Figure 16 Typical stress-strain curves of the epoxy and the composite embedded with functionalized nanowires

Table 6 Tensile properties of the epoxy and the composite samples

Sample	Tensile Strength [MPa]	Change	Elastic Modulus [GPa]	Change
Epoxy	60.0±1.3	-	1.12±0.06	-
U0.1	57.5±2.1	-4.13%	1.08±0.04	-3.76%
U0.5	59.9±3.2	-0.13%	1.09±0.10	-2.10%
U1	59.4±1.4	-0.96%	1.06±0.06	-5.27%
A0.1	61.8±1.8	+3.04%	1.13±0.07	+1.15%
A0.5	63.7±1.0	+6.19%	1.22±0.03	+9.10%
A1	65.0±2.0	+8.35%	1.26±0.07	+12.48%
A2	62.6±4.0	+4.39%	1.37±0.02	+22.98%
B1	56.6±0.7	-5.72%	1.04±0.03	-6.56%

In the case of the composites reinforced by 4ATP-functionalized nanowires, the addition of 4ATP-functionalized nanowires enhanced elastic modulus, even with a very small nanowire loading. At 2 wt.%, the elastic modulus of the composite was increased by 23% compared to the epoxy sample. For tensile strength, the maximum improvement was obtained at 1 wt.% instead of 2 wt.%, probably due to nanowire agglomeration that occurs at higher loadings [173, 186]. These results also indicate that nanowires are capable of improving the mechanical properties of an epoxy when good interfacial adhesion is achieved and when nanowire agglomeration is prevented. Agglomeration is possible even at loadings of 2 wt.%, if the matrix is highly viscous in nature [117, 134].

On the other hand, with a poorer interfacial adhesion, the addition of 1 wt.% 4tBTP-functionalized nanowires resulted in both lower tensile strength and elastic

modulus. This validated the hypothesis that interfacial adhesion plays a significant role in reinforcement. This type of results (negative impacts of fillers on mechanical properties), although not very commom, has been observed by a few studies [229-233]. For example, Dányádi *et al.* fabricated a polypropylene composite filled with wood flour, which was benzylated to reduce its water absorption, and yet found that benzylation of filler materials led to considerably poor filler-polymer interfacial interactions and thereby reduction in both elastic modulus and tensile strength [231].

Discussion

Interactions between Zn_3P_2 Nanowires and Epoxy

Reinforcement of polymeric materials can only be achieved when an external load is effectively distributed and transferred from a matrix to inorganic filler materials. Therefore, nanowires should not be simply dispersed into an epoxy during preparation, given that organic and inorganic materials typically have poor interfacial adhesion. For example, in this study, when Zn_3P_2 nanowires were incorporated into the epoxy without any surface modification, no enhancement in either tensile strength or elastic modulus was obtained (**Table 7**). This is probably caused by the fact that Zn_3P_2 doesn't have sufficient surface hydroxyl groups to establish a strong interface with the epoxy matrix. It has been reported that epoxy adheres to metal and metal oxide surface by chemical interactions, where both amine and epoxide monomers are able to react with hydroxyl groups on the surface [234-237]. Based on the FTIR and XPS analyses discussed in the proceeding

section, the surfaces of Zn_3P_2 nanowires are oxidized into $Zn_3(PO_4)_2$. Given that Zn_3P_2 nanowires lack surface hydroxyl groups, while $Zn_3(PO_4)_2$ is an ionic compound, it is hypothesized here that the epoxy matrix could not interact well with the Zn_3P_2 nanowires.

Similarly, it was found that the flexural modulus, the property of a material to resist bending, of the composites embedded with unfunctionalized nanowires failed to improve upon nanowire addition. The flexural modulus was measured by standardized flexural test (ASTM D790) on 50.8×12.7×1.6 mm specimens. **Table 7** shows the flexural modulus with respect to nanowire loading. In this study, all the specimens didn't fail at a 5% deflection level, and therefore the flexural strength was not discussed here. As discussed in the previous paragraph, because of poor interfacial adhesion between the unfunctionalized nanowires and the epoxy matrix, no enhancement in flexural modulus was observed. In fact, flexural modulus was found to be decreasing slightly with nanowire loading up until loading of 1 wt.%. This demonstrates that establishment of good interfacial adhesion is critical for improving the mechanical properties of a polymeric material.

Table 7 Tensile and flexural properties of the composites reinforced by unfunctionalized nanowires

Sample	Tensile Strength [MPa]	Elastic Modulus [GPa]	Flexural Modulus [GPa]
Epoxy	60.0±1.3	1.12±0.06	-
U0.1	57.5±2.1	1.08±0.04	5.77±0.38
U0.5	59.9±3.2	1.09±0.10	5.44±0.30
U1	59.4±1.4	1.06±0.06	5.08±0.21

Comparison with Models

Many models have been developed to predict the elastic modulus of a fiber-reinforced composite material. One of the simplest models is the rule of mixtures, i.e.,

$$E_c = V_f E_f + \left(1 - V_f\right)E_m$$

where, E_c, E_m, and E_f represent the elastic moduli of composite, matrix, and fillers, while V_f is the volume fraction of the fillers. In this study, the volume fraction of nanowires was calculated based on the density of the epoxy and nanowires. The density of epoxy was measured by Archimedes' principle, which was calculated to be 1.195 g/cm^3.

The rule of mixtures was derived based on the assumption that the specimen is deformed only by a tensile load along the fiber direction, while fillers (1) have good interfacial bonding with the matrix, (2) are perfectly aligned within the matrix, and (3) span the full length of the specimen. In the industry, fibers used in many applications are generally much shorter and randomly oriented. Therefore, this equation is highly idealized and typically imposes the physical upper limit of reinforcement effects.

Another common model used to predict the elastic modulus of a composite material is the Halpin-Tsai equation [38, 39]. For a composite with short and randomly orientated fibers that have good interfacial adhesion with the matrix, the modified Halpin-Tsai model is expressed as follows:

$$\frac{E_c}{E_m} = \frac{3}{8}\left(\frac{1 + 2f\eta_L V_f}{1 - \eta_L V_f}\right) + \frac{5}{8}\left(\frac{1 + 2\eta_T V_f}{1 - \eta_T V_f}\right)$$

where,

$$\eta_L = \frac{E_f/E_m - 1}{E_f/E_m + 2f} \text{ and } \eta_T = \frac{E_f/E_m - 1}{E_f/E_m + 2}$$

In these equations, f is the aspect ratio of fillers. Taking the average aspect ratio of 100 and the elastic modulus of 90 GPa [238], the values calculated by these models and the experimental values were plotted in **Figure 17**. Because the experimental values are higher than the values predicted by the Halpin-Tsai model, significant reinforcement was achieved by the addition of 4ATP-functionalized nanowires. On the other hand, the composite embedded with 4tBTP-functionalized nanowires exhibited a significantly lower elastic modulus and deviated significantly from the models, given that these two models assume fillers and matrix have strong adhesion.
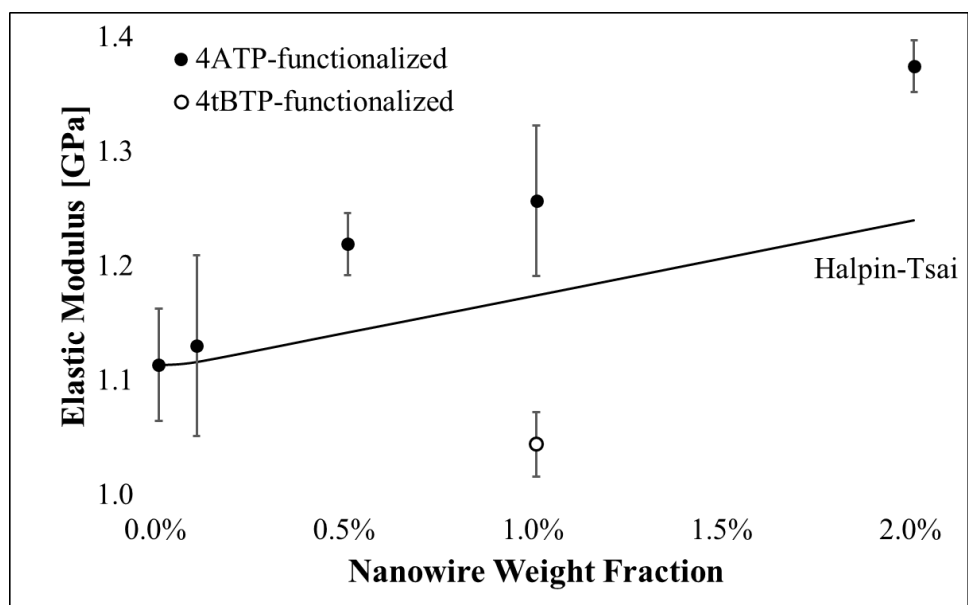
Figure 17 Comparison of experimental data with the Halpin-Tsai model

<u>Conclusions</u>

In this study, epoxy-based nanocomposites embedded with three types of Zn_3P_2 nanowires as filler materials were fabricated and studied for the mechanical properties. Unfunctionalized nanowires failed to improve the tensile strength or elastic modulus because of poor nanowire-epoxy interfacial adhesion, resulting from lack of sufficient surface hydroxyl groups on Zn_3P_2 nanowires. In order to solve this issue, 4ATP was adopted to modify the nanowire surface and able to form strong covalent bonding between nanowires and epoxy, which contributes to enhancement in elastic modulus by 23% at 2 wt.% nanowire loading. On the other hand, nanowires functionalized with 4tBTP deteriorated the tensile properties even at 1 wt.%, given that 4tBTP prevented bond formation between the nanowires and the epoxy matrix completely. This study demonstrated that the addition of inorganic filler materials, especially the ones with a

lower number of surface hydroxyl groups, does not improve the mechanical properties of a polymeric material if no care is taken regarding filler-matrix interface. Namely, deterioration in mechanical properties occurs when an effective load transfer from the matrix to fillers fails, given that the presence of nanowires reduces the number of crosslinking per volume of an epoxy and serves as voids or even defects. To overcome this problem, the functionalization of nanofillers to establish chemical bonding with matrix is proven to be an effective approach.

CHAPTER IV

FABRICATION OF TIO$_2$ NANOWIRE-EPOXY COMPOSITES AND

EXAMINATION OF NANOWIRE-EPOXY INTERFACE

Introduction

TiO$_2$ is an inorganic material widely used in the industry as photocatalyst or as additive to plastics [239, 240]. TiO$_2$ also possesses high elastic modulus and mechanical strength, which makes it promising as reinforcements for polymeric materials [239, 240]. Therefore, the nanoscale counterpart, especially the one-dimensional nanostructures such as TiO$_2$ nanowires, offer great opportunities as reinforcements due to their high surface-area-to-volume ratios and aspect ratios. It is worth noting that a large-scale synthesis approach of TiO$_2$ nanowires has been established [51] by Advanced Energy Materials, LLC, Lousville, KY, which enables the possibility of fabrication composites for commercial applications.

In the recent years, functionalization of fillers has been widely adopted to produce stronger composite materials, but a few issues are commonly present in many studies. One of the issues is limited information about the quality of functionalization. For example, even though some analyses such as Fourier-transform infrared spectroscopy (FTIR) and X-ray photoelectron spectroscopy (XPS) have been performed to confirm the presence of functional groups on fillers [241-244], the number of functional groups on filler materials is usually unreported, which renders the difficulties in evaluating the effectiveness of coupling agents as well as their effects on the mechanical properties of a composite.

Another issue is lack of understanding of interactions between fillers and a polymeric matrix. For metal and metal oxide substrates, the chemical interactions between a substrate and an epoxy resin has been investigated by several groups [234-237], but such an interaction between powder fillers and epoxy is rarely examined. Given that establishment of strong interfacial adhesion between fillers and a matrix is prerequisite for fabricating a strong composite material, understanding of filler-matrix interaction offers great insights on design of experiment such as a choice of filler and epoxy types. Similarly, interactions between functional groups grafted to fillers and a matrix needs to be investigated. For example, in many epoxy-based nanocomposites, fillers are functionalized with amine or epoxide functional groups so that they form chemical bonds with the epoxy monomers by amine-epoxide reactions [245-247]. Nevertheless, the differences in the effects of different coupling agents on filler-matrix interface as well as on the mechanical properties of a nanocomposite are still not very clear.

In this study, TiO_2 nanowires were incorporated into an epoxy resin as filler materials. They were functionalized with two types of organosilane coupling agents by a vapor-phase approach to produce different nanowire-epoxy interfaces. The silanization conditions were optimized based on multiple techniques, and the coverage of functional groups under different conditions was reported. Furthermore, the effects of coupling agents on the interactions between TiO_2 nanowires and epoxy monomers were discussed. This study is expected to serve as a starting point for the fabrication of the composites made of pre-formed TiO_2 nanowire foams discussed in **Chapter V**.

63

Experimental Details

Materials

Two types of organosilane coupling agents, (3-aminopropyl)trimethoxysilane (APTMS) and (3-glycidyloxypropyl)trimethoxysilane (GPTMS), were purchased from TCI America. All the chemicals were used without further purification. The source of other chemicals has been listed in the previous chapters.

Procedure

TiO2 nanowires were kindly provided by Advanced Energy Materials, LLC (Louisville, KY, USA) [51]. Briefly, Ti or TiO_2 powder mixed with an alkali salt was exposed to a highly dense microwave plasma at atmospheric conditions, in which a mixture of 2 L/min Ar, 11 L/min air, and 1000 SCCM H_2 was fed into the microwave plasma reactor. The collected powder was then dipped in a 1 M HCL solution for 1 h, followed by washing with deionized water. Finally the product was exposed to the plasma for 5 min for annealing.

Subsequently, prior to silane functionalization, TiO_2 nanowires were pretreated with O_2 plasma (plasma cleaner PDC-32G, Harrick Plasma) for 20 minutes to increase the number of surface hydroxyl groups [248]. Organosilane functionalization was performed via a vapor-phase route using a commercially available stainless-steel vacuum chamber that has an internal volume of 1.9 L. In the typical procedure, 500 mg plasma-treated TiO_2 nanowires and 1 mL of organosilane were placed in two polypropylene containers,

respectively. TiO_2 nanowires were spread out in a thin layer to maximize the nominal surface area for ease of organosilane vapors to diffuse to the nanowire surfaces. These containers were placed in a glass petri dish with a cover, and the petri dish was placed on a rack in the vacuum chamber (to prevent direct contact with the chamber). Subsequently, the vacuum chamber was evacuated to <5 Torr by a mechanical rotary pump, while the vacuum chamber was heated to a desired temperature by heating tapes. The temperatures for APTMS and GPTMS functionalization were maintained at 25 and 90 °C in the vacuum chamber, respectively. Duration of deposition was 2 hours. TiO_2 nanowires functionalized with APTMS and GPTMS are denominated as APTMS- and GPTMS-NWs, respectively.

The procedure to fabricate the epoxy and the composite has been described in the previous chapter. The only modification in this chapter is that the mole ratio of EPON 826, NGDE, and Jeffamine D230 employed for polymer and composite fabrication is adjusted to 1:1:1.

Characterization

Scanning Electron Microscopy (SEM) was performed to characterize the morphology of TiO_2 nanowires used in this study. The surface area of TiO_2 nanowires was measured by the Brunauer-Emmett-Teller (BET) analysis performed on Micromerics ASAP 2010 platform with automatic programs. Before the analysis, the moisture on the TiO_2 nanowires was removed in high vacuum at 110 °C overnight.

Given that the measurement of the contact angle of a loose layer of nanopowders is difficult, the contact angles of Si wafer surfaces treated in the same manner as the TiO_2

nanowires were measured. These contact angle measurements served as representations in evaluating the effect of various surface chemical modifications on the wetting behavior of TiO$_2$ nanowires. For each sample six droplets were placed at different spots on a Si wafer and the average value was reported. The contact angles were analyzed by the ImageJ software (an open-source software).

In order to estimate the number of (1) surface hydroxyl groups of original and plasma-treated nanowires, (2) organosilane functional groups on the functionalized nanowires, and (3) epoxy monomers that were attached to the TiO$_2$ nanowires, TGA was performed by TGA Q50 (TA Instruments). All the measurements were carried out at a heating rate of 10 °C/min from room temperature to 700 °C under nitrogen gas flow.

FTIR was performed using Nicolet IR100 (Thermo Fisher Scientific) to confirm the presence of functional molecules on the silanized nanowires. The reaction between TiO$_2$ nanowires and the epoxy monomers was also characterized by FTIR.

With the intent of understanding the effect of coupling agents on nanowire-epoxy interface, the mechanical properties of epoxy and epoxy composites were studied by tensile test using Instron 5567, in which the dumbbell-shape specimens (ASTM D638-V) were pulled at a strain rate of 1 mm/min with a span of 25.4 mm at room temperature. The fracture surfaces of epoxy and epoxy composites filled with various TiO$_2$ nanowires were imaged by SEM to examine the effect of fillers as reinforcements.

Results

Characterization of TiO$_2$ Nanowires

Morphology of TiO$_2$ Nanowires

   Figure 18 represents the typical morphology of TiO$_2$ nanowires used in this study. Most of the nanowires had diameters ranging from 200 to 300 nm and lengths from 2 to 4 μm. It is estimated that the average aspect ratio of these nanowires was around 10. The BET surface area was measured to be 26.61 m^2/g.
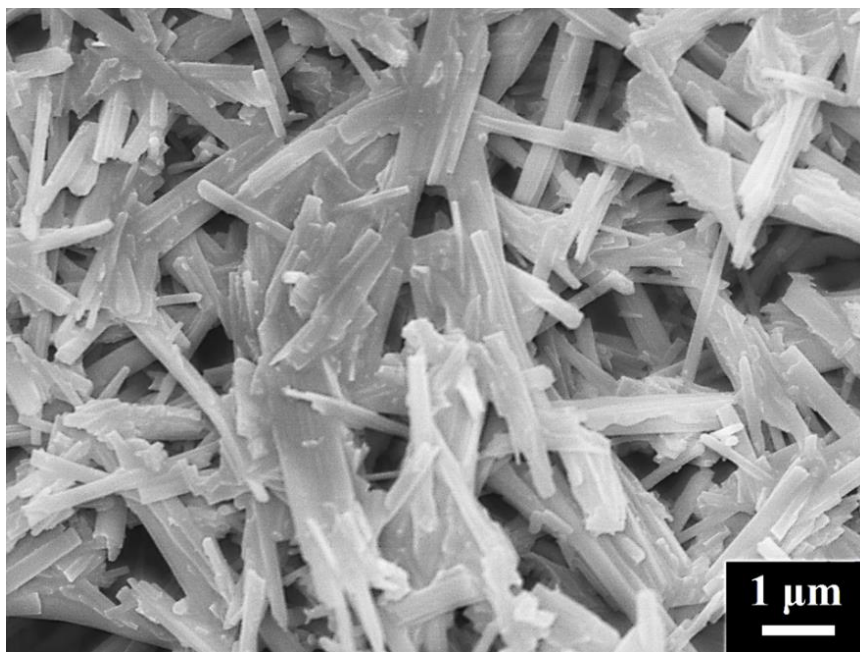
Figure 18 A representative scanning electron micrograph of TiO$_2$ nanowires used in this study

Number of Surface Hydroxyl Groups

In order to evaluate the effect of plasma treatment, the contact angles of a representative Si wafer before and after the plasma treatment were measured, given that silanization takes place on TiO_2 and SiO_2 surfaces in a similar manner [249]. The Si wafer was cut into 2×2 cm pieces and cleaned with acetone and ethanol, respectively. The contact angle of Si became 24.9° from 55.9° after the treatment. This indicates that exposure to O_2 plasma was able to activate the surface hydroxyl groups [250-252].

The number of surface hydroxyl groups on TiO_2 nanowires was estimated by TGA. The weight loss at 400–700 °C was identified as the characteristic temperature range of hydroxyl desorption, in which two surface hydroxyl groups condense and produce one water molecule [253]. This characteristic temperature range was also confirmed in this study (**Figure 19**), in which a relatively significant mass loss was observed at 400–700 °C. For the temperatures below 400 °C, the mass loss was attributed to evaporation of water physically absorbed by the nanowires, and dehydration happened mostly at 100–200 °C. Since the plasma-treated nanowires were more hydrophilic than the untreated nanowires, more mass loss was observed for plasma-treated nanowires.
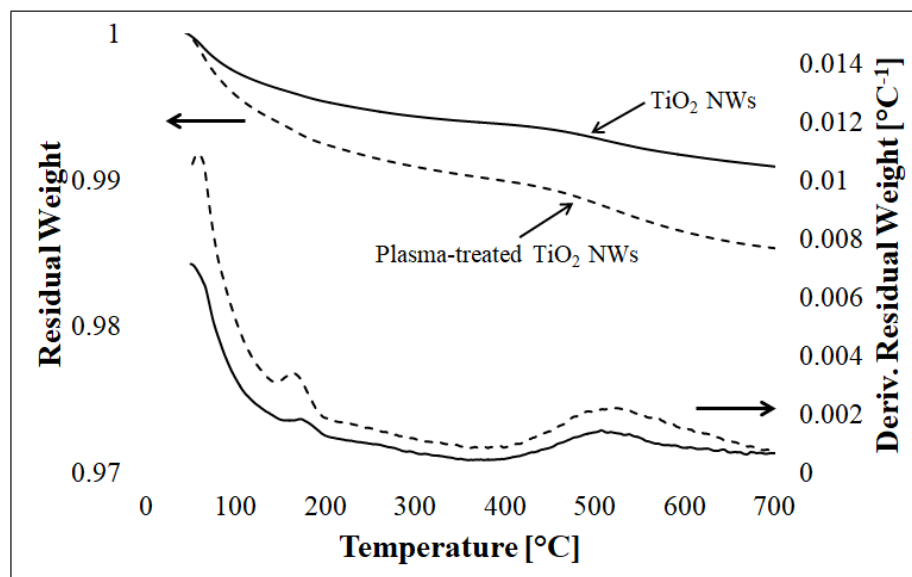
Figure 19 A TGA thermograph of original and plasma-treated TiO₂ nanowires. The mass loss up to 400 °C was attributed to evaporation of water absorbed by TiO₂ nanowires. Condensation of surface hydroxyl groups mainly occurred at higher temperatures

The number of surface hydroxyl groups on TiO₂ nanowires was determined by the following equation [254]:

$$n_{OH} = 2 \times \frac{\Delta m_{TiO_2}}{M_{water}} \frac{N_A}{S_{BET}} \times 10^{-18}$$

Here Δm_{TiO2} represents the percentage of weight loss at 400–700 °C. M_{water} is the molecular weight of water (18 g/mol) and S_{BET} is the BET surface area of TiO₂ nanowires, which was measured to be 26.61 m²/g. The unit of calculated n_{OH} is molecule/nm². Due to the fact that one desorbed water molecule is originated from two surface hydroxyl groups, the equation includes the multiplier of 2. N_A is the Avogadro constant.

Table 8 shows the results of TGA characterization of original and plasma-treated TiO₂ nanowires. Based on TGA results, the number of surface hydroxyl groups on TiO₂

nanowires was 7.3 molecule/nm^2. After O$_2$ plasma treatment, the density of surface hydroxyl groups was found to be increased to 11.5 molecule/nm^2 (or by 58%). Although, these number by themselves are larger, this data confirmed that O$_2$ plasma treatment can effectively activate the surface of TiO$_2$ nanowires.

Table 8 TGA results of O$_2$ plasma treatment

Sample	Weight Loss at 400–700 °C	Hydroxyl Coverage [molecule/nm^2]
TiO$_2$ nanowires	0.29%	7.3
Plasma-treated TiO$_2$ nanowires	0.46%	11.5

Characterization of Silanization

Figure 20 (a) shows the FTIR spectrum of TiO$_2$ nanowires. The peaks at 950, 780, and 480 cm^{-1} are assigned to the characteristic vibration mode of Ti-O, O-Ti-O, and O-Ti-O bonds of TiO$_2$ [255, 256], whereas the peak at 1630 cm^{-1} is ascribed to the bending vibration of water absorbed to the TiO$_2$ nanowires. A broad peak at 3200–3600 cm^{-1} corresponds to O-H stretching from absorbed water. These peaks were also observed in other samples.

Figure 20 (b) shows the FTIR spectrum of APTMS-functionalized nanowires. Several new peaks appeared at 2920–2850 and 1470–1380 cm^{-1}, corresponding to C-H stretching and bending modes. The peaks at 1550 and 1320 cm^{-1} are attributed to N-H bending and C-NH$_2$ (primary amine) stretching, respectively. Two small shoulders at 1200 cm^{-1} stem from C-NH and C-N, respectively. These peaks indicate that TiO$_2$ nanowires

were successfully functionalized by APTMS. In **Figure 20 (c)**, the peaks at 1340, 1250 and 1200 cm^{-1} correspond to the C-H bending mode of the epoxy ring, C-O-C stretching mode from the epoxide rings and linear chains, respectively [257], which confirmed the presence of GPTMS functional groups.
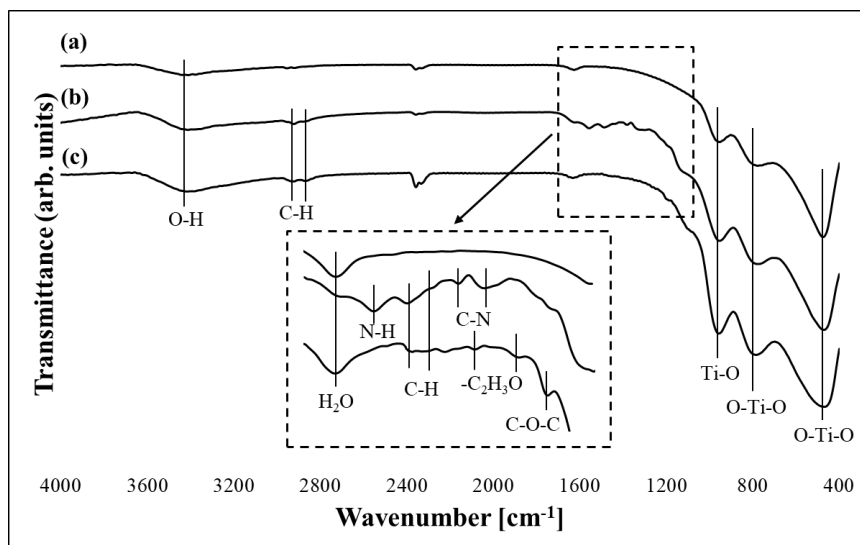
Figure 20 FTIR spectra of (a) TiO$_2$ nanowires, (b) APTMS-functionalized nanowires, and (c) GPTMS-functionalized nanowires. The boxed region shows the spectra at 1700–1100 cm^{-1}

Silane coverage was also estimated by TGA. The characteristic temperature range at which the organic part (C, H, N, and O) of attached organosilane decomposes was previous identified as 200–700 °C [258, 259]. For example, the decomposed part for APTMS is -C$_3$H$_6$NH$_2$ [260]. The equation used to determine the silane coverage is similar to the one used to calculate the density of surface hydroxyl groups of TiO$_2$ nanowires:

$$n_s = \frac{\Delta m_{s-TiO_2}}{M_s} \frac{N_A}{S_{BET}} \times 10^{-18}$$

Here n_s is the silane coverage (molecule/nm^2) and M_s is the molecular weight of decomposed part of organosilane (g/mol). $\Delta m_{s\text{-}TiO2}$ represents the percentage of weight loss at 200–700 °C. Given that the weight loss due to dehydration at 200–700 °C was not taken into account in this equation, the silane coverage obtained by this equation is slightly overestimated. It is worth noting that (1) for the nanowires functionalized with an organosilane with lower molecular weight, the deviation caused by this overestimation will be larger, since the weight ratio of water to decomposed organosilane is larger; (2) the deviation from hydrophobic nanowires will be smaller than hydrophilic one, because the former absorbs less water from the environment.

Figure 21 shows the representative TGA thermograph, and the silane coverage of each silanized TiO$_2$ nanowires is summarized in **Table 9**. The density of organosilane on GPTMS-functionalized nanowires was ~5 molecule/nm^2, which is closed to the theoretical value of the maximum silane coverage [249, 261]. On the other hand, the APTMS coverage on TiO$_2$ nanowires was higher (14.2 molecule/nm^2). As discussed in the preceding paragraph, the number of APTMS grafted to TiO$_2$ nanowires was more overestimated than the others. Nevertheless, compared to GPTMS, APTMS coverage may be higher, attributed to the fact that amine functional groups can self-catalyze silane hydrolysis/condensation and thus cause agglomeration [149]. The only deduction from this study was the fact that reduction of processing temperature is necessary to prevent agglomeration of APTMS.

72
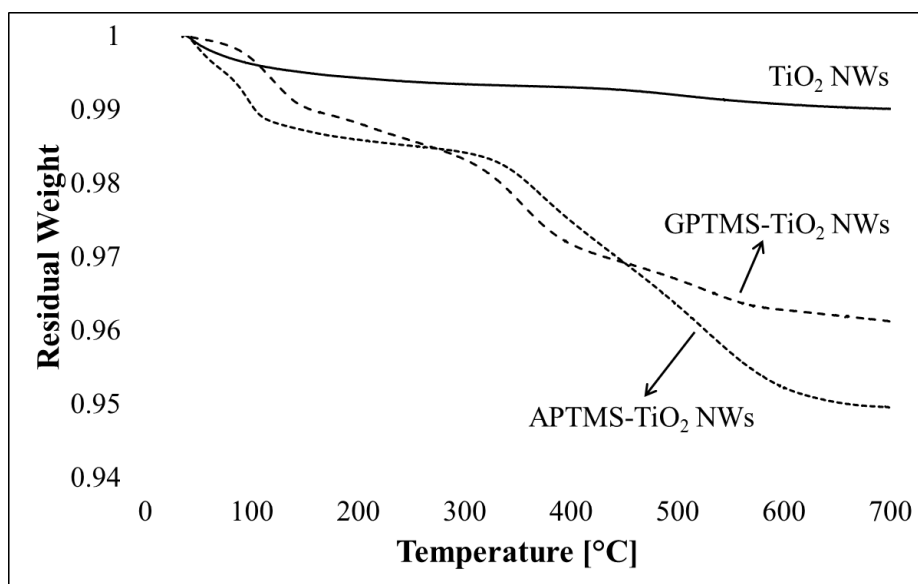
Figure 21 A TGA thermograph of silanized TiO$_2$ nanowires

Table 9 Silane coverage for each silanized TiO$_2$ nanowires, where M$_s$ stands for the molecular weight of the decomposed part

Nanowire Type	Decomposed Part	M$_s$ [g/mol]	Weight Loss at 200–700 °C	Coverage [molecule/nm^2]
APTMS-functionalized	-C$_3$H$_8$N	58	3.63%	14.2
GPTMS-functionalized	-C$_6$H$_{11}$O$_2$	115	2.67%	5.2

Mechanical Properties of Nanocomposites

ASTM D638 tensile test was performed for the epoxy and epoxy composites filled with TiO$_2$ nanowires to determine their mechanical properties. **Figure 22** shows the representative stress-strain curves. Here the epoxy composites containing 0%, 2%, 5%, and 10% plasma-treated TiO$_2$ nanowires are denominated N0, N2, N5, and N10, respectively, while the ones containing 5% APTMS- and GPTMS-functionalized

nanowires are A5 and G5, respectively. The mechanical properties of all the samples are summarized in **Table 10**, where σ_U, σ_F, E, and ε_F, represent ultimate tensile strength, fracture strength after necking (horizontal region), elastic modulus, and elongation at break. All the samples exhibited necking behavior. When a neck is initiated, stress applied to the matrix is localized, resulting in local strengthening due to partial orientation of polymer chains. As a result, necking propagates and further plastic deformation occurs (horizontal region).
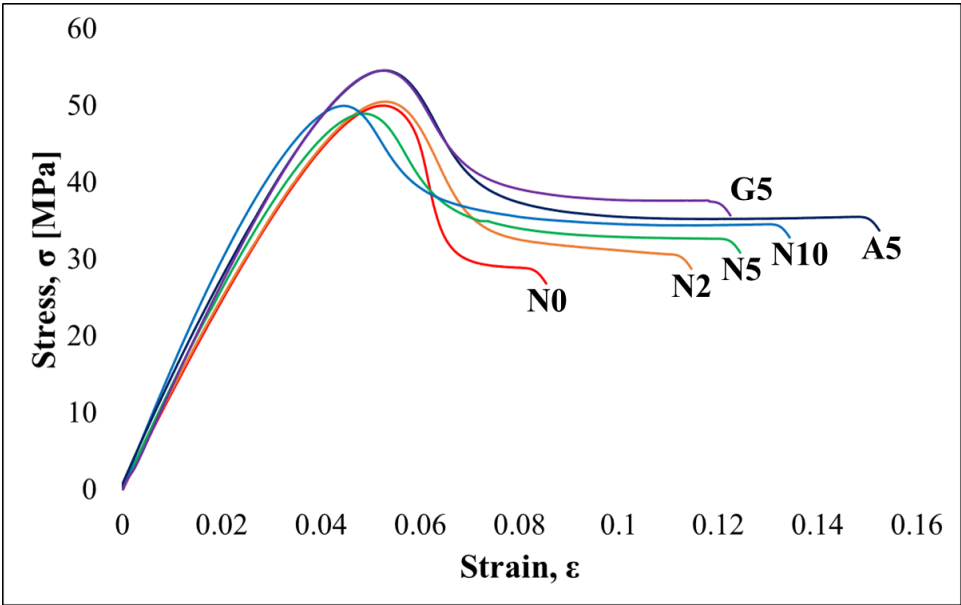
Figure 22 Representative stress-strain curves of epoxy and nanowire-reinforced epoxy composites

Table 10 Tensile properties of epoxy and epoxy composite samples, where E, σ_U, σ_F, and ε_F represent the elastic modulus, ultimate tensile strength, fracture strength after necking, and elongation at failure, respectively

Sample	nanowire	Loading	E [GPa]	σ_U [MPa]	σ_F [MPa]	ε_F
N0	-	-	1.19±0.07	50.1±3.5	25.2±4.9	0.085±0.004
N2	TiO_2	2%	1.22±0.02	50.6±2.0	28.7±2.4	0.116±0.013
N5	TiO_2	5%	1.33±0.08	49.0±1.7	29.0±1.7	0.124±0.023
N10	TiO_2	10%	1.51±0.08	50.0±3.3	32.2±1.8	0.134±0.027
A5	APTMS-TiO_2	5%	1.33±0.08	54.6±1.8	34.0±3.2	0.152±0.025
G5	GPTMS-TiO_2	5%	1.32±0.06	54.6±2.1	36.0±1.9	0.122±0.024

Figure 23(a) shows the ultimate tensile strength. For the composites filled with unfunctionalized nanowires, the ultimate tensile strength was unaffected by nanowire loading. On the other hand, the ultimate tensile strength of the composites with silanized nanowires was improved by 10% compared to either epoxy or the composites embedded with unfunctionalized nanowires.

As shown in **Figure 23(b)**, the fracture strength of unfunctionalized nanowire-epoxy composites seems to be improved with respect to nanowire loading. In order to confirm if this observation is valid, a two-tailed statistical test was conducted, in which the p values of the pair of (1) N0 and N10, (2) N2 and N10, and (3) N5 and N10 were 0.14, 0.04, and 0.04, respectively. This means that the difference between N10 and N2 or N5 was statistically significant, whereas the difference between N0 and N10 was not (probably because of the large standard deviation and small sample size). Given that the fracture strength of N10 was proved to be higher than N2 or N5 based on the statistical

test, incorporation of TiO_2 nanowires might have positive effects on the fracture strength. On the other hand, the fracture strength was further improved by incorporating silanized nanowires, in which A5 and G5 had similar fracture strength and they exhibited ~20% and ~40% higher fracture strength than N5 and N0, respectively.

For the epoxy composites reinforced by unfunctionalized TiO_2 nanowires, elastic modulus was increased with respect to nanowire loading. For N10 the elastic modulus was enhanced to 1.51 GPa by 27% compared to N0. This observation is in agreement with the values predicted by the Guth [37] and Halpin-Tsai [38, 39] equations, as shown in **Figure 23(c)** (for these equations, the density of epoxy is 1.178 g/cm^3, measured by Archimedes' principle, while the density of anatase TiO_2 is 3.84 g/cm^3). For the composites reinforced by APTMS- or GPTMS-functionalized nanowires, it was found that the elastic modulus was not affected much by functionalization at the same nanowire loading. Given that elastic modulus is typically determined at small deformation or displacement, debonding between nanowires and the matrix does not take place when the interfacial adhesion is sufficiently strong. As a result, elastic modulus is not sensitive to filler-matrix interaction when good interfacial adhesion has been established [262]. On the other hand, if the interfacial adhesion is very poor, decrease in elastic modulus may occur [231, 232].

Elongation at break (**Figure 23(d)**) was improved with respect to the nanowire loading compared to that of the epoxy, but further investigation is necessary to understand the effects of nanowire loading on the elongation at break, because of the large standard deviation obtained for the epoxy composites with 2–10% nanowire loadings.
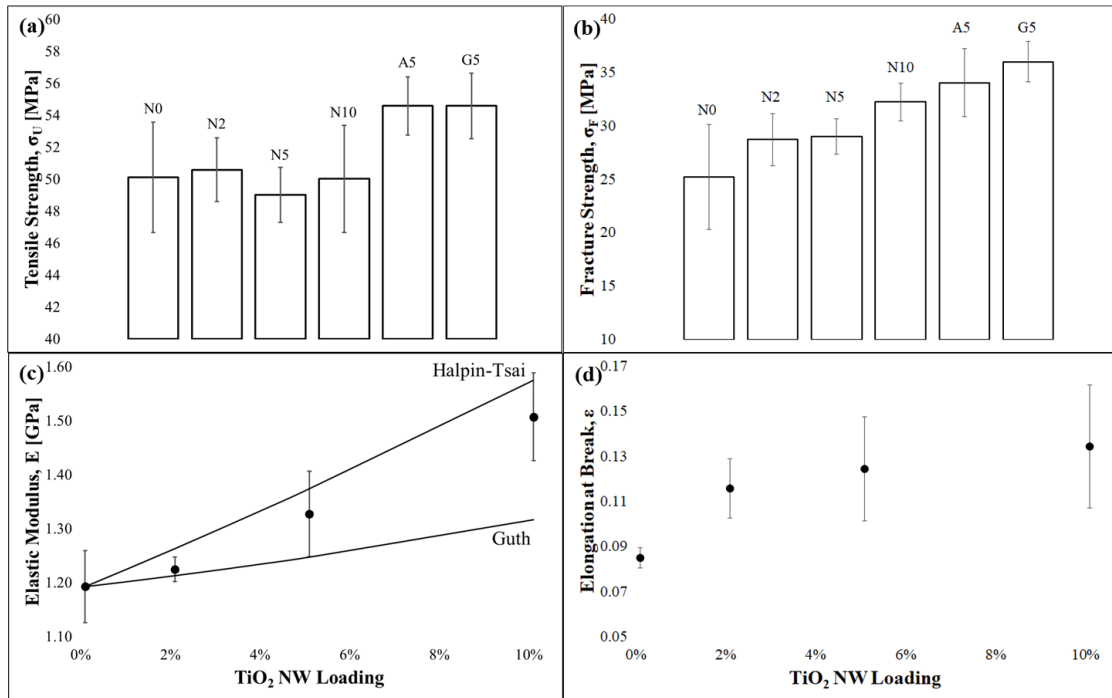
Figure 23 Mechanical properties of epoxy and the composites: (a) tensile strength, (b) fracture strength after necking, (c) elastic modulus compared with the Guth and Halpin-Tsai equations, and (d) elongation at break

Discussion

Optimization of Silanization Conditions

In order to determine the optimal functionalization conditions for each organosilane, the contact angles and silane coverage were obtained for each condition and compared, as summarized in **Table 11.** Given that the functional groups originated from these silanes are more hydrophobic than original Si surface, producing the maximum contact angle will be one of the criteria for the optimal functionalization condition. On the other hand, the silane coverage was measured using TGA, in which the condition resulting in the amount of organosilane closed to the theoretical value (5 molecule/nm^2 [249, 261])

would be optimal. Based on these criteria, the optimal functionalization temperatures for GPTMS was determined to be 90 °C. For APTMS, functionalization at room temperature was selected as the optimal condition, considering that the density of APTMS attached to Si at 40 °C was far more than that the theoretical value. This suggests that functionalization at both 25 °C and 40 °C produced multiple layers by self-polymerization, instead of forming a monolayer of APTMS. Therefore, it is expected that a lower temperature, together with the control of the amount of APTMS source material, may facilitate the formation of monolayer of APTMS by suppressing its vapor pressure.

Table 11 Contact angles and silane coverage for different silanization conditions

Organosilane	Temperature [°C]	Duration [h]	Contact Angle [°]	Silane Coverage [molecule/nm^2]
APTMS	25	2	61.1±2.2	15.5
	40	2	60.9±2.1	27.9
GPTMS	40	2	47.7±2.1	4.7
	50	2	51.7±3.1	4.6
	60	2	55.8±2.5	4.7
	80	2	56.0±3.5	5.2
	90	2	59.6±1.1	5.3
	110	2	56.1±2.0	4.7

Interactions between TiO_2 Nanowires and Epoxy Monomers

Number of Epoxy Monomers Attached to Nanowires

Unlike unfunctionalized Zn_3P_2 nanowires discussed in the previous chapter, the addition of unfunctionalized TiO_2 nanowires had a positive impact on elastic modulus, and silanized TiO_2 nanowires reinforced the nanocomposite by the same degree. This indicates that good interfacial adhesion has been established between TiO_2 nanowires and the epoxy, and silanization did not have extra impacts on interfacial adhesion as well as elastic modulus.

Strong interfacial adhesion between fillers and a matrix is of necessity to take full advantages of filler materials to reinforce the polymeric matrix. If a good filler-matrix interaction fails to be achieved, slippage at the interface occurs, and the load applied to the matrix cannot be transferred to fillers effectively. In order to evaluate the degree of interactions between TiO_2 nanowires and epoxy monomers used in this study, plasma-treated TiO_2 nanowires were dispersed in NGDE or Jeffamine D230, respectively, under three conditions: (1) kept at room temperature for 3 days, (2) heated at 100 °C for 90 minutes, and (3) heated at 100 °C for 90 minutes, followed by at 130 °C for 60 minutes (the conditions used in epoxy synthesis). TiO_2 nanowires were dispersed by sonication and washed with ethanol for five times after the treatment. TiO_2 nanowires treated with NGDE at these conditions are denominated as NGDE-NWs@RT, NGDE-NWs@100°C, and NGDE-NWs@130°C, respectively, whereas those with Jeffamine D230 are J-NWs@RT, J-NWs@100°C, and J-NWs@130°C.

Similar to quantification of silane coverage in the proceeding sections, the amount of NGDE or Jeffamine molecules attached to TiO_2 nanowires ($n_{monomer}$) was determined by the following equation:

$$n_{monomer} = \frac{\Delta m_{m-TiO_2} - \Delta m_{TiO_2}}{M_{monomer}} \frac{N_A}{S_{BET}} \times 10^{-18}$$

where Δm_{m-TiO2} represents the percentage of weight loss of monomer-treated TiO_2 nanowires, and $M_{monomer}$ is the molecular weight of the monomer. The molecular weights of NGDE and Jeffamine are 216 and 230 g/mol, respectively. It was assumed that the weight loss difference between monomer-treated and untreated TiO_2 nanowires at 200–700 °C is ascribed to the monomer molecules that are either covalently bonded to or strongly adhered by TiO_2 nanowires.

Figure 24(a) shows the TGA thermograph of NGDE-NWs, and the amounts of NGDE molecules attached to TiO_2 nanowires at various conditions were determined by TGA, as summarized in **Table 12**. It was observed that the NGDE coverage increased with respect to the treating temperature, as higher temperatures promoted the epoxy monomers to diffuse in and react with the TiO_2 surface. After full curing, 1.7 NGDE molecules were crosslinked with TiO_2 nanowires at every nm^2. This demonstrates that unfunctionalized TiO_2 nanowires were able to chemically bond with an epoxy matrix.

The TGA thermograph and the coverage of J-NWs are shown in **Figure 24(b)** and **Table 12**, respectively. Similarly, the amount of Jeffamine D230 attached to TiO_2 nanowires increased with respect to the treating temperature. Under the same conditions in which fully cured epoxy was synthesized in this study, the Jeffamine D230 coverage was found to be 0.8 molecule/nm^2. Although the reason for this difference in coverage is

80

unclear, this finding may suggest that epoxide monomers more readily interact with TiO_2 than amine monomers, when their molecular weights are nearly the same.
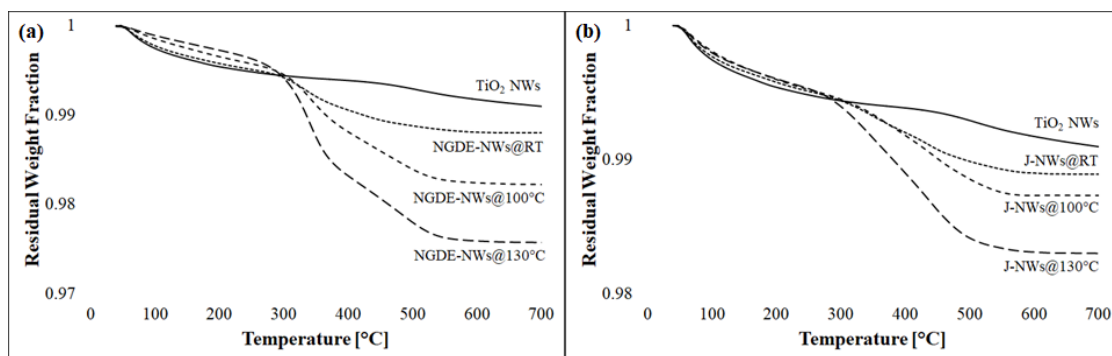
Figure 24 TGA thermographs of (a) NGDE-NWs and (b) J-NWs

Table 12 Epoxy monomer coverage on TiO_2 nanowires

Sample	Weight Loss at 200–700 °C	Monomer Coverage [molecule/nm^2]
Plasma-treated nanowires	0.47%	-
NGDE-NWs @RT	0.75%	0.3
NGDE- NWs @100°C	1.40%	1.0
NGDE- NWs @130°C	2.12%	1.7
J- NWs @RT	0.63%	0.2
J- NWs @100°C	0.83%	0.4
J- NWs @130°C	1.25%	0.8

Effect of O$_2$ Plasma Treatment

The effect of O$_2$ plasma treatment on the mechanical properties was also investigated. The results of epoxy composites filled with 5% plasma-treated (N5) and untreated (U5) TiO$_2$ nanowires are summarized in **Table 13**. Although plasma-treated TiO$_2$ nanowires had ~58% more surface hydroxyl groups than untreated ones, the mechanical properties were almost identical or only slightly higher (each value was within the standard deviation). This suggests that increase in the number of surface hydroxyl groups may only have marginal effects on the mechanical properties when good interfacial adhesion is formed. This is because strength is determined by the weakest failure scenario associated with all the possible failure mechanisms, and not by the statistically averaged values among these mechanisms [262].

Table 13 Mechanical properties of N5 and U5

Specimen	σ$_U$ [MPa]	σ$_F$ [MPa]	E [GPa]	ε$_F$
N5	49.0±1.7	29.0±1.7	1.33±0.08	0.124±0.023
U5	48.3±2.4	27.7±3.0	1.30±0.06	0.131±0.037

Interactions between Silanized TiO$_2$ Nanowires and Epoxy Monomers

Nanowire-epoxy Interfaces by Silanized Nanowires

Owing to different functional groups to be grafted on fillers, it is anticipated that the effect of different organosilane coupling agents may not be identical. The difference can be ascribed to the type or the number of bonds formed between the functional groups

and epoxy monomers. In this study, as shown in **Figure 25**, two types of interfaces were generated by functionalizing TiO_2 nanowires with APTMS and GPTMS. APMTS appends amine functional groups to nanowires, which react with epoxide monomers to establish a strong interface with the epoxy network (**Figure 25(a)**). Given that one part of amines can react with two parts of epoxide groups, the number of chemical bonds is up to 200% of that of active amine groups, if the reaction is fully completed. On the other hand, GPTMS-functionalized nanowires react with amine monomers, and the maximum number of bonds can be either 100% or 50%, as illustrated in **Figure 25(b-i)** and **Figure 25(b-ii)**, respectively. Consequently, considering that APTMS- and GPTMS-functionalized nanowires essentially form the same type of bonding with an epoxy network, APTMS-functionalized nanowires should generate a stronger interface than GPTMS-functionalized nanowires. Namely, interfacial adhesion between APTMS-functionalized nanowires and epoxy is stronger than that between GPTMS-functionalized nanowires and epoxy, if all the functional groups are able to react with epoxy monomers in both cases. This will lead to higher mechanical properties for a composite reinforced by APTMS-functionalized nanowires than GPTMS-functionalized nanowires at the same loading.
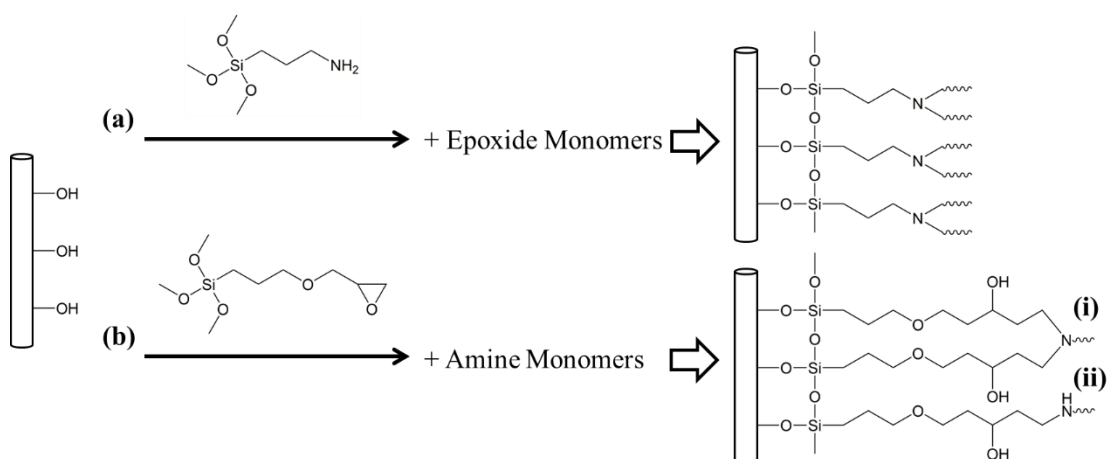
Figure 25 A scheme of different nanowire-epoxy interfaces created by (a) APTMS-functionalized nanowires and (b) GPTMS-functionalized nanowires. One of the major differences is the number of bonds that can form between nanowires and an epoxy matrix. For APTMS-functionalized nanowires, up to 200% of the number of active functional groups at surface, whereas GPTMS-functionalized nanowires can form up to (i) 100% or (ii) 50% of the number of surface epoxide groups

Nevertheless, based on the tensile test, the mechanical properties of A5 and G5 were almost identical. This leads to a hypothesis that the reaction between the functional groups and the epoxy monomers was not complete, and the number of bonds is similar in two cases. Therefore, interactions between silanized nanowires and corresponding epoxy monomers was examined, as discussed in the following sections.

Number of Epoxy Monomers Attached to Silanized Nanowires

In order to confirm that chemical bonds were actually formed between silanized nanowires and the epoxy matrix, the reaction between nanowires and epoxy monomers was examined. Similar to the proceeding section, APTMS-functionalized nanowires were dispersed in NGDE and heated at 100 °C for 90 minutes and 130 °C for 60 minutes.

Subsequently, the nanowires were filtered and washed with ethanol for five times. **Figure 26(b)** shows the spectrum of APTMS-functionalized nanowires reacted with NGDE (NGDE-A-nanowires). Compared to APTMS-functionalized nanowires (**Figure 26(a)**), a few peaks at 1290 and 1190 cm^{-1} corresponding to C-O-C stretching from epoxide rings and linear chains showed up, while the peaks at 1550 and 1320 cm^{-1} corresponding to N-H stretching and C-NH$_2$ stretching disappeared. The intensity of two peaks at 1470 and 1350 cm^{-1} were also increased, originated from C-H stretching from NGDE molecules. This confirmed that APTMS-functionalized nanowires were able to form chemical bonding with NGDE.

Similarly, **Figure 26(d)** shows the spectrum of GPTMS-functionalized nanowires reacted with Jeffamine (J-G-NWs). Several new peaks attributed to the amine functional groups from Jeffamine showed up after the reaction. The peaks at 1570 and 1530 cm^{-1} correspond to N-H stretching from primary and secondary amines, respectively. The peak at 1360 cm^{-1} and the shoulder at 1270 cm^{-1} are attributed to C-NH$_2$ and C-NH/C-N stretching. This demonstrated that the epoxide functional groups from GPTMS-functionalized nanowires were able to react with the amine groups from Jeffamine.
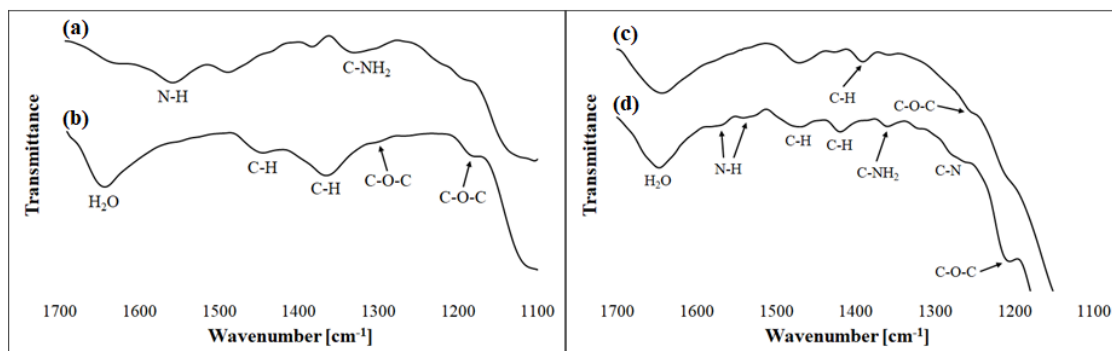
Figure 26 FTIR spectra of (a) APTMS-NWs, (b) NGDE-A-NWs, (c) GPTMS-NWs, and (d) J-G-NWs

TGA was performed to estimate the density of epoxy monomers interacted with silanized TiO_2 nanowires. **Figure 27** shows the TGA thermograph of silanized and monomer-treated silanized TiO_2 nanowires. Considering the weight loss up to 200 °C was attributed mainly to dehydration for each specimen, the weight loss at 200–700 °C was mainly caused by decomposition of organic molecules attached to TiO_2 nanowires. Accordingly, the difference in weight loss at this temperature range between silanized and monomer-treated silanized nanowires would equal to the amount of epoxy monomers decomposed at elevated temperatures. **Table 14** summarized the results of the TGA characterization. Compared to unfunctionalized TiO_2 nanowires, APTMS-functionalized nanowires were able to bind a higher number of NGDE molecules, which was increased from 1.7 to 3.7 molecule/nm^2. This indicates that the functionalization of TiO_2 nanowires with APTMS can significantly improve nanowire-epoxy interaction. On the other hand, the amount of Jeffamine attached to GPTMS-functionalized nanowires was increased only slightly from 0.8 to 1.0 molecule/nm^2, suggesting that GPTMS might not be as effective as APTMS in improving nanowire-epoxy interaction. Nevertheless, this observation may

vary depending on the type of epoxy monomers (both epoxide and amine monomers), and further investigations will provide more insights to understand nanowire-epoxy interaction.
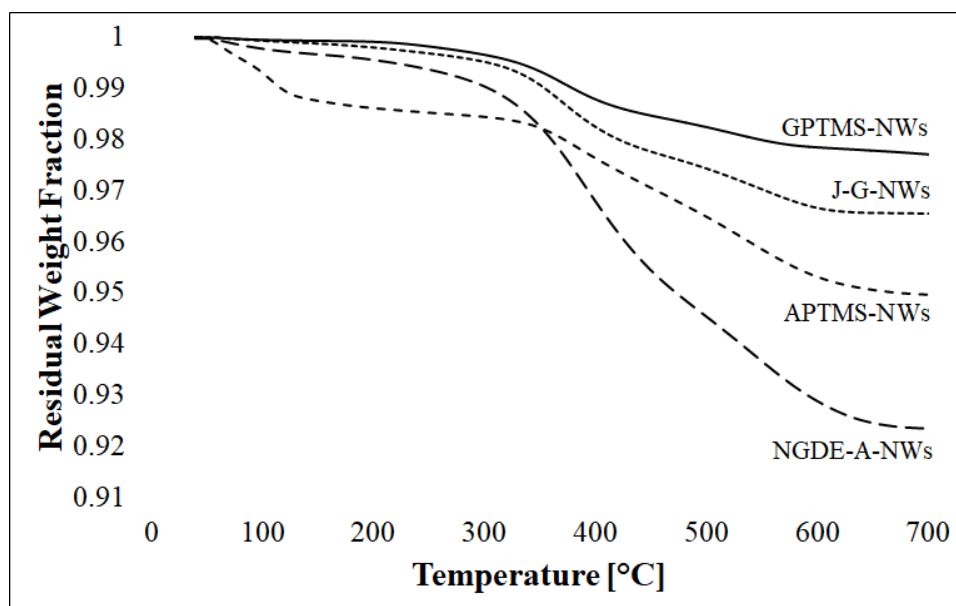
Figure 27 A TGA thermograph of silanized nanowires and silanized nanowires reacted with monomers

Table 14 Epoxy monomer coverage on silanized TiO₂ nanowires

Sample	Weight Loss at 200–700 °C	Monomer Coverage [molecule/nm²]
APTMS-NWs	3.63%	-
NGDE-A-NWs	7.17%	3.7
GPTMS-NWs	2.22%	-
J-G-NWs	3.20%	1.0

Based on the TGA results, it was found that the number of bonds between nanowires and the epoxy matrix was different for APTMS- and GPTMS-functionalized nanowires. Therefore, in addition to improved interfacial adhesion, improved nanowire dispersion (i.e., fewer nanowire agglomerates) is expected to contribute to the improved strength of the composites by APTMS and GPTMS functionalization of nanowires. This is also supported by SEM analysis of the fractured surfaces of the composites, which is discussed in the following section.

Fracture Surface of Epoxy and Composites

Figure 28 shows the scanning electron micrographs of the fracture surfaces of epoxy and epoxy composites. The epoxy had a smooth, featureless fracture surface (**Figure 28(a)**), whereas nanowire-reinforced epoxy composites showed rough, complex surfaces with nanowires protruding out (**Figure 28(b)-(d)**). As the nanowire loading increased, more nanowires appeared at the surface, and the number of lines induced by localized shear stress increased. As a result, the fracture surface became more complex and fracture surface area increased with respect to nanowire loading, leading to more energy absorption during deformation.

Compared to N5 (**Figure 28(c)**), in which some small bundles of a few nanowires were found, the nanowire distribution in A5 (**Figure 28(e)**) and G5 (**Figure 28(f)**) was more homogeneous, which confirmed the previous hypothesis that silanization of TiO_2 nanowires was able not only to improve the interfacial adhesion between nanowires and the matrix, but also to improve the dispersion of the nanowires within the epoxy matrix.
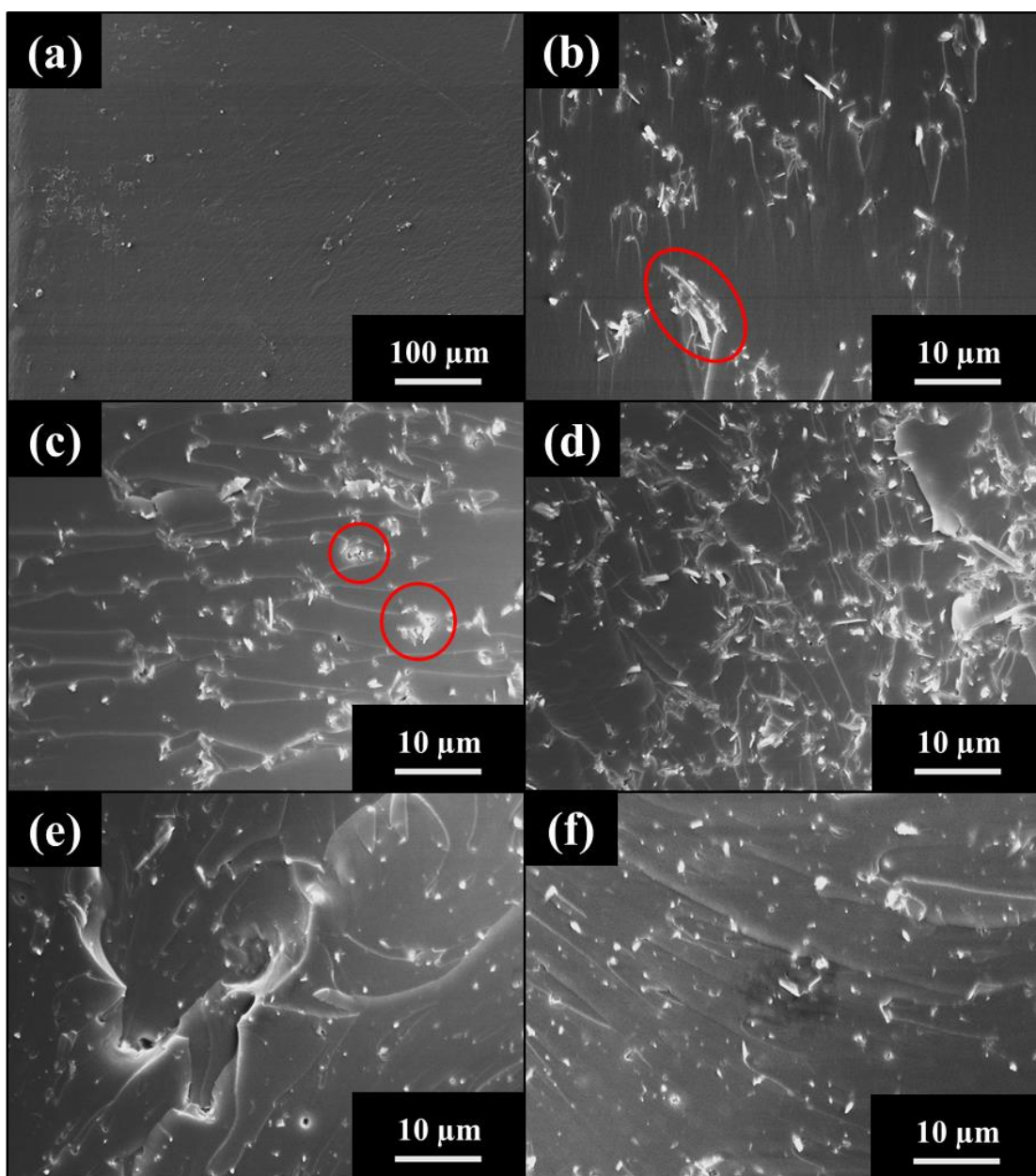
Figure 28 Fracture surface of (a) epoxy (N0), (b) N2, (c) N5, (d) N10, (e) A5, and (f) G5. The red circles represent the slight agglomeration of nanowires

Conclusions

In this study, a vapor-phase process was developed to functionalize TiO_2 nanowires with organosilane coupling agents, and the quality of silanization was

scrutinized by different techniques. TGA is a powerful tool to determine the silane coverage on filler materials, which allows to further evaluate the number of chemical bonds able to form between fillers and epoxy monomers. Based on TGA, the silane coverage of APTMS and GPTMS was 15.2 and 5.2 molecule/nm^2, respectively. This indicates that APTMS was more reactive and formed multi-layers (i.e., oligolayers), whereas GPTMS probably formed a self-assembled monolayer (SAM).

The interactions between unfunctionalized TiO$_2$ nanowires and epoxy monomers was examined by FTIR and TGA, which confirmed that the functional groups were capable of forming chemical bonding with epoxy monomers. For unfunctionalized nanowires, both Jeffamine D230 (amine) and NGDE (epoxide) molecules from the epoxy resin were able to attach to the nanowires, the density of these two monomers being 1.7 and 0.8 molecule/nm^2, respectively. Similarly, the functional groups on the silanized TiO$_2$ nanowires were able to form chemical bonding by amine-epoxide reactions. However, the number of bonds formed between APTMS-functionalized nanowires and NGDE was larger than that between GPTMS-functionalized nanowires and Jeffamine D230 by a factor of 3.7. This suggests that the functionalization of TiO$_2$ nanowires with APTMS might be more favorable.

To evaluate the effects of functionalization with various organosilanes on the mechanical properties of an epoxy composite, tensile test on the composites filled with unfunctionalized and silanized nanowires were performed. It was observed that the elastic modulus of the nanocomposites depended only on nanowire loading and was essentially unaffected by silanization. On the other hand, silanization of TiO$_2$ nanowires was capable

of improving the ultimate tensile strength and fracture strength. Nevertheless, APTMS- and GPTMS-functionalized nanowires had similar effects on strength, despite the fact that the difference in the number of bonds between TiO_2 nanowires and the epoxy monomers was quite significant. This suggests that improvement in mechanical strength was ascribed not only to improved interfacial adhesion, but also to the improved dispersion of nanowires within the matrix, which was confirmed by their fracture surface observed by SEM. Additionally, comparison between two epoxy composites containing nanowires with different numbers of surface hydroxyl groups also showed almost the same mechanical properties, indicating that the number of bonds does not affect the mechanical properties of a nanocomposite when good interfacial adhesion has been established.

CHAPTER V

FABRICATION OF EPOXY COMPOSITES REINFORCED BY

INTERCONNECTED NANOWIRE NETWORK

<u>Introduction</u>

As discussed earlier, nanowires are a class of materials that are useful as reinforcements for SMPCs. Their addition to polymers leads to improved mechanical properties through an effective load transfer from a host matrix to fillers [30, 31]. Moreover, it has been reported that excellent mechanical performance of a nanocomposite is achieved when a continuous network of filler materials is established within a polymeric matrix [33, 34, 190, 191]. Currently, a major approach towards the fabrication of nanocomposites involves blending pre-determined quantities of nanowires and polymers together. In this approach, agglomeration and non-uniform dispersion of fillers within a polymeric matrix prevent maximizing the mechanical properties of the resulting composites. In addition, direct interaction among nanofillers cannot be established. An alternative approach, therefore, is to pre-fabricate an interconnected structure of nanofillers and infiltrate a polymer dispersion or an epoxy resin into the structure [192-195]. Freeze casting [196-198] and gelation [199-201] for fabricating interconnected nanofillers are typically implemented, but these methods result in mechanically weak reinforcements owing to the formation of only physical bonds between the nanofillers [199, 201]. In turn, this results in the formation of nanocomposites that exhibit poor mechanical properties. For example, He *et al.* fabricated an aerogel consisting of Ag

nanowires from a Ag nanowire suspension, where the three-dimensional nanowire network was constructed based on physical bonds among nanowires [201]. It was also reported that the conformal coatings on the nanowire network prepared by *in-situ* polymerization of pyrrole improved the structural elasticity of the aerogel by welding the nanowires through the polymer coatings [201].

In this context, the aim of this chapter is to explore the possibility of using powder metallurgy techniques for forming nanowire networks (or nanowire foams) that have nanowires covalently bonded to each other, and further explore the possibility of forming mechanically strong SMPCs from the nanowire foams thus obtained. In this technique, nanowires are mixed with a sacrificial space holder, followed by consolidation of the resulting mixtures into the desired shape. Removal of the space holder results in the formation of porous nanowire foams. In the current study, $(NH_4)_2CO_3$ was selected as the sacrificial salt, as it readily decomposes at a low temperature (58 °C), while leaving behind no solid residue. In the past, our group also has employed this technique to fabricate thermally conducting zinc foams useful for the byproduct-free synthesis of Zn_3P_2 nanowires using NH_4Cl as a sacrificial salt [165].

More specifically, SMPCs were fabricated from mechanically strong TiO_2 nanowire foams and presented in this study. A 300% increase in elastic modulus achieved in the SMPCs relative to that observed in the corresponding SMP, which is much higher than the enhancement predicted by the well-known Halpin-Tsai model (~80%), will be discussed. Finally, the shape memory properties of the SMPCs and their behavior under cyclic compression will be discussed in detail in this paper.

Experimental Details

Materials

Polyvinylpyrrolidone (PVP) with average molecular weight of 360,000 g/mol and $(NH_4)_2CO_3$ were obtained from Sigma-Aldrich. All the chemicals were used without further purification. The source of other chemicals has been listed in the previous chapters.

Procedure

As depicted in **Figure 29**, preparation of a SMPC required five major steps: (1) silanization of TiO$_2$ nanowires, (2) synthesis of space holder microcrystals by antisolvent crystallization, (3) pelletization of TiO$_2$ nanowires and the space holder, (4) evaporation of the space holder, and (5) infiltration of an epoxy resin into nanowire foams.
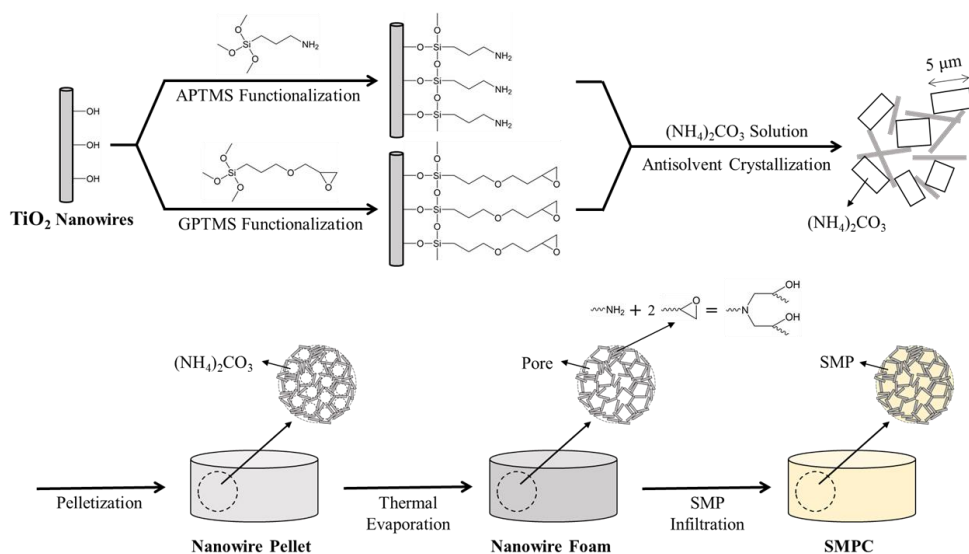
Figure 29 A schematic illustration representing the steps involved in the fabrication of SMPCs reinforced with TiO$_2$ nanowire foams

The first step is to functionalize TiO_2 nanowires with APTMS and GPTMS. Prior to silanization, TiO_2 nanowires were exposed to O_2 plasma (plasma cleaner PDC-32G, Harrick Plasma) for 20 minutes to introduce hydroxyl groups on their surfaces [248]. Following this, functionalization of TiO_2 nanowire surfaces with APTMS or GPTMS was performed using the vapor-phase functionalization method in a commercially-available stainless-steel vacuum chamber (AblazeCustom) as follows. In a typical procedure, plasma-treated TiO_2 nanowires were spread as a thin layer in a polypropylene container and exposed to an organosilane placed in an adjacent polypropylene container inside the vacuum chamber. Subsequently, the vacuum chamber was evacuated to <3 Torr using a mechanical rotary pump, while the vacuum chamber was heated to an elevated temperature using heating tapes. The temperatures of the chamber were maintained at 25 °C and 90 °C, respectively, for nanowire functionalization by APTMS and GPTMS. This procedure lasted a duration of 1 hour.

Subsequently, an *in-situ* method for simultaneously synthesizing $(NH_4)_2CO_3$ microcrystals and mixing the microcrystals with TiO_2 nanowires was performed. Considering that fabrication of a densely crosslinked foam requires reducing the pore sizes, crystals with smaller sizes are preferred as a space holder. Similar to our attempts of mass producing nanowires using porous foams [165], Attempts to obtain $(NH_4)_2CO_3$ microcrystals using a well-known mechanochemical method [263, 264], or simple grinding, resulted in irregular shaped crystals that had wide distribution of sizes. Antisolvent crystallization [265, 266], which has been widely used to crystallize pharmaceuticals [267, 268], was therefore employed as an alternative. In a typical process,

0.45 g APTMS-functionalized nanowires and 0.45 g GPTMS-functionalized nanowires were first fully dispersed in 18 mL of 1 wt.% PVP aqueous solution. Next, 4.5 g $(NH_4)_2CO_3$ was dissolved into this nanowire dispersion, and the dispersion was quickly poured into 90 mL of refrigerated acetone (-7 °C) under constant stirring. White powder formed immediately and precipitated quickly to the bottom of the container. The precipitate was filtered and washed with acetone three times to remove water. Subsequently, the precipitate was dried naturally in a fume hood.

The dried mixture of APTMS- and GPTMS-functionalized TiO_2 nanowires and $(NH_4)_2CO_3$ microcrystals was consolidated into pellets by a uniaxial press at a pressure of 350 MPa at room temperature. A custom-made stainless-steel die was employed for this purpose. Then 1.2 cm-diameter pellets thus obtained were heated at 60 °C for 4 hours in an oven, for removing the $(NH_4)_2CO_3$ by thermal decomposition into NH_3, H_2O and CO_2. Subsequently, the nanowire foams thus obtained were dried at 120 °C for 2 hours. This step also aided in the formation of bonds between the epoxide groups of GPTMS and amine groups of APTMS. For comparison purposes, unfunctionalized TiO_2 nanowires were also fabricated into foams using the same procedure described above.

Finally, NGDE and Jeffamine D230 were fully mixed at a mole ratio of 2:1, and the resin was infiltrated into the TiO_2 nanowire foams under a vacuum. After the samples were fully degassed, the resin was cured at 100 °C for 90 minutes and 130 °C for 60 minutes, respectively. The samples examined in this study have been listed in **Table 15**.

Table 15 A list of all the SMPs, nanowire foams, and SMPCs prepared in this study

Sample	Type	Description
Reference #1	SMP	Composed of NGDE and Jeffamine D230 in 2:1 mole ratio
Foam #1	Nanowire foam	Made by consolidating as-obtained TiO_2 nanowires and $(NH_4)_2CO_3$ microcrystals into cylindrical pellets, followed by removal of the $(NH_4)_2CO_3$ microcrystal space holders
Foam #2	Nanowire foam	Made by consolidating APTMS- and GPTMS-functionalized TiO_2 nanowires and $(NH_4)_2CO_3$ microcrystals into cylindrical pellets, followed by removal of the $(NH_4)_2CO_3$
Reference #2	SMPC	Made by casting a mixture of the SMP and TiO_2 nanowires
SMPC #1	SMPC	Composed of Foam #1 infiltrated with the SMP
SMPC #2	SMPC	Composed of Foam #2 infiltrated with the SMP

Characterization

The morphology of TiO_2 nanowires, the crystal size of $(NH_4)_2CO_3$, and the inner structure of TiO_2 nanowire foams were observed by Scanning Electron Microscopy (SEM). The presence of functional groups grafted on TiO_2 nanowires was confirmed by Fourier-transform Infrared Spectroscopy (FTIR) using Nicolet IR100 (Thermo Fisher Scientific). The mechanical properties of TiO_2 nanowire foams and foam composites were examined by compression test performed by Instron 5944. For this purpose, the crosshead speed was set at 1 mm/min, and the specimens were compressed until the compressive strains reached 0.2. To ensure reproducibility of the results, six specimens were tested for

each sample. For cyclic compression test, the crosshead speed, the compressive strain, and the number of cycles were 1 mm/min, 0.1, and 250.

Results

Characterization of TiO_2 Nanowires and $(NH_4)_2CO_3$ Microcrystals

Figure 30(a) represents the typical morphology of TiO_2 nanowires imaged by SEM. As mentioned previously, most of the nanowires had diameters ranging from 200 to 300 nm and lengths ranging from 2 to 4 μm. It is therefore estimated that the average aspect ratio of these nanowires was 10.

In order to examine the effectiveness of antisolvent crystallization process, the sizes of the as-received $(NH_4)_2CO_3$ crystals (**Figure 30(b)**) and those of the as-synthesized microcrystals (**Figure 30(c) and (d)**) were compared. While the as-obtained $(NH_4)_2CO_3$ crystals had a very wide crystal size distribution, ranging from a few microns to hundreds of microns, most of the $(NH_4)_2CO_3$ microcrystals produced by the antisolvent crystallization process had the size of a few microns. Moreover, the size distribution of the $(NH_4)_2CO_3$ microcrystals was narrower.
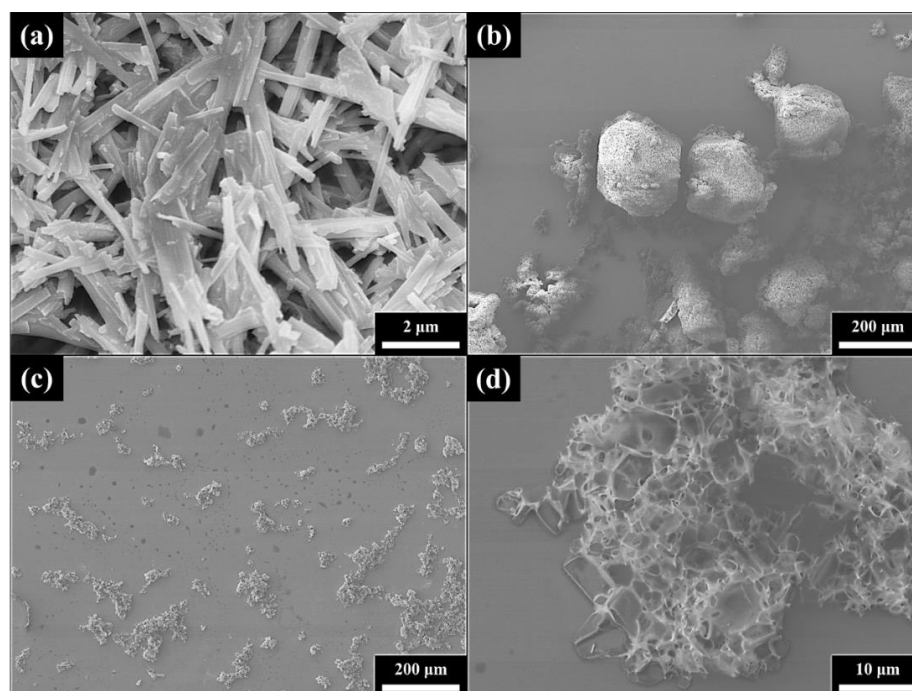
Figure 30 Scanning electron micrographs of (a) TiO₂ nanowires, (b) as-received (NH₄)₂CO₃ crystals, and (c) and (d) (NH₄)₂CO₃ microcrystals produced by antisolvent crystallization at lower and higher magnifications, respectively

Characterization of Nanowire Foams

Optical micrographs of Foam #2, SMPC #2, and Reference #1 are presented in **Figure 31(a)**. In all, the nanowire foam cylinders retained their shape after polymer infiltration for the formation of SMPCs.

SEM analyses of the inner structure of Foam #2 indicated a highly porous, interconnected nanowire structure (**Figure 31(c) and (d)**). Since the size of the space holder is on the order of a few microns, the spacing between the nanowires is also in a similar range. Accordingly, the use of $(NH_4)_2CO_3$ is an effective approach to producing a porous structure, given that direct compression of nanowires without $(NH_4)_2CO_3$ generated only a fraction of porosity (**Figure 31(b)**). Due to the loss of $(NH_4)_2CO_3$ during

the antisolvent crystallization and subsequent drying processes, the final fraction of TiO_2

nanowires became 22 wt.% (8 vol.%), after the thermally-assisted removal of all the

$(NH_4)_2CO_3$ crystals. Overall, the porosity of the as-synthesized TiO_2 nanowire foams was

around 92% for both Foam #1 and #2.
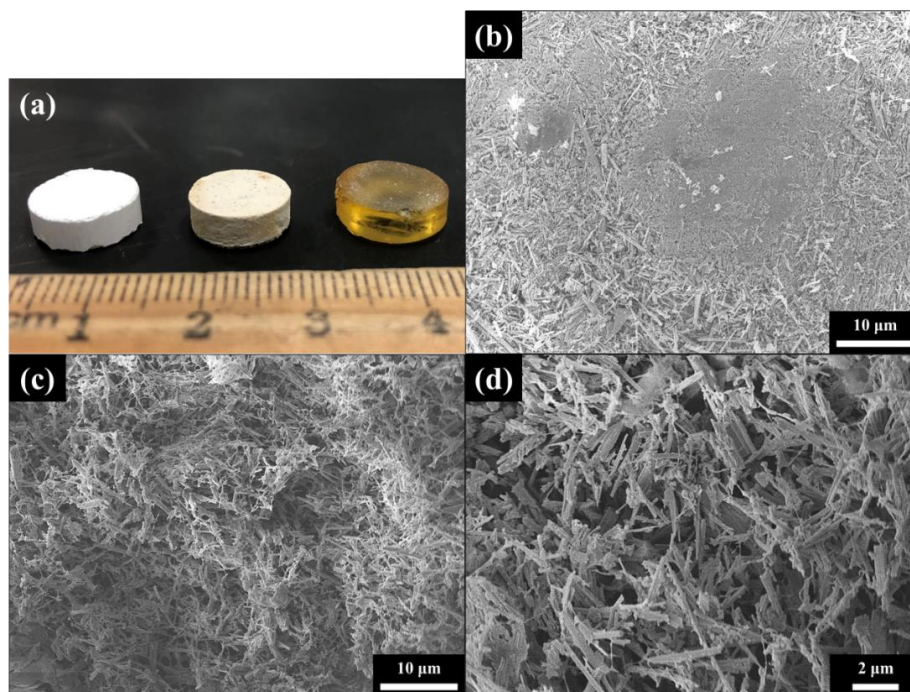
Figure 31 (a) A photograph of Foam #2, SMPC #2, and Reference #1. Due to the excess epoxy being polished off from the surface, the SMPC specimen may look slightly smaller than the other two. (b) A scanning electron micrograph of the inner structure of a pellet compressed by only TiO_2 nanowires without $(NH_4)_2CO_3$. Scanning electron micrographs of Foam #2 in a (c) low and (d) high magnification, respectively

<u>Mechanical Properties of Nanowire Foam Composites</u>

Compression Test

The compressive stress-strain curves of Reference #1, Reference #2, SMPC #1 and SMPC #2 samples are shown in **Figure 32**, and their elastic moduli are also summarized in **Table 16**. When compared to Reference #1 that exhibits an elastic modulus of 5.98 MPa, SMPC #2 exhibited a remarkably improved elastic modulus of 25.60 MPa. In contrast, the elastic moduli of Reference #2 and SMPC #1 were improved only to 10.09 and 14.88 MPa, respectively. Taking the nanowire aspect ratio of 10, the density of 3.84 g/cm^3, and the elastic modulus of 170 GPa for anatase TiO_2 [269], the theoretical value of the elastic modulus of 22 wt.% (8 vol.%) of the TiO_2 nanowire-epoxy composite is expected to be 11 MPa using the Halpin-Tsai model, which is closed to the experimental values obtained for Reference #2 samples. This indicates prefabrication of filler foams and their subsequent infiltration with polymers is a better route for the fabrication of composites, relative to casting of mixtures of polymers matrices and fillers. A major difference between SMPC #1 and SMPC #2 is the type of bond formed among the nanowires. While simple Van der Waals interaction exists between the nanowires in SMPC #1[199, 201], covalent bonds between the amine and the epoxide groups exists between the APTMS- and GPTMS-functionalized nanowires in SMPC #2.
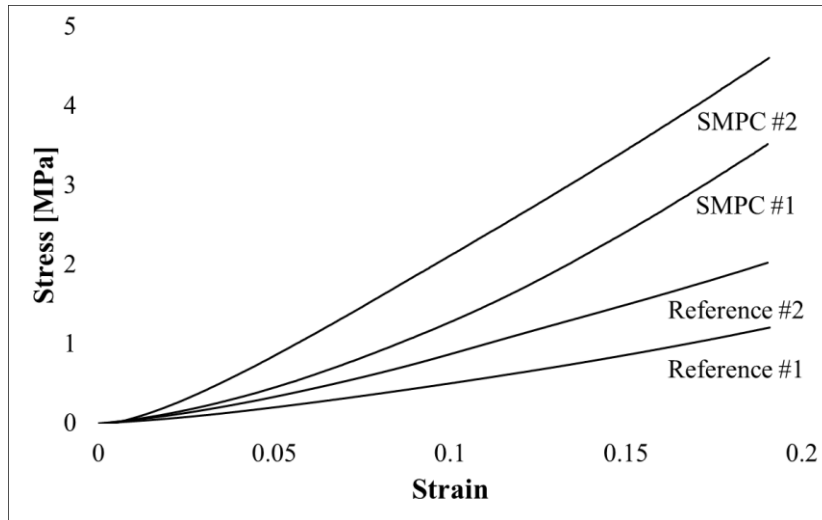
Figure 32 Stress-strain curves of SMPC #1 and SMPC #2 fabricated in this study. For reference, stress-strain curves of Reference #1 and Reference #2 are also included in the figure

Table 16 Elastic moduli of the References and SMPCs

Sample	E_c [MPa]	Change
Reference #1	5.98	-
Reference #2	10.09	69%
SMPC #1	14.88	149%
SMPC #2	25.60	328%

Cyclic Compression Test

Figure 33(a) shows the representative cyclic behavior of Reference #1 and SMPC #2. The loading/unloading curves of Reference #1 followed almost the same path over 250 cycles, whereas SMPC #2 demonstrated cyclic stress softening, where the maximum stress of each cycle decreased with respect to the number of cycles, well-known as the Mullins effect [270]. This decrease in stress is only pronounced in the first several cycles

102

(typically 5-10 cycles). The Mullins effect is a phenomenon commonly observed in filled rubbers, yet many composite hydrogels also exhibit this type of behavior in cyclic tests [271, 272].

One of the features of the Mullins effect is that the stress reduction can be recovered if the composite is allowed to relax for a period of time (typically at an elevated temperature). As shown in **Figure 33(b)**, the second cyclic behavior of the same SMPC #2 specimen was almost identical after the specimen was treated at 100 °C for 2 hours.

To date, a consensus on the physical mechanism of the Mullins effect has not been achieved [273], but several models have been developed to explain this phenomenon, including bond rupture, molecules slipping, filler rupture, disentanglement, and double layer models [273]. With the intent of understanding the physical source of the Mullins effect in SMPC #2, several derivatives of foam composites, including normal composites, were fabricated. **Figure 33(b)** also shows the cyclic stress-strain curves of Reference #1 and #2. Given that a hysteresis was not observed for Reference #1, it can be excluded the possibility that cyclic stress softening was caused by polymer chain ruptures or slippage. For Reference #2, a slight decrease in stress was observed, probably resulted from filler-filler ruptures or bond ruptures between nanowires and an epoxy matrix, but the effect is relatively minor. On the other hand, a significant hysteresis was observed for SMPC #2. It has been reported that the formation of a filler network, or percolation, within a rubbery matrix plays an important role in the Mullins effect [274]. For instance, Ivanoska-Dacikj *et al.* observed that, for a natural rubber reinforced by multiwalled carbon nanotubes (MWCNTs), stress softening became profound when the MWCNT loading exceeded the

percolation threshold [275]. Therefore, it is postulated that the reduction in modulus may be ascribed to the temporary alteration of the microstructure of a nanowire foam over loading/unloading cycles.
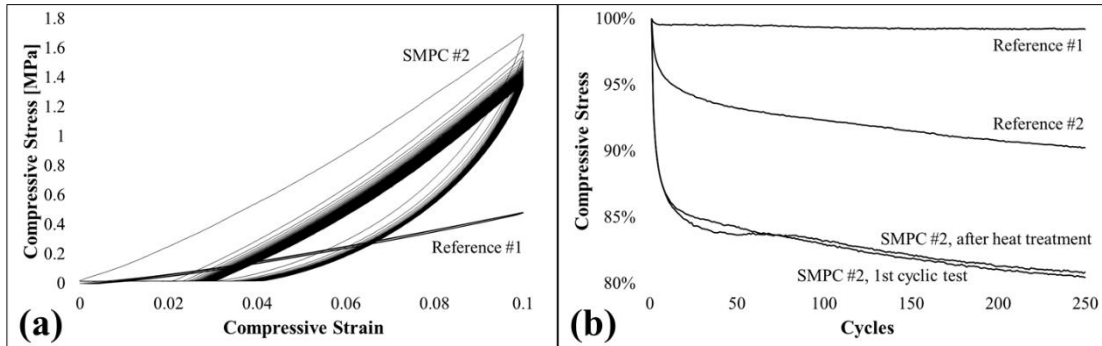
Figure 33 (a) Cyclic stress-strain curves of Reference #1 and SMPC #2. (b) Residual stress with respect to the number of cycles of Reference #1, Reference #2, and SMPC #2 at the first and subsequent cycles

Shape Memory Properties of Nanowire Foam Composites

In order to confirm that the addition of nanowire foams does not deteriorate shape memory properties of the epoxy, a simple shape recovery experiment was performed. Two stripes of Reference #1 and SMPC #2 were first bent at the same angle, then the shape of these two stripes was fixed in refrigerated water, and they were dropped in hot water to initiate shape recovery. **Figure 34** shows a series of snapshots of shape recovery process, in which both bent stripes recovered back to the original, straight form quickly. Therefore, both Reference #1 and SMPC #2 were capable of recovering back to their original shape when they were thermally activated. This suggests that the use of nanowire foams as reinforcements didn't deteriorate the shape memory properties.
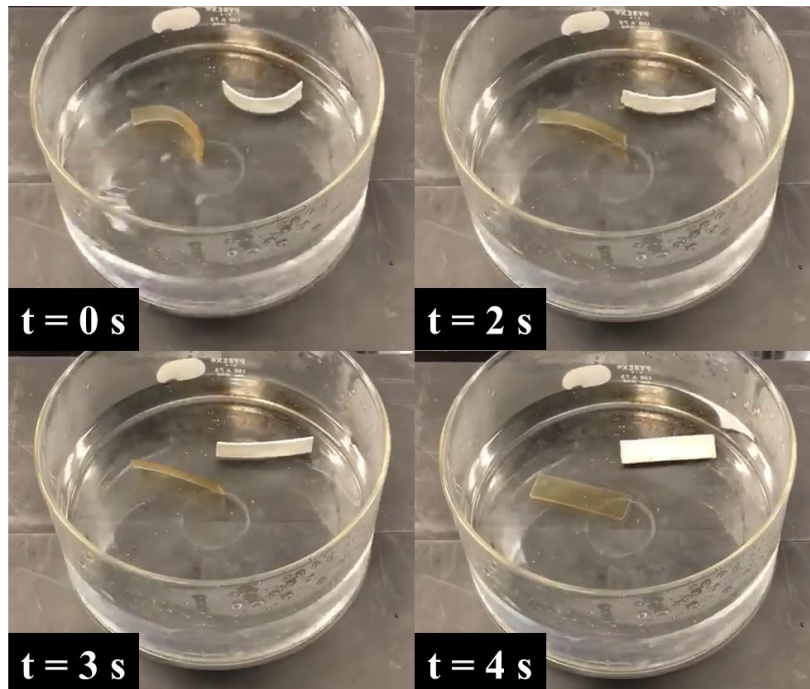
Figure 34 A series of snapshots of shape recovery process. Before being submerged into hot water, both Reference #1 and SMPC #2 stripes were bent and fixed at the same angle. Both of them recovered back to the original shape quickly, no significant difference being observed

Discussion

Role of Polyvinylpyrrolidone

The addition of a small amount of a polymer as a binder is a very common approach to make a foam more robust. For example, Tang *et al.* added polyvinyl alcohol to a Cu nanowire aerogel monolith during synthesis, which substantially improved its mechanical performance [192]. In this study, PVP was used as the binder. For comparison, a nanowire foam without PVP was fabricated, but it was found that the nanowire foam was too fragile and collapsed during the removal of $(NH_4)_2CO_3$.

It has been reported that many water-soluble polymers, such as PVP, are able to break up agglomerates of nanoparticles and stabilize the dispersion [276-278]. Furthermore, PVP also facilitated a uniform mixing of TiO_2 nanowires and $(NH_4)_2CO_3$ crystals during the antisolvent crystallization process. Given that PVP is soluble in water but not in most of organic solvents, e.g., acetone, when an aqueous solution of $(NH_4)_2CO_3$, TiO_2 nanowires, and PVP was poured into acetone, not only $(NH_4)_2CO_3$ crystals but also PVP precipitated simultaneously. During this precipitation process, PVP molecules quickly wrapped up both TiO_2 nanowires and $(NH_4)_2CO_3$ crystals, which prevented the separation of nanowires and $(NH_4)_2CO_3$ crystals during precipitation. As shown in **Figure 35(a) and (b)**, all the particles sedimented quickly with PVP, whereas some TiO_2 nanowires were still suspended in the dispersion if antisolvent crystallization of $(NH_4)_2CO_3$ crystals took place without PVP. Accordingly, a well-dispersed mixture of nanowires and $(NH_4)_2CO_3$ crystals was attained after dried, as shown in **Figure 35(c)**. On the contrary, if they were mixed in the state of dry powders, instead of a well-dispersed mixture of individual nanowires and $(NH_4)_2CO_3$ crystals, a mixture of their agglomerates was obtained. In this case, the as-synthesized nanowire foams cannot fully utilize the mechanical strength of nanowires.

As a comparison, a nanowire foam was produced via pelletization of PVP-treated TiO_2 nanowires and $(NH_4)_2CO_3$ crystals (produced by antisolvent crystallization) in dry powders (namely, nanowires and $(NH_4)_2CO_3$ were not mixed in a solvent). After $(NH_4)_2CO_3$ was removed, it was found that the entire structure collapsed by itself. This result can be attributed to two factors: (1) non-uniform mixing of nanowires and

(NH$_4$)$_2$CO$_3$, as discussed above, and (2) the excessively large pores, perhaps up to even hundreds of μm, created by large (NH$_4$)$_2$CO$_3$ crystal agglomerates. Due to the sparsely connected structure, this type of nanowire foams were too fragile to maintain their structure integrity.
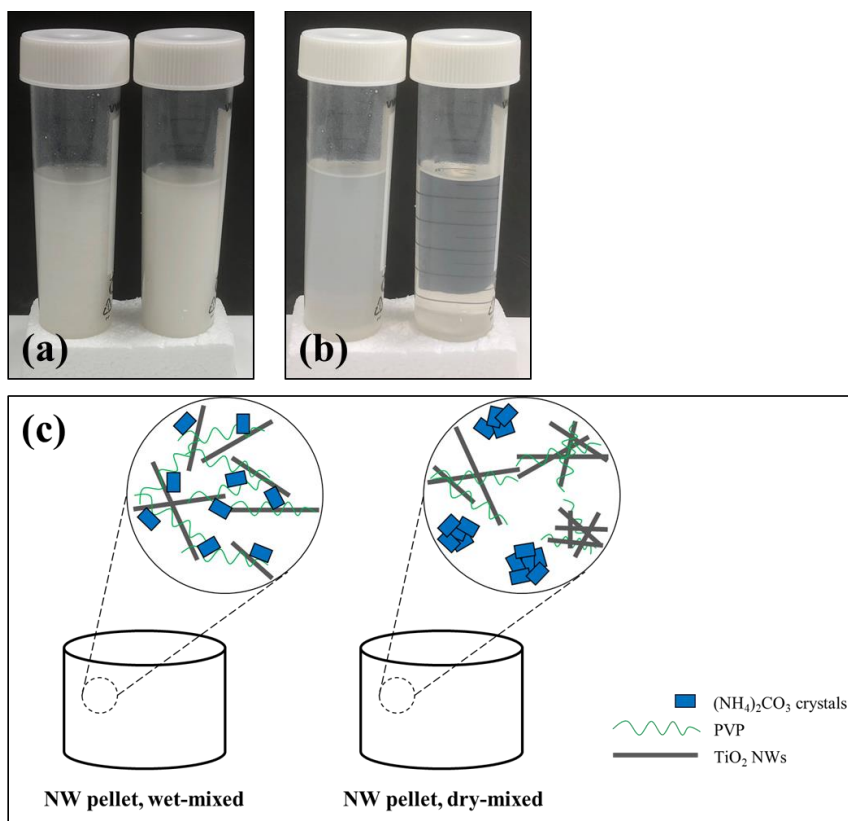
Figure 35 Photographs of the acetone dispersion of TiO$_2$ nanowires with (NH$_4$)$_2$CO$_3$ microcrystals produced by antisolvent crystallization with no PVP (left) and with PVP (right), (a) taken immediately after the dispersion was vigorously shaken, and (b) taken 30 minutes after allowing the particles to sediment by gravity. (c) A scheme of the microstructures of the nanowire pellets produced from wet- and dry-mixed powders, which were subsequently used for synthesis of nanowire foams after (NH$_4$)$_2$CO$_3$ was thermally removed

Conclusions

In this study, a non-conventional approach was employed to fabricate a nanowire-based SMPCs. Nanowire foams were produced by a powder metallurgy technique, where $(NH_4)_2CO_3$ was selected a space holder. In order to produce nanowire foams with a more closely packed structure, $(NH_4)_2CO_3$ microcrystals were synthesized via antisolvent crystallization. After thermal treatment, the nanowire foams were crosslinked and subsequently infiltrated with an epoxy resin. The resulting foam composite exhibited a remarkable elastic modulus, with more than 300% improvement compared to the epoxy. Considering that powder metallurgy has been extensively performed to produce various parts and products in the industry, this approach enables to fabricate shape memory devices based on foam composites with different shapes and dimensions.

CHAPTER VI

SUMMARY AND FUTURE WORK

Summary of Work

Overall, this dissertation consists of three sections: (1) synthesis of nanowires in a byproduct-free manner using a sacrificial salt, (2) examination of the effects of filler-matrix interaction on the mechanical properties of the nanowire-based epoxy composite, and (3) fabrication of foam composites by powder metallurgy with a space holder. It is worth noting that the employment of sacrificial materials is a powerful method for both the mass production of nanowires and the fabrication of nanocomposites from the mass-produced nanowires.

In Chapter II, porous Zn pellets were produced by powder metallurgy with NH_4Cl as a space holder, and they were subsequently used as a substrate to grow Zn_3P_2 nanowires. The as-grown Zn_3P_2 nanowires contained no byproduct. This study hopefully provides a new avenue to synthesize nanomaterials in a non-traditional approach, as well as enables the exploration of the possibility of nanowire-based devices, provided that the applications of nanowires require large quantities of byproduct-free nanowires.

In Chapter III and Chapter IV, the epoxy composites reinforced by Zn_3P_2 and TiO_2 nanowires were respectively fabricated, and the effects of these nanowires on the mechanical properties were examined. Given the variances in their surface characteristics, it was found that Zn_3P_2 and TiO_2 nanowires interact with an epoxy matrix in different manners. For Zn_3P_2 nanowires, provided that epoxy monomers cannot bind with their

oxide surface, i.e., $Zn_3(PO_4)_2$, the addition of pristine nanowires resulted in no change or even slight reduction in the tensile strength and elastic modulus. On the other hand, the TiO_2 nanowire-epoxy composite exhibited enhanced mechanical performance compared to the epoxy, owing to the formation of a good interface by the reaction between the surface hydroxyl groups on the nanowires and epoxy monomers. This observation will offer a guideline of selection for appropriate types of fillers as reinforcements for polymeric materials, from the perspective of epoxy interaction with the nanowire surfaces.

Furthermore, the effects of the degree of interactions, i.e., interfacial adhesion, on the mechanical properties of the nanocomposite were studied. The surface characteristics of these two nanowires were respectively engineered by two types of coupling agents, i.e., thiols and organosilanes. For Zn_3P_2 nanowires, 4ATP and 4tBTP were applied to produce good and poor interfaces, respectively, where improvement and deterioration in mechanical properties were obtained as speculated. This showed that, when interfacial adhesion between nanowires and a matrix is not sufficiently strong, the use of coupling agents will mainly impact the interfacial bonding. In contrast, TiO_2 nanowires were respectively functionalized by APTMS and GPTMS. Thereupon, it was expected to produce improved interfaces but by different degrees; namely, because of the difference in the number bonds formed between nanowires and the matrix, APTMS-functionalized nanowires will have a stronger interface than GPTMS-functionalized nanowires, even though both of them will produce stronger interface than pristine nanowires. Nevertheless, despite the fact that these two nanocomposites successfully exhibited enhanced mechanical properties than the epoxy composite reinforced by pristine TiO_2 nanowires,

110

no discrepancies in mechanical properties were attained between the composites reinforced by APTMS- and GPTMS-functionalized nanowires. In view of this, their fracture surfaces were inspected, and it was observed that APTMS and GPTMS were able to improve the degree of dispersion of nanowires within the epoxy matrix by almost the same degree. This concluded that, when strong interfacial adhesion has been achieved, the application of coupling agents has only minor effects on the degree of interactions, while the enhancement in the mechanical performance of a nanocomposite is attributed to the higher degree of nanowire dispersion. These results may explain some ambiguities found in literature, such as the reasons for the improved mechanical properties of nanocomposites by the functionalization of nanofillers.

Finally, with the intent of fabricating a nanowire-based epoxy composite with considerably enhanced mechanical properties, as well as studying the effects of nanowire-nanowire interactions, foam composites were developed in Chapter V. Considering that an interconnected filler network results in a significant reinforcement, it was proposed to use nanowire foams as fillers. The nanowire foams were synthesized by a powder metallurgy technique with $(NH_4)_2CO_3$ as a sacrificial salt. Based on compression test, more than 300% enhancement in elastic modulus was obtained, superior to the prediction made by the Halpin-Tsai model (~80%). Hopefully this study opens an avenue for fabricating a nanocomposite with excellent properties.

Future Research Directions

Byproduct-free Production of Nanowires

A novel concept, in which highly porous Zn pellets were used as both the reactant and the substrate to synthesize Zn_3P_2 nanowires, was successfully demonstrated in this dissertation. Reasonable extensions to this work are (1) to synthesize other types of nanowires, e.g., ZnO, CuO and TiO_2 nanowires, from porous pellets of corresponding metals; (2) to synthesize nanowires from porous sheets that have large areas. Former will prove this method is generic and not specific to Zn_3P_2 nanowires, while latter aids in achieving nanowire mass production with the simultaneous production of no byproducts.

Nanowire-based Polymer Composites

In this dissertation, an epoxy was used as the matrix to study the effects of nanowires as reinforcements. Considering that an epoxy is amorphous in nature, the addition of nanowires did not cause any changes in crystallinity and glass transition behavior of the matrix. Typically, if a crystalline or semicrystalline polymer are used as the matrix, the addition of fillers alters the crystallinity and glass transition temperature, resulting in changes in mechanical and thermal performances. For example, when nanowires are incorporated into a semicrystalline polymer, the crystallinity and the glass transition temperature will increase, given that fillers serves as heterogeneous nucleation sites for polymer crystallization [181, 184, 186]. Nevertheless, the effect of surface characteristics of fillers on these changes has not been examined yet. Therefore, addition

of nanowires into a crystalline or semicrystalline polymer might be of interest to investigate, especially the effects of nanowires with different surface characteristics on crystallinity and glass transition temperature.

Besides, as mentioned briefly in Chapter III, the epoxy used in this dissertation exhibit shape memory effects. Notwithstanding, the effects of nanowires on the shape memory properties were not discussed in details. Based on tensile test, significant improvements on elastic modulus at room temperature (below T_g) was observed, whereas mechanical properties at elevated temperatures (above T_g) were not examined. Considering that a shape memory polymer needs to be designed to be capable of maintaining its structural integrity during deformation and shape recovery at temperatures above and below its T_g, mechanical properties above T_g is of great interest to complement the understanding of the effects of nanowires on the mechanical properties of a shape memory polymer.

Nanowire Foam Polymer Composites

In terms of foam composites, one another direction might be of interest to pursue. Given that the ease of the formation of an interconnected structure of particles is dependent on their aspect ratio, the nanowires with higher aspect ratios are more preferable to be employed to fabricate nanowire foams. Since the nanowires used in this dissertation has aspect ratios of only 10–20, it is expected that the same or even greater mechanical performance can be achieved with far lower a nanowire loading, if nanowire foams or foam composites are produced from nanowires with much higher aspect ratios.

REFERENCES

1.   Sun, J. and S.L. Simon, *The melting behavior of aluminum nanoparticles.* Thermochimica Acta, 2007. **463**(1-2): p. 32-40.

2.   Sheng, H.W., et al., *Superheating and melting-point depression of Pb nanoparticles embedded in Al matrices.* Philosophical Magazine Letters, 1996. **73**(4): p. 179-186.

3.   Daniel, M.C. and D. Astruc, *Gold nanoparticles: Assembly, supramolecular chemistry, quantum-size-related properties, and applications toward biology, catalysis, and nanotechnology.* Chemical Reviews, 2004. **104**(1): p. 293-346.

4.   Haruta, M., *When gold is not noble: catalysis by nanoparticles.* The Chemical Record, 2003. **3**(2): p. 75-87.

5.   Wu, Y., W. Tsui, and T. Liu, *Experimental analysis of tribological properties of lubricating oils with nanoparticle additives.* Wear, 2007. **262**(7-8): p. 819-825.

6.   Gulzar, M., et al., *Tribological performance of nanoparticles as lubricating oil additives.* Journal of Nanoparticle Research, 2016. **18**(8): p. 223.

7.   Corma, A. and H. Garcia, *Supported gold nanoparticles as catalysts for organic reactions.* Chemical Society Reviews, 2008. **37**(9): p. 2096-2126.

8.   Astruc, D., F. Lu, and J.R. Aranzaes, *Nanoparticles as recyclable catalysts: the frontier between homogeneous and heterogeneous catalysis.* Angewandte Chemie International Edition, 2005. **44**(48): p. 7852-7872.

9.   Mashford, B.S., et al., *High-efficiency quantum-dot light-emitting devices with enhanced charge injection.* Nature Photonics, 2013. **7**(5): p. 407-412.

10.   Shirasaki, Y., et al., *Emergence of colloidal quantum-dot light-emitting technologies.* Nature Photonics, 2013. **7**(1): p. 13.

11.   Soppimath, K.S., et al., *Biodegradable polymeric nanoparticles as drug delivery devices.* Journal of Controlled Release, 2001. **70**(1-2): p. 1-20.

12.   De Jong, W.H. and P.J. Borm, *Drug delivery and nanoparticles: applications and hazards.* International Journal of Nanomedicine, 2008. **3**(2): p. 133.

13.   Chan, W.C. and S. Nie, *Quantum dot bioconjugates for ultrasensitive nonisotopic detection.* Science, 1998. **281**(5385): p. 2016-2018.

14.   Wang, S., et al., *Antigen/antibody immunocomplex from CdTe nanoparticle bioconjugates.* Nano Letters, 2002. **2**(8): p. 817-822.

15.   Ali, A., et al., *Nanowire-based thermoelectrics.* Nanotechnology, 2017. **28**(28).

16.   Brockway, L., et al., *Large-scale synthesis and in situ functionalization of Zn_3P_2 and Zn_4Sb_3 nanowire powders.* Physical Chemistry Chemical Physics, 2013. **15**(17): p. 6260-6267.

17.   Gordon, M.J., et al., *Size effects in mechanical deformation and fracture of cantilevered silicon nanowires.* Nano Letters, 2009. **9**(2): p. 525-529.

18.   Hsin, C.L., et al., *Elastic properties and buckling of silicon nanowires.* Advanced Materials, 2008. **20**(20): p. 3919-3923.

19.   Wu, B., A. Heidelberg, and J.J. Boland, *Mechanical properties of ultrahigh-strength gold nanowires.* Nature Materials, 2005. **4**(7): p. 525-529.

20.   Yang, P., et al., *Controlled growth of ZnO nanowires and their optical properties.* Advanced Functional Materials, 2002. **12**(5): p. 323-331.

21.   Rao, C., et al., *Inorganic nanowires.* Progress in Solid State Chemistry, 2003. **31**(1-2): p. 5-147.

22.   Lu, W. and C.M. Lieber, *Semiconductor nanowires.* Journal of Physics D: Applied Physics, 2006. **39**(21): p. R387.

23.   Callister, W.D. and D.G. Rethwisch, *Materials science and engineering: an introduction.* Vol. 7. 2007: John wiley & sons New York.

24.   Soutis, C., *Carbon fiber reinforced plastics in aircraft construction.* Materials Science and Engineering: A, 2005. **412**(1-2): p. 171-176.

25.   Yu, M.-F., et al., *Tensile loading of ropes of single wall carbon nanotubes and their mechanical properties.* Physical Review Letters, 2000. **84**(24): p. 5552.

26.   Yu, M.-F., et al., *Strength and breaking mechanism of multiwalled carbon nanotubes under tensile load.* Science, 2000. **287**(5453): p. 637-640.

27.   Ajayan, P., et al., *Aligned carbon nanotube arrays formed by cutting a polymer resin-nanotube composite.* Science-AAAS-Weekly Paper Edition, 1994. **265**(5176): p. 1212-1214.

28.   Iijima, S., *Helical microtubules of graphitic carbon.* Nature, 1991. **354**(6348): p. 56.

29.   Vivekchand, S., U. Ramamurty, and C. Rao, *Mechanical properties of inorganic nanowire reinforced polymer-matrix composites.* Nanotechnology, 2006. **17**(11): p. S344.

30. Denver, H., et al., *Fabrication of polydimethylsiloxane composites with nickel nanoparticle and nanowire fillers and study of their mechanical and magnetic properties.* Journal of Applied Physics, 2009. **106**(6): p. 064909.

31. Ayatollahi, M., et al., *Effect of multi-walled carbon nanotube aspect ratio on mechanical and electrical properties of epoxy-based nanocomposites.* Polymer Testing, 2011. **30**(5): p. 548-556.

32. Lonjon, A., et al., *Mechanical improvement of P(VDF-TrFE)/nickel nanowires conductive nanocomposites: Influence of particles aspect ratio.* Journal of Non-crystalline Solids, 2012. **358**(2): p. 236-240.

33. Favier, V., et al., *Mechanical percolation in cellulose whisker nanocomposites.* Polymer Engineering & Science, 1997. **37**(10): p. 1732-1739.

34. Park, S.-H. and P.R. Bandaru, *Improved mechanical properties of carbon nanotube/polymer composites through the use of carboxyl-epoxide functional group linkages.* Polymer, 2010. **51**(22): p. 5071-5077.

35. Han, Y. and J. Elliott, *Molecular dynamics simulations of the elastic properties of polymer/carbon nanotube composites.* Computational Materials Science, 2007. **39**(2): p. 315-323.

36. Frankland, S., et al., *The stress-strain behavior of polymer-nanotube composites from molecular dynamics simulation.* Composites Science and Technology, 2003. **63**(11): p. 1655-1661.

37. Guth, E., *Theory of filler reinforcement.* Journal of Applied Physics, 1945. **16**(1): p. 20-25.

38. Halpin, J.C., *Stiffness and Expansion Estimates for Oriented Short Fiber Composites.* Journal of Composite Materials, 1969. **3**(4): p. 732-&.

39. Affdl, J.H. and J. Kardos, *The Halpin-Tsai equations: a review.* Polymer Engineering & Science, 1976. **16**(5): p. 344-352.

40. Sun, Y. and Y. Xia, *Large-scale synthesis of uniform silver nanowires through a soft, self-seeding, polyol process.* Advanced Materials, 2002. **14**(11): p. 833-837.

41. Greene, L.E., et al., *Low-temperature wafer-scale production of ZnO nanowire arrays.* Angewandte Chemie International Edition, 2003. **42**(26): p. 3031-3034.

42. Song, X.C., et al., *Large-scale hydrothermal synthesis of WO$_3$ nanowires in the presence of K$_2$SO$_4$.* Materials Letters, 2007. **61**(18): p. 3904-3908.

43. Chang, Y., M.L. Lye, and H.C. Zeng, *Large-scale synthesis of high-quality ultralong copper nanowires.* Langmuir, 2005. **21**(9): p. 3746-3748.

44. Banerjee, D., et al., *Large-quantity free-standing ZnO nanowires.* Applied Physics Letters, 2003. **83**(10): p. 2061-2063.

45. Jiang, X., T. Herricks, and Y. Xia, *CuO nanowires can be synthesized by heating copper substrates in air.* Nano Letters, 2002. **2**(12): p. 1333-1338.

46. Wan, Q., et al., *Low-field electron emission from tetrapod-like ZnO nanostructures synthesized by rapid evaporation.* Applied Physics Letters, 2003. **83**(11): p. 2253-2255.

47. Zhou, W.M., et al., *Large-scale synthesis and characterization of SiC nanowires by high-frequency induction heating.* Applied Surface Science, 2006. **252**(14): p. 5143-5148.

48. Chang, P.-C., et al., *ZnO nanowires synthesized by vapor trapping CVD method.* Chemistry of Materials, 2004. **16**(24): p. 5133-5137.

49. Thangala, J., et al., *Large-scale, Hot-filament-assisted Synthesis of Tungsten Oxide and Related Transition Metal Oxide Nanowires.* Small, 2007. **3**(5): p. 890-896.

50. Xiang, X., et al., *Large-scale crystalline GaN nanowires synthesized through a chemical vapor deposition method.* Applied Physics A, 2005. **80**(5): p. 1129-1132.

51. Kumar, V., et al., *Alkali-assisted, atmospheric plasma production of titania nanowire powders and arrays.* Crystal Growth & Design, 2011. **11**(7): p. 2913-2919.

52. Lan, X., et al., *Fiber reinforced shape-memory polymer composite and its application in a deployable hinge.* Smart Materials and Structures, 2009. **18**(2): p. 024002.

53. Lendlein, A. and R. Langer, *Biodegradable, elastic shape-memory polymers for potential biomedical applications.* Science, 2002. **296**(5573): p. 1673-1676.

54. Liu, C., H. Qin, and P.T. Mather, *Review of progress in shape-memory polymers.* Journal of Materials Chemistry, 2007. **17**(16): p. 1543-1558.

55. Mu, T., et al., *Shape memory polymers for composites.* Composites Science and Technology, 2018. **160**: p. 169-198.

56. Meng, H. and G. Li, *A review of stimuli-responsive shape memory polymer composites.* Polymer, 2013. **54**(9): p. 2199-2221.

57. Liu, Y.J., et al., *Review of electro-active shape-memory polymer composite.* Composites Science and Technology, 2009. **69**(13): p. 2064-2068.

58.   Meng, Q.H. and J.L. Hu, *A review of shape memory polymer composites and blends.* Composites Part a-Applied Science and Manufacturing, 2009. **40**(11): p. 1661-1672.

59.   Li, F.K., et al., *Polyurethane/conducting carbon black composites: Structure, electric conductivity, strain recovery behavior; and their relationships.* Journal of Applied Polymer Science, 2000. **75**(1): p. 68-77.

60.   Gunes, I.S., F. Cao, and S.C. Jana, *Evaluation of nanoparticulate fillers for development of shape memory polyurethane nanocomposites.* Polymer, 2008. **49**(9): p. 2223-2234.

61.   Gunes, I.S., F. Cao, and S.C. Jana, *Effect of thermal expansion on shape memory behavior of polyurethane and its nanocomposites.* Journal of Polymer Science Part B-Polymer Physics, 2008. **46**(14): p. 1437-1449.

62.   Wang, X.Y., et al., *Improved Self-healing of Polyethylene/Carbon Black Nanocomposites by Their Shape Memory Effect.* Journal of Physical Chemistry B, 2013. **117**(5): p. 1467-1474.

63.   Gall, K., et al., *Shape memory polymer nanocomposites.* Acta Materialia, 2002. **50**(20): p. 5115-5126.

64.   Gall, K., et al., *Internal stress storage in shape memory polymer nanocomposites.* Applied Physics Letters, 2004. **85**(2): p. 290-292.

65.   Liu, Y.P., et al., *Thermomechanics of shape memory polymer nanocomposites.* Mechanics of Materials, 2004. **36**(10): p. 929-940.

66.   Cao, F. and S.C. Jana, *Nanoclay-tethered shape memory polyurethane nanocomposites.* Polymer, 2007. **48**(13): p. 3790-3800.

67.   Rezanejad, S. and M. Kokabi, *Shape memory and mechanical properties of cross-linked polyethylene/clay nanocomposites.* European Polymer Journal, 2007. **43**(7): p. 2856-2865.

68.   Xu, B., et al., *Mechanical properties of attapulgite clay reinforced polyurethane shape-memory nanocomposites.* European Polymer Journal, 2009. **45**(7): p. 1904-1911.

69.   Haghayegh, M. and G.M.M. Sadeghi, *Synthesis of shape memory polyurethane/clay nanocomposites and analysis of shape memory, thermal, and mechanical properties.* Polymer Composites, 2012. **33**(6): p. 843-849.

70.   Gall, K., et al., *Carbon fiber reinforced shape memory polymer composites.* Journal of Intelligent Material Systems and Structures, 2000. **11**(11): p. 877-886.

71.   Tang, Z.H., et al., *Vapor grown carbon nanofiber reinforced bio-based polyester for electroactive shape memory performance.* Composites Science and Technology, 2013. **75**: p. 15-21.

72.   Cho, J.W., et al., *Electroactive shape-memory polyurethane composites incorporating carbon nanotubes.* Macromolecular Rapid Communications, 2005. **26**(5): p. 412-416.

73.   Sahoo, N.G., et al., *Influence of carbon nanotubes and polypyrrole on the thermal, mechanical and electroactive shape-memory properties of polyurethane nanocomposites.* Composites Science and Technology, 2007. **67**(9): p. 1920-1929.

74.   Jung, Y.C., et al., *Electroactive shape memory performance of polyurethane composite having homogeneously dispersed and covalently crosslinked carbon nanotubes.* Carbon, 2010. **48**(5): p. 1598-1603.

75.   Xiao, Y., et al., *Electro-active Shape Memory Properties of Poly(epsilon-caprolactone)/Functionalized Multiwalled Carbon Nanotube Nanocomposite.* ACS Applied Materials & Interfaces, 2010. **2**(12): p. 3506-3514.

76.   Raja, M., S.H. Ryu, and A.M. Shanmugharaj, *Thermal, mechanical and electroactive shape memory properties of polyurethane (PU)/poly(lactic acid) (PLA)/CNT nanocomposites.* European Polymer Journal, 2013. **49**(11): p. 3492-3500.

77.   Yang, P., Y. Wu, and R. Fan, *Inorganic semiconductor nanowires.* International Journal of Nanoscience, 2002. **1**(01): p. 1-39.

78.   Ye, C., et al., *Zinc oxide nanostructures: morphology derivation and evolution.* The Journal of Physical Chemistry B, 2005. **109**(42): p. 19758-19765.

79.   Wu, J.-M., et al., *Thermal evaporation growth and the luminescence property of TiO$_2$ nanowires.* Journal of crystal Growth, 2005. **281**(2-4): p. 384-390.

80.   Park, M.S., et al., *Preparation and electrochemical properties of SnO$_2$ nanowires for application in lithium‑ion batteries.* Angewandte Chemie International Edition, 2007. **46**(5): p. 750-753.

81.   Law, M., J. Goldberger, and P. Yang, *Semiconductor nanowires and nanotubes.* Annu. Rev. Mater. Res., 2004. **34**: p. 83-122.

82.   Cao, G., *Nanostructures and nanomaterials: synthesis, properties and applications*. 2004: World scientific.

83.   Xia, Y., et al., *One-dimensional nanostructures: synthesis, characterization, and applications.* Advanced Materials, 2003. **15**(5): p. 353-389.

84.   Zhang, R.Q., Y. Lifshitz, and S.T. Lee, *Oxide‐assisted growth of semiconducting nanowires.* Advanced Materials, 2003. **15**(7‐8): p. 635-640.

85.   Wang, N., Y. Cai, and R. Zhang, *Growth of nanowires.* Materials Science and Engineering: R: Reports, 2008. **60**(1-6): p. 1-51.

86.   Wagner, R. and W. Ellis, *Vapor-liquid-solid mechanism of single crystal growth.* Applied Physics Letters, 1964. **4**(5): p. 89-90.

87.   Wagner, R. and W. Ellis, *Vapor-liquid-solid mechanism of crystal growth and its application to silicon.* Transactions of the Metallurgical Society of AIME, 1965. **233**: p. 1053-1064.

88.   Morales, A.M. and C.M. Lieber, *A laser ablation method for the synthesis of crystalline semiconductor nanowires.* Science, 1998. **279**(5348): p. 208-211.

89.   Wu, Y. and P. Yang, *Direct observation of vapor-liquid-solid nanowire growth.* Journal of the American Chemical Society, 2001. **123**(13): p. 3165-3166.

90.   Hannon, J., et al., *The influence of the surface migration of gold on the growth of silicon nanowires.* Nature, 2006. **440**(7080): p. 69-71.

91.   Dasgupta, N.P., et al., *25th anniversary article: semiconductor nanowires-synthesis, characterization, and applications.* Advanced Materials, 2014. **26**(14): p. 2137-2184.

92. He, M., et al., *Growth of GaN nanowires by direct reaction of Ga with NH₃.* Journal of Crystal Growth, 2001. **231**(3): p. 357-365.

93. Meyyappan, M. and M.K. Sunkara, *Inorganic nanowires: applications, properties, and characterization*. 2018: CRC Press.

94. Xia, Y., et al., *Shape-controlled synthesis of metal nanocrystals: simple chemistry meets complex physics?* Angewandte Chemie International Edition, 2009. **48**(1): p. 60-103.

95. Kuno, M., *An overview of solution-based semiconductor nanowires: synthesis and optical studies.* Physical Chemistry Chemical Physics, 2008. **10**(5): p. 620-639.

96. Sun, Y., et al., *Polyol synthesis of uniform silver nanowires: a plausible growth mechanism and the supporting evidence.* Nano Letters, 2003. **3**(7): p. 955-960.

97. Sun, Y., et al., *Uniform silver nanowires synthesis by reducing AgNO₃ with ethylene glycol in the presence of seeds and poly(vinyl pyrrolidone).* Chemistry of Materials, 2002. **14**(11): p. 4736-4745.

98. Amin, G., et al., *Influence of pH, precursor concentration, growth time, and temperature on the morphology of ZnO nanostructures grown by the hydrothermal method.* Journal of Nanomaterials, 2011. **2011**.

99. He, T., L. Xiang, and S. Zhu, *Different nanostructures of boehmite fabricated by hydrothermal process: effects of pH and anions.* CrystEngComm, 2009. **11**(7): p. 1338-1342.

100. Furneaux, R., W. Rigby, and A. Davidson, *The formation of controlled-porosity membranes from anodically oxidized aluminium.* Nature, 1989. **337**(6203): p. 147.

101. Schönenberger, C., et al., *Template synthesis of nanowires in porous polycarbonate membranes: electrochemistry and morphology.* The Journal of Physical Chemistry B, 1997. **101**(28): p. 5497-5505.

102. Walter, E.C., et al., *Metal nanowire arrays by electrodeposition.* ChemPhysChem, 2003. **4**(2): p. 131-138.

103. Cao, G. and D. Liu, *Template-based synthesis of nanorod, nanowire, and nanotube arrays.* Advances in Colloid and Interface Science, 2008. **136**(1-2): p. 45-64.

104. Sauer, G., et al., *Highly ordered monocrystalline silver nanowire arrays.* Journal of Applied Physics, 2002. **91**(5): p. 3243-3247.

105. Yin, A., et al., *Fabrication of highly ordered metallic nanowire arrays by electrodeposition.* Applied Physics Letters, 2001. **79**(7): p. 1039-1041.

106. Zheng, M., et al., *Fabrication and optical properties of large-scale uniform zinc oxide nanowire arrays by one-step electrochemical deposition technique.* Chemical Physics Letters, 2002. **363**(1-2): p. 123-128.

107. Prieto, A.L., et al., *Electrodeposition of ordered Bi_2Te_3 nanowire arrays.* Journal of the American Chemical Society, 2001. **123**(29): p. 7160-7161.

108. Whitney, T., et al., *Fabrication and magnetic properties of arrays of metallic nanowires.* Science, 1993. **261**(5126): p. 1316-1319.

109. Coleman, J.N., U. Khan, and Y.K. Gun'ko, *Mechanical reinforcement of polymers using carbon nanotubes.* Advanced Materials, 2006. **18**(6): p. 689-706.

110. Moniruzzaman, M. and K.I. Winey, *Polymer nanocomposites containing carbon nanotubes.* Macromolecules, 2006. **39**(16): p. 5194-5205.

111.   Huang, W., et al., *Sonication-assisted functionalization and solubilization of carbon nanotubes.* Nano Letters, 2002. **2**(3): p. 231-234.

112.   Lu, K., et al., *Mechanical damage of carbon nanotubes by ultrasound.* Carbon, 1996. **34**(6): p. 814-816.

113.   Gelves, G.A., et al., *Enhancing dispersion of copper nanowires in melt-mixed polystyrene composites.* Journal of Polymer Science Part B: Polymer Physics, 2008. **46**(19): p. 2064-2078.

114.   Yu, Z., et al., *Highly Dispersible Silver Nanowires via Diblock Copolymer Approach for Potential Application in Transparent Conductive Composite.* New Journal of Chemistry, 2017. **41**(14): p. 6349-6358.

115.   Kango, S., et al., *Surface modification of inorganic nanoparticles for development of organic-inorganic nanocomposites-a review.* Progress in Polymer Science, 2013. **38**(8): p. 1232-1261.

116.   Yang, K., et al., *Effects of carbon nanotube functionalization on the mechanical and thermal properties of epoxy composites.* Carbon, 2009. **47**(7): p. 1723-1737.

117.   Huang, Y.Y. and E.M. Terentjev, *Dispersion of carbon nanotubes: mixing, sonication, stabilization, and composite properties.* Polymers, 2012. **4**(1): p. 275-295.

118.   Cadek, M., et al., *Reinforcement of polymers with carbon nanotubes: the role of nanotube surface area.* Nano Letters, 2004. **4**(2): p. 353-356.

119.   Coleman, J.N., et al., *Small but strong: a review of the mechanical properties of carbon nanotube-polymer composites.* Carbon, 2006. **44**(9): p. 1624-1652.

120.   Vollenberg, P., D. Heikens, and H. Ladan, *Experimental determination of thermal and adhesion stress in particle filled thermoplasts.* Polymer Composites, 1988. **9**(6): p. 382-388.

121.   Dekkers, M. and D. Heikens, *The effect of interfacial adhesion on the tensile behavior of polystyrene-glass-bead composites.* Journal of Applied Polymer Science, 1983. **28**(12): p. 3809-3815.

122.   Bose, S., R.A. Khare, and P. Moldenaers, *Assessing the strengths and weaknesses of various types of pre-treatments of carbon nanotubes on the properties of polymer/carbon nanotubes composites: A critical review.* Polymer, 2010. **51**(5): p. 975-993.

123.   Rahmat, M. and P. Hubert, *Carbon nanotube-polymer interactions in nanocomposites: a review.* Composites Science and Technology, 2011. **72**(1): p. 72-84.

124.   Byrne, M.T. and Y.K. Gun'ko, *Recent advances in research on carbon nanotube-polymer composites.* Advanced Materials, 2010. **22**(15): p. 1672-1688.

125.   Wang, L., et al., *One-pot synthesis and bioapplication of amine-functionalized magnetite nanoparticles and hollow nanospheres.* Chemistry-A European Journal, 2006. **12**(24): p. 6341-6347.

126.   Xin, X., et al., *Highly efficient removal of heavy metal ions by amine-functionalized mesoporous Fe_3O_4 nanoparticles.* Chemical Engineering Journal, 2012. **184**: p. 132-140.

127. Sayyar, M., et al., *High performance pseudoelastic metal nanowire reinforced elastomeric composite.* Industrial & Engineering Chemistry Research, 2014. **53**(34): p. 13329-13339.

128. Massoumi, B., et al., *Ag/polyaniline nanocomposites: synthesize, characterization, and application to the detection of dopamine and tyrosine.* Journal of Applied Polymer Science, 2013. **130**(4): p. 2780-2789.

129. Byrne, M.T., et al., *Chemical functionalisation of titania nanotubes and their utilisation for the fabrication of reinforced polystyrene composites.* Journal of Materials Chemistry, 2007. **17**(22): p. 2351-2358.

130. Tee, D., et al., *Effect of silane-based coupling agent on the properties of silver nanoparticles filled epoxy composites.* Composites Science and Technology, 2007. **67**(11-12): p. 2584-2591.

131. Ma, P.C., J.-K. Kim, and B.Z. Tang, *Effects of silane functionalization on the properties of carbon nanotube/epoxy nanocomposites.* Composites Science and Technology, 2007. **67**(14): p. 2965-2972.

132. Zhao, Y.-L. and J.F. Stoddart, *Noncovalent functionalization of single-walled carbon nanotubes.* Accounts of Chemical Research, 2009. **42**(8): p. 1161-1171.

133. Kim, S.W., et al., *Surface modifications for the effective dispersion of carbon nanotubes in solvents and polymers.* Carbon, 2012. **50**(1): p. 3-33.

134. Ma, P.-C., et al., *Dispersion and functionalization of carbon nanotubes for polymer-based nanocomposites: a review.* Composites Part A: Applied Science and Manufacturing, 2010. **41**(10): p. 1345-1367.

135. Yu, Y.-H., et al., *Enhanced thermal and mechanical properties of epoxy composites filled with silver nanowires and nanoparticles.* Journal of The Taiwan Institute of Chemical Engineers, 2013. **44**(4): p. 654-659.

136. Velasco-Santos, C., et al., *Improvement of thermal and mechanical properties of carbon nanotube composites through chemical functionalization.* Chemistry of Materials, 2003. **15**(23): p. 4470-4475.

137. Bartholome, C., et al., *Influence of surface functionalization on the thermal and electrical properties of nanotube-PVA composites.* Composites Science and Technology, 2008. **68**(12): p. 2568-2573.

138. Porter, M.D., et al., *Spontaneously organized molecular assemblies. 4. Structural characterization of n-alkyl thiol monolayers on gold by optical ellipsometry, infrared spectroscopy, and electrochemistry.* Journal of the American Chemical Society, 1987. **109**(12): p. 3559-3568.

139. Jadzinsky, P.D., et al., *Structure of a thiol monolayer-protected gold nanoparticle at 1.1 Å resolution.* Science, 2007. **318**(5849): p. 430-433.

140. Laibinis, P.E., et al., *Comparison of the structures and wetting properties of self-assembled monolayers of n-alkanethiols on the coinage metal surfaces, copper, silver, and gold.* Journal of the American Chemical Society, 1991. **113**(19): p. 7152-7167.

141. Anyaogu, K.C., A.V. Fedorov, and D.C. Neckers, *Synthesis, characterization, and antifouling potential of functionalized copper nanoparticles.* Langmuir, 2008. **24**(8): p. 4340-4346.

142. Herradura, P.S., K.A. Pendola, and R.K. Guy, *Copper-mediated cross-coupling of aryl boronic acids and alkyl thiols.* Organic Letters, 2000. **2**(14): p. 2019-2022.

143. Love, J.C., et al., *Self-assembled monolayers of thiolates on metals as a form of nanotechnology.* Chemical Reviews, 2005. **105**(4): p. 1103-1170.

144. Vericat, C., et al., *Self-assembled monolayers of thiols and dithiols on gold: new challenges for a well-known system.* Chemical Society Reviews, 2010. **39**(5): p. 1805-1834.

145. Zerulla, D. and T. Chassé, *X-ray induced damage of self-assembled alkanethiols on gold and indium phosphide.* Langmuir, 1999. **15**(16): p. 5285-5294.

146. Yamamoto, H., et al., *Characterization of the surface to thiol bonding in self-assembled monolayer films of $C_{12}H_{25}SH$ on InP (100) by angle-resolved X-ray photoelectron spectroscopy.* Langmuir, 1999. **15**(25): p. 8640-8644.

147. Zerulla, D. and T. Chassé, *Structure and self-assembly of alkanethiols on III-V semiconductor (110) surfaces.* Journal of Electron Spectroscopy and Related Phenomena, 2009. **172**(1-3): p. 78-87.

148. Lunt, S.R., et al., *Chemical studies of the passivation of GaAs surface recombination using sulfides and thiols.* Journal of Applied Physics, 1991. **70**(12): p. 7449-7467.

149. Sterman, S. and Marsden, J. G., *Silane coupling agents*. Industrial & Engineering Chemistry, 1966. **58**(3): p. 33-37.

150.   Xie, Y., et al., *Silane coupling agents used for natural fiber/polymer composites: A review.* Composites Part A: Applied Science and Manufacturing, 2010. **41**(7): p. 806-819.

151.   Jung, G.-Y., et al., *Vapor-phase self-assembled monolayer for improved mold release in nanoimprint lithography.* Langmuir, 2005. **21**(4): p. 1158-1161.

152.   Anderson, A.S., et al., *Functional PEG-modified thin films for biological detection.* Langmuir, 2008. **24**(5): p. 2240-2247.

153.   Li, G.-y., et al., *Large areas of centimeters-long SiC nanowires synthesized by pyrolysis of a polymer precursor by a CVD route.* The Journal of Physical Chemistry C, 2009. **113**(41): p. 17655-17660.

154.   Fang, L., et al., *Catalyst-free growth of millimeter-long topological insulator Bi_2Se_3 nanoribbons and the observation of the π-Berry phase.* Nano Letters, 2012. **12**(12): p. 6164-6169.

155.   Zhai, T., et al., *Centimeter-Long V_2O_5 Nanowires: From Synthesis to Field-Emission, Electrochemical, Electrical Transport, and Photoconductive Properties.* Advanced Materials, 2010. **22**(23): p. 2547-2552.

156.   Yu, K., et al., *Growth and optical applications of centimeter-long ZnO nanocombs.* Nano Research, 2008. **1**(3): p. 221-228.

157.   Chen, S., et al., *Dense and vertically-aligned centimetre-long ZnS nanowire arrays: ionic liquid assisted synthesis and their field emission properties.* Nanoscale, 2012. **4**(8): p. 2658-2662.

158. Park, W.I., et al., *Controlled synthesis of millimeter-long silicon nanowires with uniform electronic properties.* Nano Letters, 2008. **8**(9): p. 3004-3009.

159. Smith, J.B., et al., *Ultra-long Crystalline Red Phosphorus Nanowires from Amorphous Red Phosphorus Thin Films.* Angewandte Chemie International Edition, 2016. **55**(39): p. 11829-11833.

160. Shi, W.-S., et al., *Synthesis of large areas of highly oriented, very long silicon nanowires.* Advanced Materials, 2000. **12**(18): p. 1343-1345.

161. Kumar, V., et al., *Gas-Phase, Bulk Production of Metal Oxide Nanowires and Nanoparticles Using a Microwave Plasma Jet Reactor.* The Journal of Physical Chemistry C, 2008. **112**(46): p. 17750-17754.

162. Bogart, T.D., et al., *Lithium Ion Battery Peformance of Silicon Nanowires with Carbon Skin.* ACS Nano, 2013. **8**(1): p. 915-922.

163. Lu, X. and B.A. Korgel, *A Single-step Reaction for Silicon and Germanium Nanorods.* Chemistry-A European Journal, 2014. **20**(20): p. 5874-5879.

164. Heurlin, M., et al., *Continuous gas-phase synthesis of nanowires with tunable properties.* Nature, 2012. **492**(7427): p. 90-94.

165. Chen, Y., R. Polinnaya, and S. Vaddiraju, *Byproduct-free mass production of compound semiconductor nanowires: zinc phosphide.* Materials Research Express, 2018. **5**(5): p. 055042.

166. Hannon, J.B., et al., *The influence of the surface migration of gold on the growth of silicon nanowires.* Nature, 2006. **440**(7080): p. 69-71.

167.   Jarrett, R. and R. Crook, *Silver nanowire purification and separation by size and shape using multi-pass filtration.* Materials Research Innovations, 2016. **20**(2): p. 86-91.

168.   Rakesh, *Large-scale Synthesis of Zn_3P_2 Nanowires Using Porous Zinc Pellets.* 2017, Master's thesis, Texas A&M University.

169.   Langley, D., et al., *Flexible transparent conductive materials based on silver nanowire networks: a review.* Nanotechnology, 2013. **24**(45): p. 452001.

170.   Abbasi, N.M., et al., *Preparation of silver nanowires and their application in conducting polymer nanocomposites.* Materials Chemistry and Physics, 2015. **166**: p. 1-15.

171.   Wei, J., et al., *High Enhanced Efficiency and Mechanism of Ultra-long SiC Nanowires in Composites.* Advanced Engineering Materials, 2015. **17**(4): p. 539-544.

172.   Meng, S., et al., *Tailoring and application of SiC nanowires in composites.* Materials Science and Engineering: A, 2010. **527**(21): p. 5761-5765.

173.   Vijayan P, P., et al., *Mechanical and thermal properties of epoxy/silicon carbide nanofiber composites.* Polymers for Advanced Technologies, 2015. **26**(2): p. 142-146.

174.   Nhuapeng, W., et al., *Fabrication and mechanical properties of silicon carbide nanowires/epoxy resin composites.* Current Applied Physics, 2008. **8**(3): p. 295-299.

175. Keshoju, K. and L. Sun, *Mechanical characterization of magnetic nanowire-polydimethylsiloxane composites.* Journal of Applied Physics, 2009. **105**(2): p. 023515.

176. Xu, Q., et al., *Copper nanowire/PA6 composites prepared by in situ polymerization and its properties.* Journal of Polymer Research, 2013. **20**(10): p. 257.

177. Lin, B., et al., *Electrical, rheological, and mechanical properties of polystyrene/copper nanowire nanocomposites.* Industrial & Engineering Chemistry Research, 2007. **46**(8): p. 2481-2487.

178. Liang, H. and D. Yu, *Mechanical and thermal properties of (Ag/C nanocable)/epoxy resin composites.* Polymer Science Series B, 2011. **53**(11): p. 601-605.

179. Paszkiewicz, S., et al., *Comparative study on the properties of poly(trimethylene terephthalate)-based nanocomposites containing multi-walled carbon (MWCNT) and tungsten disulfide (INT-WS$_2$) nanotubes.* Polymers for Advanced Technologies, 2017. **28**(6): p. 645-657.

180. Naffakh, M. and A.M. Díez-Pascual, *WS$_2$ inorganic nanotubes reinforced poly(l-lactic acid)/hydroxyapatite hybrid composite biomaterials.* RSC Advances, 2015. **5**(80): p. 65514-65525.

181. Naffakh, M., et al., *New inorganic nanotube polymer nanocomposites: improved thermal, mechanical and tribological properties in isotactic polypropylene*

incorporating INT-MoS₂. Journal of Materials Chemistry, 2012. **22**(33): p. 17002-17010.

182. Huskić, M., et al., *The effect of Mo₆S₃I₆ nanowires on the thermal and mechanical properties of polyamide 12.* Composites Part B: Engineering, 2014. **56**: p. 62-67.

183. Chin, S.J., et al., *Composites of poly(ε-caprolactone) and Mo₆S₃I₆ Nanowires.* Polymers for Advanced Technologies, 2012. **23**(2): p. 149-160.

184. Mancic, L., et al., *Application of silane grafted titanate nanotubes in reinforcing of polyamide 11 composites.* Composites Part B: Engineering, 2016. **93**: p. 153-162.

185. Mancic, L., et al., *Thermal and mechanical properties of polyamide 11 based composites reinforced with surface modified titanate nanotubes.* Materials & Design, 2015. **83**: p. 459-467.

186. Doganay, D., et al., *Electrical, mechanical and thermal properties of aligned silver nanowire/polylactide nanocomposite films.* Composites Part B: Engineering, 2016. **99**: p. 288-296.

187. Mi, H.-Y., et al., *Silver nanowire/thermoplastic polyurethane elastomer nanocomposites: Thermal, mechanical, and dielectric properties.* Materials & Design (1980-2015), 2014. **56**: p. 398-404.

188. Lima, G.R., et al. *Thermal, Mechanical, and Morphological Properties of DPU/Titanate Nanotubes Nanocomposites*. in *Macromolecular Symposia*. 2019. Wiley Online Library.

189.   Zhang, P., et al., *Enhanced electrochemical and mechanical properties of P(VDF-HFP)-based composite polymer electrolytes with SiO$_2$ nanowires.* Journal of Membrane Science, 2011. **379**(1): p. 80-85.

190.   Favier, V., H. Chanzy, and J. Cavaillé, *Polymer nanocomposites reinforced by cellulose whiskers.* Macromolecules, 1995. **28**(18): p. 6365-6367.

191.   Nikfar, N., Y. Zare, and K.Y. Rhee, *Dependence of mechanical performances of polymer/carbon nanotubes nanocomposites on percolation threshold.* Physica B: Condensed Matter, 2018. **533**: p. 69-75.

192.   Tang, Y., et al., *Manufacturable conducting rubber ambers and stretchable conductors from copper nanowire aerogel monoliths.* ACS Nano, 2014. **8**(6): p. 5707-5714.

193.   áSatcher Jr, J.H., *Stiff and electrically conductive composites of carbon nanotube aerogels and polymers.* Journal of Materials Chemistry, 2009. **19**(21): p. 3370-3372.

194.   Hu, H., et al., *Polymer casting of ultralight graphene aerogels for the production of conductive nanocomposites with low filling content.* Journal of Materials Chemistry A, 2014. **2**(11): p. 3756-3760.

195.   Tang, G., et al., *Three dimensional graphene aerogels and their electrically conductive composites.* Carbon, 2014. **77**: p. 592-599.

196.   Qian, F., et al., *Ultralight conductive silver nanowire aerogels.* Nano Letters, 2017. **17**(12): p. 7171-7176.

197. Tang, Y., et al., *Ultralow-density copper nanowire aerogel monoliths with tunable mechanical and electrical properties.* Journal of Materials Chemistry A, 2013. **1**(23): p. 6723-6726.

198. Han, D., et al., *Porous SiC$_{nw}$/SiC ceramics with unidirectionally aligned channels produced by freeze-drying and chemical vapor infiltration.* Journal of the European Ceramic Society, 2017. **37**(3): p. 915-921.

199. Jung, S.M., et al., *A facile route for 3D aerogels from nanostructured 1D and 2D materials.* Scientific Reports, 2012. **2**: p. 849.

200. Jung, S.M., et al., *Porous Cu nanowire aerosponges from one-step assembly and their applications in heat dissipation.* Advanced Materials, 2016. **28**(7): p. 1413-1419.

201. He, W., et al., *Polypyrrole/silver coaxial nanowire aero-sponges for temperature-independent stress sensing and stress-triggered joule heating.* ACS Nano, 2015. **9**(4): p. 4244-4251.

202. Bhushan, M. and A. Catalano, *Polycrystalline Zn$_3$P$_2$ Schottky barrier solar cells.* Applied Physics Letters, 1981. **38**(1): p. 39-41.

203. Fessenden, R., J. Sobhanadri, and V. Subramanian, *Minority carrier lifetime in thin films of Zn$_3$P$_2$ using microwave and optical transient measurements.* Thin Solid Films, 1995. **266**(2): p. 176-181.

204. Shen, G., et al., *Single-crystalline and twinned Zn$_3$P$_2$ nanowires: synthesis, characterization, and electronic properties.* The Journal of Physical Chemistry C, 2008. **112**(42): p. 16405-16410.

205. Wu, P., et al., *Fast-speed and high-gain photodetectors of individual single crystalline Zn₃P₂ nanowires.* Journal of Materials Chemistry, 2011. **21**(8): p. 2563-2567.

206. Vaddiraju, S., et al., *Mechanisms of 1D crystal growth in reactive vapor transport: Indium nitride nanowires.* Nano Letters, 2005. **5**(8): p. 1625-1631.

207. Qiu, Y. and L. Gao, *Novel way to synthesize nanocrystalline aluminum nitride from coarse aluminum powder.* Journal of the American Ceramic Society, 2003. **86**(7): p. 1214-1216.

208. Vaddiraju, S., et al., *Synthesis of group III antimonide nanowires.* Journal of Physical Chemistry C, 2007. **111**(20): p. 7339-7347.

209. Ashby, M.F., et al., *Metal foams: a design guide*. 2000: Elsevier.

210. Solórzano, E., M. Rodriguez‐Perez, and J. de Saja, *Thermal conductivity of cellular metals measured by the transient plane sour method.* Advanced Engineering Materials, 2008. **10**(4): p. 371-377.

211. Ho, M.-W., et al., *Mechanical properties of epoxy-based composites using nanoclays.* Composite Structures, 2006. **75**(1-4): p. 415-421.

212. Zhu, J., et al., *Reinforcing epoxy polymer composites through covalent integration of functionalized nanotubes.* Advanced Functional Materials, 2004. **14**(7): p. 643-648.

213. Hsieh, T., et al., *The toughness of epoxy polymers and fibre composites modified with rubber microparticles and silica nanoparticles.* Journal of Materials Science, 2010. **45**(5): p. 1193-1210.

214.   Zhou, Y., et al., *Fabrication and evaluation of carbon nano fiber filled carbon/epoxy composite.* Materials Science and Engineering: A, 2006. **426**(1-2): p. 221-228.

215.   Kosmidou, T.V., et al., *Structural, mechanical and electrical characterization of epoxy-amine/carbon black nanocomposites.* Express Polymer Letters, 2008. **2**(5): p. 364-372.

216.   Khalil, H.A., et al., *Exploring biomass based carbon black as filler in epoxy composites: Flexural and thermal properties.* Materials & Design, 2010. **31**(7): p. 3419-3425.

217.   Wang, L., et al., *Preparation, morphology and thermal/mechanical properties of epoxy/nanoclay composite.* Composites Part A: Applied Science and Manufacturing, 2006. **37**(11): p. 1890-1896.

218.   Sprenger, S., *Epoxy resin composites with surface-modified silicon dioxide nanoparticles: A review.* Journal of Applied Polymer Science, 2013. **130**(3): p. 1421-1428.

219.   Gojny, F., et al., *Carbon nanotube-reinforced epoxy-composites: enhanced stiffness and fracture toughness at low nanotube content.* Composites Science and Technology, 2004. **64**(15): p. 2363-2371.

220.   Brockway, L., et al., *Thermoelectric properties of large-scale Zn_3P_2 nanowire assemblies.* Nanotechnology, 2014. **25**(14): p. 145401.

221.   Xie, T. and I.A. Rousseau, *Facile tailoring of thermal transition temperatures of epoxy shape memory polymers.* Polymer, 2009. **50**(8): p. 1852-1856.

222. Rousseau, I.A. and T. Xie, *Shape memory epoxy: Composition, structure, properties and shape memory performances.* Journal of Materials Chemistry, 2010. **20**(17): p. 3431-3441.

223. Luna Zaragoza, D., E.T. Romero Guzmán, and L.R. Reyes Gutiérrez, *Surface and physicochemical characterization of phosphates vivianite, $Fe_2(PO_4)_3$ and hydroxyapatite, $Ca_5(PO_4)_3OH$.* Journal of Minerals and Materials Characterization and Engineering, 2009, **8**(8): p. 591-609.

224. Jung, S.-H., et al., *Sonochemical synthesis of amorphous zinc phosphate nanospheres.* Bull. Korean Chem. Soc, 2009. **30**(10): p. 2281.

225. Rosario-Castro, B.I., et al., *Single-wall carbon nanotube chemical attachment at platinum electrodes.* Applied Surface Science, 2010. **257**(2): p. 340-353.

226. Lim, H., et al., *Chemical and thermal stability of alkanethiol and sulfur passivated InP (100).* Langmuir, 2004. **20**(3): p. 743-747.

227. Wang, S., et al., *Effective amino-functionalization of carbon nanotubes for reinforcing epoxy polymer composites.* Nanotechnology, 2006. **17**(6): p. 1551.

228. Naffakh, M. and A.M. Díez-Pascual, *Nanocomposite biomaterials based on poly(ether-ether-ketone) (PEEK) and WS_2 inorganic nanotubes.* Journal of Materials Chemistry B, 2014. **2**(28): p. 4509-4520.

229. Dominkovics, Z., L. Dányádi, and B. Pukanszky, *Surface modification of wood flour and its effect on the properties of PP/wood composites.* Composites Part A: Applied Science and Manufacturing, 2007. **38**(8): p. 1893-1901.

230.   Li, S., et al., *Effect of acid and TETA modification on mechanical properties of MWCNTs/epoxy composites.* Journal of Materials Science, 2008. **43**(8): p. 2653-2658.

231.   Dányádi, L., J. Móczó, and B. Pukánszky, *Effect of various surface modifications of wood flour on the properties of PP/wood composites.* Composites Part A: Applied Science and Manufacturing, 2010. **41**(2): p. 199-206.

232.   Li, P., et al., *Enhancement of the interfacial interaction between poly(vinyl chloride) and zinc oxide modified reduced graphene oxide.* RSC Advances, 2016. **6**(7): p. 5784-5791.

233.   Pehlivan, H., et al., *Characterization of pure and silver exchanged natural zeolite filled polypropylene composite films.* Composites Science and Technology, 2005. **65**(13): p. 2049-2058.

234.   Marsh, J., et al., *Interaction of epoxy model molecules with aluminium, anodised titanium and copper surfaces: an XPS study.* Applied Surface Science, 1998. **133**(4): p. 270-286.

235.   Wielant, J., et al., *Influence of the iron oxide acid-base properties on the chemisorption of model epoxy compounds studied by XPS.* The Journal of Physical Chemistry C, 2007. **111**(35): p. 13177-13184.

236.   Kollek, H., *Some aspects of chemistry in adhesion on anodized aluminium.* International Journal of Adhesion and Adhesives, 1985. **5**(2): p. 75-80.

237.   Nigro, J. and H. Ishida, *Cure behavior of very thin epoxy resin films on steel.* Journal of Applied Polymer Science, 1989. **38**(12): p. 2191-2204.

238.   Gaillac, R., P. Pullumbi, and F.-X. Coudert, *ELATE: an open-source online application for analysis and visualization of elastic tensors.* Journal of Physics: Condensed Matter, 2016. **28**(27): p. 275201.

239.   Konnola, R., et al., *Fabrication and Characterization of Toughened Nanocomposites Based on TiO$_2$ Nanowire-Epoxy System.* Polymer Composites, 2019. **40**(7): p. 2629-2638.

240.   Saritha, A., et al., *Mechanical, thermophysical, and diffusion properties of TiO$_2$-filled chlorobutyl rubber composites.* Polymer Composites, 2011. **32**(10): p. 1681-1687.

241.   Hashimoto, M., et al., *Enhancement of mechanical strength of TiO$_2$/high-density polyethylene composites for bone repair with silane-coupling treatment.* Materials Research Bulletin, 2006. **41**(3): p. 515-524.

242.   Erdem, B., et al., *XPS and FTIR surface characterization of TiO$_2$ particles used in polymer encapsulation.* Langmuir, 2001. **17**(9): p. 2664-2669.

243.   Lou, Y., et al., *Improvement of the mechanical properties of nano-TiO$_2$/poly(vinyl alcohol) composites by enhanced interaction between nanofiller and matrix.* Polymer Composites, 2010. **31**(7): p. 1184-1193.

244.   Huaiyuan, W., et al., *The effect of self-assembly modified potassium titanate whiskers on the friction and wear behaviors of PEEK composites.* Wear, 2010. **269**(1-2): p. 139-144.

245.   Wang, H., G. Xian, and H. Li, *Grafting of nano-TiO$_2$ onto flax fibers and the enhancement of the mechanical properties of the flax fiber and flax fiber/epoxy*

composite. Composites Part A: Applied Science and Manufacturing, 2015. **76**: p. 172-180.

246.   Li, J., et al., *The improvement in cryogenic mechanical properties of nano-ZrO₂/epoxy composites via surface modification of nano-ZrO₂.* RSC Advances, 2016. **6**(66): p. 61393-61401.

247.   Srivastava, S. and R.K. Tiwari, *Synthesis of epoxy-TiO₂ nanocomposites: A study on sliding wear behavior, thermal and mechanical properties.* International Journal of Polymeric Materials, 2012. **61**(13): p. 999-1010.

248.   Kim, W.-J., et al., *Enhanced protein immobilization efficiency on a TiO₂ surface modified with a hydroxyl functional group.* Langmuir, 2009. **25**(19): p. 11692-11697.

249.   Fadeev, A.Y., R. Helmy, and S. Marcinko, *Self-assembled monolayers of organosilicon hydrides supported on titanium, zirconium, and hafnium dioxides.* Langmuir, 2002. **18**(20): p. 7521-7529.

250.   Demirel, G.B., et al., *Molecular design of photoswitchable surfaces with controllable wettability.* Journal of Materials Chemistry, 2011. **21**(9): p. 3189-3196.

251.   Satyanarayana, N. and S.K. Sinha, *Tribology of PFPE overcoated self-assembled monolayers deposited on Si surface.* Journal of Physics D: Applied Physics, 2005. **38**(18): p. 3512.

252.   Wang, Y. and M. Lieberman, *Growth of ultrasmooth octadecyltrichlorosilane self-assembled monolayers on SiO₂.* Langmuir, 2003. **19**(4): p. 1159-1167.

253. Abboud, M., et al., *PMMA-based composite materials with reactive ceramic fillers. Part 1.-Chemical modification and characterisation of ceramic particles.* Journal of Materials Chemistry, 1997. **7**(8): p. 1527-1532.

254. Goren, K., et al., *Influence of nanoparticle surface chemistry and size on supercritical carbon dioxide processed nanocomposite foam morphology.* The Journal of Supercritical Fluids, 2010. **51**(3): p. 420-427.

255. Chatterjee, S., et al., *Photocatalytic properties of one-dimensional nanostructured titanates.* The Journal of Physical Chemistry C, 2010. **114**(20): p. 9424-9430.

256. Santara, B., et al., *Evidence of oxygen vacancy induced room temperature ferromagnetism in solvothermally synthesized undoped TiO_2 nanoribbons.* Nanoscale, 2013. **5**(12): p. 5476-5488.

257. Carli, L.N., et al., *The effects of silane coupling agents on the properties of PHBV/halloysite nanocomposites.* Applied Clay Science, 2014. **87**: p. 311-319.

258. Rostamzadeh, P., S.M. Mirabedini, and M. Esfandeh, *APS-silane modification of silica nanoparticles: effect of treatment's variables on the grafting content and colloidal stability of the nanoparticles.* Journal of Coatings Technology and Research, 2014. **11**(4): p. 651-660.

259. López-Periago, A.M., W. Sandoval, and C. Domingo, *Chemical modification of nanometric TiO_2 particles by anchoring functional silane molecules in supercritical CO_2.* Applied Surface Science, 2014. **296**: p. 114-123.

260. Liu, Y., et al., *Kinetics of (3-aminopropyl)triethoxylsilane (APTES) silanization of superparamagnetic iron oxide nanoparticles.* Langmuir, 2013. **29**(49): p. 15275-15282.

261. Helmy, R. and A.Y. Fadeev, *Self-assembled monolayers supported on TiO₂: comparison of $C_{18}H_{37}SiX_3$ (X=H, Cl, OCH₃), $C_{18}H_{37}Si(CH_3)_2Cl$, and $C_{18}H_{37}PO(OH)_2$.* Langmuir, 2002. **18**(23): p. 8924-8928.

262. Fu, S.-Y., et al., *Effects of particle size, particle/matrix interface adhesion and particle loading on mechanical properties of particulate-polymer composites.* Composites Part B: Engineering, 2008. **39**(6): p. 933-961.

263. Baláž, P., et al., *Hallmarks of mechanochemistry: from nanoparticles to technology.* Chemical Society Reviews, 2013. **42**(18): p. 7571-7637.

264. Tsuzuki, T. and P.G. McCormick, *Mechanochemical synthesis of nanoparticles.* Journal of Materials Science, 2004. **39**(16-17): p. 5143-5146.

265. Joye, I.J. and D.J. McClements, *Production of nanoparticles by anti-solvent precipitation for use in food systems.* Trends in Food Science & Technology, 2013. **34**(2): p. 109-123.

266. Nalesso, S., et al., *Development of Sodium Chloride Crystal Size during Antisolvent Crystallization under Different Sonication Modes.* Crystal Growth & Design, 2018. **19**(1): p. 141-149.

267. Guo, Z., et al., *Effect of ultrasound on anti-solvent crystallization process.* Journal of Crystal Growth, 2005. **273**(3-4): p. 555-563.

268. Zhou, G.X., et al., *Direct design of pharmaceutical antisolvent crystallization through concentration control.* Crystal Growth & Design, 2006. **6**(4): p. 892-898.

269. Zywitzki, O., et al., *Structure and properties of crystalline titanium oxide layers deposited by reactive pulse magnetron sputtering.* Surface and Coatings Technology, 2004. **180**: p. 538-543.

270. Cantournet, S., R. Desmorat, and J. Besson, *Mullins effect and cyclic stress softening of filled elastomers by internal sliding and friction thermodynamics model.* International Journal of Solids and Structures, 2009. **46**(11-12): p. 2255-2264.

271. Khoushabi, A., et al., *Tailoring swelling to control softening mechanisms during cyclic loading of PEG/cellulose hydrogel composites.* Composites Science and Technology, 2018. **168**: p. 88-95.

272. Zhang, L., et al., *Anisotropic tough poly(vinyl alcohol) hydrogels.* Soft Matter, 2012. **8**(40): p. 10439-10447.

273. Diani, J., B. Fayolle, and P. Gilormini, *A review on the Mullins effect.* European Polymer Journal, 2009. **45**(3): p. 601-612.

274. Srivastava, S.K. and Y.K. Mishra, *Nanocarbon reinforced rubber nanocomposites: detailed insights about mechanical, dynamical mechanical properties, Payne, and Mullin effects.* Nanomaterials, 2018. **8**(11): p. 945.

275. Ivanoska-Dacikj, A., et al., *Fine tuning of the dynamic mechanical properties of natural rubber/carbon nanotube nanocomposites by organically modified*

montmorillonite: A first step in obtaining high-performance damping material suitable for seismic application. Applied Clay Science, 2015. **118**: p. 99-106.

276. Xu, H., et al., *PVP-stabilized PdAu nanowire networks prepared in different solvents endowed with high electrocatalytic activities for the oxidation of ethylene glycol and isopropanol.* Colloids and Surfaces A: Physicochemical and Engineering Aspects, 2017. **522**: p. 335-345.

277. Wajid, A.S., et al., *Polymer-stabilized graphene dispersions at high concentrations in organic solvents for composite production.* Carbon, 2012. **50**(2): p. 526-534.

278. Bourlinos, A.B., et al., *Aqueous-phase exfoliation of graphite in the presence of polyvinylpyrrolidone for the production of water-soluble graphenes.* Solid State Communications, 2009. **149**(47-48): p. 2172-2176.